

Dissertation ETH number 17331

# **Ultrasonic In-Line Characterization of Suspensions**

A dissertation submitted to

ETH Zurich

for the degree of

Doctor of Sciences

presented by

**Beat H. Birkhofer**

Dipl.-Ing. ETH Zurich

born January 14, 1977

citizen of Liestal (BL) and Neuhausen am Rheinfall (SH)

accepted on the recommendation of

Prof. Dr.-Ing. Erich J. Windhab, examiner

Prof. Yasushi Takeda, co-examiner

Dr. Shaik A. K. Jeelani, co-examiner

2007

Copyright © 2007 Beat H. Birkhofer  
Laboratory of Food Process Engineering (ETH Zurich)  
All rights reserved.

## Ultrasonic In-Line Characterization of Suspensions

ISBN: 978-3-905609-34-7

Food Process Engineering series no. 30

*Published and distributed by:*

Laboratory of Food Process Engineering  
Institute of Food Science and Nutrition  
Swiss Federal Institute of Technology (ETH) Zurich  
ETH Zentrum, LFO  
8092 Zurich  
Switzerland  
<http://www.ilw.agrl.ethz.ch/vt/>

*Printed in Switzerland by:*

ETH Reprozentrale Höggerberg  
HIL C45  
8093 Zurich  
Switzerland





# Acknowledgements

This research work was carried out at the Food Process Engineering (FPE) Laboratory of the Swiss Federal Institute of Technology Zurich between July 2003 and June 2007. The project (no. 6215.1 KTS) was sponsored by the CTI (Swiss Federal Innovation Promotion Agency) and the two industrial partners Bühler AG (Uzwil) and Met-Flow SA (Lausanne).

I wish to thank Prof. Dr.-Ing. E. J. Windhab for giving me the opportunity to do this thesis in his Laboratory. His visions and ideas contributed to the achievements of this project.

I also would like to thank Prof. Dr. Y. Takeda for this scientific consulting throughout the work and for taking over the co-examination of my thesis and reviewing the manuscript. I will also remember his hospitality in Sapporo during the 4th ISUD.

I would like to express my gratitude to Dr. S. A. K. Jeelani who constantly supported me throughout this research work. His scientific advise was an invaluable contribution to the work. I appreciated to have the opportunity to learn from his scientific methodology. The collaboration was a pleasure for me.

The project would not have been possible without the support from the industrial partners of the CTI project. I thank B. Ouriev, J. Lisner, Y. Zeng, A. Ziegler, P. Braun, M. Höhner, and T. Scheiwiller from Bühler AG for their direct collaboration and encouragement in the project team, setup and maintenance of the cocoa butter shear crystallizer flow loop in Uzwil and their input for the development of the electronics. I am also very grateful to G. Gogniat and O. Mariette from Met-Flow SA for their open ears for our requests. We benefited from the know-how of the ultrasound wizard P. Pinter and the software programmer J. Kroupa. Thanks also to P. Dumas and his team from Imasonic SA for their contributions.

J. Wiklund from SIK Gothenburg was working in parallel on a similar UVP-PD project. I would like to thank him and his supervisor M. Stading for the scientific collaboration and fruitful discussions. I had the pleasure to conduct the model suspension measurements together with Johan at SIK Gothenburg in autumn 2006.

## *Acknowledgements*

---

Many thanks to T. Meile and G. de Cesare from the laboratory of hydraulic constructions at the Swiss federal institute of technology, Lausanne. Tobias spent a day with me in the hydraulics hall where we conducted the open channel flow measurements.

Thanks to my diploma students G. Rivara from the Politecnico di Torino and T. Shafiei for the countless measurements of acoustic suspension properties, the investigation of the rotating cylinder and the flow profile measurements in the beginning of my thesis.

Special thanks go to the skilled technical staff of the FPE Laboratory, namely P. Bigler, J. Corsano, D. Kiechl, B. Koller and B. Pfister for manufacturing the flow adapters and other constructions, the setup of the measurement equipment and the computer support.

J. C. Eischen motivated me to learn in a real programming language (C++) which helped me in many ways for the coding of the software during my doctoral work. I also enjoyed that I was always welcome in his office. I would like to thank P. Fischer for helping me to get my first publication out. His know-how was also invaluable for the organization of the 5th ISUD in 2006.

I really enjoyed the time in the team of Prof. Windhab and I thank all of the members. Special thanks to Beate, Christoph, Hans, Ketan, Matthias, Muriel, Natalie, Phillip, Rok, Silja, Stefan, Verena, Vishwa and Yvonne as they all contributed to the work one or another way.

Thanks to my parents, family members and friends who supported and encouraged me throughout the work.

Last but not least I would like to thank my wife Tina for all her support and proofreading the manuscript.

Zurich, July 2007

Beat H. Birkhofer

# Contents

<b>Acknowledgements</b>	<b>v</b>
<b>Notation</b>	<b>xi</b>
<b>Abstract</b>	<b>xv</b>
<b>Kurzfassung</b>	<b>xvii</b>
<b>1. Introduction</b>	<b>1</b>
1.1. Aims of the work . . . . .	2
<b>2. Ultrasound Doppler velocimetry</b>	<b>5</b>
2.1. Blood flow measurement . . . . .	5
2.2. Influence of the sample volume . . . . .	6
2.3. Test setups . . . . .	9
2.4. Signal processing . . . . .	10
2.4.1. Anti-aliasing . . . . .	11
2.4.2. Spectral broadening and signal to noise ratio . . . . .	11
2.5. Instruments . . . . .	12
<b>3. Particulate Suspensions</b>	<b>15</b>
3.1. Rheology . . . . .	15
3.1.1. Shear thinning . . . . .	16
3.1.2. Aggregation and flocculation . . . . .	17
3.1.3. Creaming or sedimentation . . . . .	18
3.1.4. Particle migration . . . . .	18
3.2. Ultrasound based in-line rheometry . . . . .	20
3.2.1. Existing literature on UVP-PD . . . . .	21
3.2.2. Power law fluid model . . . . .	26
3.2.3. Herschel-Bulkley fluid model . . . . .	26
3.2.4. Gradient method . . . . .	27
3.2.5. Direct ultrasonic measurement of viscoelasticity . . . . .	27
3.2.6. Ultrasonic blood viscosity estimation . . . . .	28
3.3. Acoustic properties . . . . .	28
3.3.1. Propagation . . . . .	29

3.3.2.	Attenuation . . . . .	29
3.3.3.	Sound velocity . . . . .	30
3.3.4.	Scattering . . . . .	31
3.3.4.1.	Thermal scattering . . . . .	31
3.3.4.2.	Visco-inertial scattering . . . . .	31
3.3.4.3.	Scattering in suspensions and emulsions . . . . .	32
3.3.4.4.	Ultrasound spectroscopy . . . . .	32
3.3.4.5.	Backscattering of Ultrasound from blood and tissue . . . . .	33
3.3.4.6.	Backscattering theories . . . . .	34
3.3.4.7.	Backscattering measurement techniques . . . . .	34
3.3.4.8.	Backscattering data analysis . . . . .	35
3.3.4.9.	Spectral analysis of backscattered signal . . . . .	37
3.3.4.10.	Backscattering in hydraulic engineering . . . . .	37
3.3.5.	Fat crystallization and ultrasonic monitoring . . . . .	38
3.3.6.	Application in food systems . . . . .	40
3.3.6.1.	Characterization of edible oils and fats . . . . .	40
3.3.6.2.	Measurement methods . . . . .	42
<b>4.</b>	<b>Materials and Methods</b>	<b>43</b>
4.1.	Suspensions . . . . .	43
4.1.1.	Model suspensions of polyamide particles in rapeseed oil . . . . .	43
4.1.2.	Model suspensions of polyamide particles in water . . . . .	43
4.1.3.	Cocoa butter suspension . . . . .	44
4.1.4.	Chocolate suspension . . . . .	45
4.2.	Analytical techniques . . . . .	45
4.2.1.	Off-line rheometry . . . . .	45
4.2.2.	Nuclear Magnetic Resonance Technique (NMR) . . . . .	46
4.2.3.	Laser Diffraction Particle Size Analyzer . . . . .	46
4.2.4.	Rotating cylinder . . . . .	46
4.3.	Instrumentation . . . . .	48
4.3.1.	UVP . . . . .	48
4.3.2.	Ultrasound Transducer . . . . .	50
4.3.3.	Flow adapters . . . . .	51
4.3.4.	Oscilloscope . . . . .	53
4.3.5.	Pressure sensors . . . . .	54
4.3.6.	Temperature sensors . . . . .	54
4.4.	Data acquisition software . . . . .	54
4.5.	Process flow loops . . . . .	56
4.5.1.	Model suspension . . . . .	56
4.5.2.	Cocoa butter shear crystallization . . . . .	57
4.5.3.	Seeded chocolate suspension . . . . .	58



<b>5. Results and Discussion</b>	<b>59</b>
5.1. Model suspensions . . . . .	59
5.1.1. Polyamide particle size distribution . . . . .	59
5.1.2. Velocity of sound . . . . .	61
5.1.3. Influence of particle migration . . . . .	62
5.1.4. Off-line rheometry . . . . .	64
5.1.5. Velocity profiles and in-line rheometry . . . . .	66
5.1.6. Comparison between in-line and off-line rheometry . . . . .	72
5.2. Cocoa butter crystallization . . . . .	74
5.2.1. Crystal concentration and sound velocity . . . . .	74
5.2.2. Crystallization process . . . . .	77
5.2.3. Measured parameters . . . . .	77
5.2.4. Temporal evolution of velocity profiles . . . . .	80
5.2.5. Ultrasound scatterers in the cocoa butter . . . . .	81
5.2.5.1. Shear crystallizer start . . . . .	81
5.2.5.2. Echo development during crystallization . . . . .	81
5.2.6. Rheological parameters . . . . .	86
5.2.7. Limitations of the current ultrasound transducers and adapter . . . . .	88
5.3. Seeded chocolate suspension . . . . .	89
5.3.1. Attenuation of transmitted pulse signal . . . . .	89
5.3.2. Number of cycles per pulse . . . . .	92
5.3.2.1. Baseband signal amplitude . . . . .	92
5.3.2.2. Velocity profiles . . . . .	92
5.3.3. Frequency . . . . .	93
5.3.4. Comparison of TN and TX transducers . . . . .	97
5.3.5. Influence of cocoa butter seeding on sound velocity . . . . .	99
5.4. Open channel flow with hydrogen bubbles . . . . .	99
5.4.1. Flow profiles and baseband signal . . . . .	99
5.4.2. Concentration of gas bubbles . . . . .	104
5.5. Rotating cylinder evaluation . . . . .	105
5.5.1. Polyamide reflector particles . . . . .	105
5.5.2. Velocity development . . . . .	106
5.5.3. Reference measurement . . . . .	106
5.5.4. UVP parameters . . . . .	107
5.5.4.1. Number of repetitions . . . . .	107
5.5.4.2. Number of cycles . . . . .	108
5.5.4.3. Rotation speed of cylinder . . . . .	108
5.5.4.4. FFT based measurement . . . . .	108
<b>6. Conclusions</b>	<b>111</b>

<b>Appendix</b>	<b>113</b>
<b>A. Near field pressure field</b>	<b>115</b>
<b>Bibliography</b>	<b>117</b>
<b>List of Figures</b>	<b>141</b>
<b>List of Tables</b>	<b>145</b>
<b>Curriculum Vitae</b>	<b>147</b>

# Notation

## Latin Letters

Symbol	Unit	Definition
$a$	m	particle radius
$B$	Pa	bulk modulus of elasticity
$c$	m/s	sound velocity
$d$	mm	channel (gate) distance
$D$	-	dilation
$E$	Pa	complex elastic modulus
$f$	Hz	frequency
$g$	m/s <sup>2</sup>	gravitational constant
$I$	-	intensity distribution
$k$	1/m	wave vector
$k_B$	-	Boltzmann's constant, $1.380 \times 10^{-23}$ J/K
$K$	Pa·s <sup>n</sup>	power law consistency index
$L$	m	length
$n$	-	power law exponent
$N$	-	number
$Q$	ℓ/min	volume flow rate
$P$	Pa	pressure
$r$	m	radius respectively radial position
$R$	m	pipe radius
$R_*$	m	Radius of plug
$R^2$	-	Coefficient of determination
$s$	-	condensation
$t$	s	time
$T$	°C	temperature
$v$	m/s	flow velocity
$V$	m <sup>3</sup>	volume
$X$	m	distance
$z$	m	distance or length

## Greek Letters

Symbol	Unit	Definition
$\alpha$	–	attenuation coefficient
$\beta$	–	backscattering coefficient
$\delta$	–	degree of orientation
$\dot{\gamma}$	1/s	shear rate
$\delta$	–	degree of orientation
$\eta$	Pa s	viscosity
$\eta_r$	–	$\eta/\eta_s$ , relative viscosity
$\kappa$	1/Pa	compressibility
$\lambda$	m	wavelength
$\xi$	–	ultrasound signal amplitude
$\pi$	–	Pi-number
$\rho$	kg/m <sup>3</sup>	density
$\sigma$	Pa	shear stress
$\tau$	Pa	shear stress
$\tau$	s	duration
$\tau_0$	Pa	Yield stress
$\phi$	–	volume fraction
$\phi_m$	–	maximum-packing volume fraction
$\Phi$	–	volume fraction
$\Psi$	–	angle distribution factor
$\omega$	1/s	angular velocity

## Subscripts

Symbol	Definition
c	compression wave
D	diffusion
eff	effective
<i>i</i>	counter
l	liquid phase
max	maximum

continued on next page

---

---

Symbol (cont.)	Definition (cont.)
n	normal
p	profile
p	particle
pr	pulse repetition
r	repetition
s	suspending fluid
s	solid phase
S	Stokes
S	Surface
t	true
y	yield

---

## Dimensionless Numbers

---

Symbol	Definition
$Pe$	Péclet number
$Re$	Reynolds number

---

## Abbreviations

---

Abbrev.	Definition
ADC	Analog to Digital Converter
API	Application Programming Interface
ARMA	Autoregressive Moving Average
BSC	BackScattering Coefficient
BPM	Beats Per Minute
CFD	Computational Fluid Dynamics
DC	Direct Current
DSC	Differential Scanning Calorimetry
DSP	Digital Signal Processor
DMEA	Demodulated Echo Amplitude

---

continued on next page

---

## Notation

---

Abbrev. (cont.)	Definition (cont.)
ECAH	Epstein, Carhart, Allegra and Hawley
EPFL	Ecole Polytechnique Fédérale, Lausanne (Switzerland)
ERT	Electrical Resistance Tomography
ETH	Swiss Federeal Institute of Technology
F	Focal Point
FF	Far Field
FFT	Fast Fourier Transformation
FPGA	Field-Programmable Gate Array
gr	gradient
GUI	Graphical User Interface
HB	Herschel-Bulkley
LDA	Laser Doppler Anemometry
MIT	Massachusetts Institute of Technology
MRI	Magnetic Resonance Imaging
MUSIC	MULTiple SIGNAL Classification
NMR	Nuclear Magnetic Resonance
NF	Near Field
OLR	Off-Line Rheometer
PC	Personal Computer
PCI	Peripheral Component Interconnect
PD	Pressure Difference
PEHD	High Density Polyethylene
PET	Polyethylene Terephthalate
PIDS	Polarization Intensity Differential Scattering
PEEK	Polyetheretherketone
PEG	Polyethylene Glycol
PID	Proportional Integral Derivative controller
pl	power law
PMMA	Polymethyl Methacrylate
ppm	parts per million
PRF	Pulse Repetition Frequency
PVC	Polyvinyl Chloride
RF	Radio Frequency
RMS	Root Mean Square
SIK	Swedish Institute for Food and Biotechnology
SDS	Sodium Dodecyl Sulfate
SFC	Solid Fat Content
SNR	Signal to Noise Ratio
Td	Transducer
UVP	Ultrasound Velocity Profiler

---

# Abstract

The simultaneous in-line measurement of ultrasonic Doppler based velocity profiles (UVP) and pressure drop (PD) over a pipe section during the laminar flow of Newtonian or non-Newtonian fluids enables determination of rheological properties such as shear stress, shear rate and hence shear rate dependent viscosity. This involves the application of an appropriate rheological model such as power law or the direct determination of the shear rate from the velocity gradient. The method can, in principle, be used for particulate or fiber suspensions or droplet emulsions or colloidal solutions. The concentration of dispersed phase can be determined from the measured sound velocity.

Although the UVP-PD technique for in-line rheometry was investigated for the first time over a decade ago, there exists little literature on the systematic investigation of the effect of various parameters of model suspensions (e.g. particle size distribution and concentration) on the in-line rheology and comparison with those results obtained using off-line rheometers. In addition, the verification of the applicability of this in-line method is essential for industry as the suspensions encountered are not only opaque but could also be highly attenuating due to high particulate concentrations. Consequently, the present work investigates model and industrial suspensions.

The rheology of model suspensions of polyamide particles of two size distributions (mean diameters of 11  $\mu\text{m}$  and 90  $\mu\text{m}$ ) and different concentrations (up to 25% by volume) in rapeseed oil was investigated during the steady state fully developed flow through a pipe using the in-line UVP-PD method. The results were compared with those measured with an off-line stress controlled rheometer. The shear rate dependent viscosities obtained with velocity gradient method agreed reasonably well with those measured using off-line rheometer. This implies that this method is less influenced by the convolution of velocity profile with the sample volume as the most affected pipe wall region is not considered. The suspensions were shear thinning as indicated by the decrease in the viscosity with the shear rate for both the size distributions. The viscosity increased with increase in concentration of particles but decreased with increase in diameter of particles. The velocity of sound was found to increase with particle concentration and to decrease with particle size.

The temporal variation in rheological properties and velocity of sound of cocoa butter crystal suspension due to a step change in process parameters of shear crystallizer was continuously monitored using the UVP-PD technique. The suspension was found to be shear thinning and the viscosity increased with the concentration of crystals. The latter (determined by nuclear magnetic resonance, NMR) resulted in higher velocity of sound.

The method of spectral analysis of the baseband signal for the computation of the velocity profiles was adopted to acquire quantitative quality information such as signal amplitude and signal to noise ratio. This enabled the detection of most of the sources of errors associated with the inconsistencies in the velocity profiles. The method was integrated as part of the software interfacing the UVP device and hardware acquiring the data of pressure difference, velocity of sound and temperature. It also allows for the rheometric calculations using different approaches and a versatile data visualization.

The experimental investigations of reference rotating cylinder containing dilute aqueous suspensions of reflector particles enabled the determination of the accuracy of measurement of flow velocities using UVP. The minimum concentration of ultrasound tracer reflectors necessary for measurement of the actual velocity profile was obtained using electrolysis to generate gas bubbles in open channel flow.

Investigations showed that it was possible to measure the velocity profiles of milk chocolate suspension, which is highly concentrated, flowing through a pipe. However, further refinements of the measurement equipment would improve the quality of the velocity profiles.

The present work on model suspensions reveals that the spatial distribution of the shear rate dependant viscosity in the pipe flow is influenced by the local particle size, shape and concentration, which are governed by local physical mechanisms such as particle migration, creaming or sedimentation, Brownian collisions and aggregation. In addition, the local rheology of cocoa butter crystal suspensions produced under applied shear depend on the kinetics of isothermal or non-isothermal crystallization, the morphology of crystals and their network. Consequently, the application of the in-line UVP-PD technique in combination with simultaneous tomography of velocity of sound and possibly spectroscopy, would enable determination of the local rheology depending on the corresponding microstructure.



# Kurzfassung

Die Doppler Ultraschall basierte Inline-Messung von Geschwindigkeitsprofilen (Ultrasonic Velocity Profiles, UVP) und die gleichzeitige Erfassung der Druckdifferenz (Pressure Difference, PD) über einem Rohrabschnitt in einem laminar fließenden newtonschen oder nicht-newtonschen System ermöglicht die Bestimmung rheologischer Eigenschaften wie zum Beispiel Schubspannung oder Schergeschwindigkeit und der davon abhängigen Viskosität. Das Verfahren beinhaltet die Verwendung eines entsprechenden rheologischen Modells wie beispielsweise Power Law oder die direkte Bestimmung der Schergeschwindigkeit aus dem gemessenen Geschwindigkeitsgradienten. Die Methode kann prinzipiell in partikulären oder fasrigen Suspensionen, Emulsionen und kolloidalen Lösungen verwendet werden. Die Konzentration der dispersen Phase kann über die gemessene Schallgeschwindigkeit bestimmt werden.

Auch wenn die erste Publikation zu UVP-PD Messungen schon über zehn Jahre zurück liegt, gibt es nur eine beschränkte Auswahl an Literatur zu systematischen Untersuchungen des Einflusses von verschiedenen Parametern von Modellsuspensionen (beispielsweise Partikelgrößenverteilung und Konzentration) auf die inline gemessene Rheologie und Vergleiche mit den offline, mittels Rheometer, gemessenen Eigenschaften. Gleichzeitig ist die Überprüfung der Anwendbarkeit der UVP-PD Methode für die industrielle Anwendung wichtig, weil die dort zu verarbeitenden Suspensionen oft opak sind und aufgrund der hohen Partikelkonzentration den Ultraschall stark abdämpfen. Daher wurden in der vorliegenden Arbeit sowohl Modellsuspensionen als auch für die Lebensmittelindustrie relevante Systeme untersucht.

Für die Geschwindigkeitsprofil-Messungen in einer voll entwickelten, stationären Rohrströmung wurden aus Polyamid-Partikeln und Rapsöl bestehende Modellsuspensionen verwendet. Dabei wurden zwei verschiedene Partikelgrößenverteilungen (um 11 und 90  $\mu\text{m}$  Durchmesser) sowie Partikelkonzentrationen bis zu 25 % verwendet. Die Inline-Messungen wurden mit denjenigen von einem offline Rheometer (spannungsgesteuert) verglichen. Die mit der Gradienten-Methode erhaltene Viskosität als Funktion der Schergeschwindigkeit wies dabei eine relativ gute Übereinstimmungen mit den offline gemessenen Werten auf. Das impliziert, dass diese Methode weniger von der Faltung von Geschwindigkeitsprofil und Probe-Volumen betroffen ist, weil die am meisten verzerrte Region in der Nähe der Rohrwand

nicht für die rheologischen Berechnungen berücksichtigt wird. Für beide Gröszenverteilungen waren die Suspensionen strukturviskos. Die Viskosität nahm mit zunehmender Partikel-Konzentration zu, aber mit zunehmender Partikel-Grösse wiederum ab.

In einem Scherkristallisationsprozess für Kakaobutter wurde die zeitabhängige Variation der rheologischen Eigenschaften und der Schallgeschwindigkeit als Folge der Änderung von Prozessparametern mit Ultraschall überwacht. Die Kristall-Suspension erwies sich dabei als strukturviskos, die Viskosität stieg mit der Kristallkonzentration. Letzteres resultierte auch in einer Erhöhung der Schallgeschwindigkeit.

Die Spektralanalyse des Basisband Signals für die Berechnung der Geschwindigkeitsprofile diente gleichzeitig dazu die Signalqualität über Störabstand und Signalstärke zu quantifizieren. Die Verfügbarkeit der Spektren ermöglichte die einfache Erkennung der meisten Ursachen für Störungen im Fliessprofil. Die spektrale Signalverarbeitung war integraler Bestandteil der während der Arbeit entwickelten Software die für die Datenerfassung vom UVP sowie von der Hardware für Druckdifferenz, Temperatur und Schallgeschwindigkeit verwendet wurde. Diese Software beinhaltet auch die rheologischen Berechnungen unter der Verwendung verschiedener Ansätze und eine vielseitige Datenvisualisierung.

Ein mit einer niedrig konzentrierten Suspension gefüllter rotierender Zylinder wurde für die experimentelle Bestimmung der Präzision der UVP Messung verwendet. Die minimale Konzentration an Ultraschall-Reflektoren die für eine korrekte Fliessgeschwindigkeitsmessung notwendig ist, wurde in einem offenen Kanal mit Hilfe von durch Elektrolyse erzeugten Gasblasen untersucht.

Weitere Untersuchungen zeigten, dass es selbst in hochkonzentrierten Suspensionen wie Milkschokolade möglich ist, Geschwindigkeitsprofile der Rohrströmung zu messen. Allerdings sind weitere Verbesserungen an der Messeinrichtung nötig, um die Qualität der Fliessprofile zu verbessern.

Die vorliegende Arbeit über die Modellsuspensionen zeigt, dass die räumliche Verteilung der scherratenabhängigen Viskosität in der Rohrströmung von der örtlichen Verteilung von Partikelgrösse, -form und -konzentration abhängt, welche wiederum über lokale physikalische Mechanismen wie beispielsweise Partikel-Migration, Aufrahmen, Sedimentation, brownsche Kollisionen und Aggregation bestimmt werden. Die lokale Rheologie von unter Scherung produzierter Kakaobutter Kristallsuspension hängt von der Kinetik der isothermalen oder anisothermischen Kristallisation, der Morphologie der Kristalle und deren Netzwerk ab. Folglich würde die Kombination von UVP-PD mit einer Tomographie der Schallgeschwindigkeit und eventuell Spektroskopie eine lokale Bestimmung der Rheologie in Abhängigkeit der entsprechenden Mikrostruktur ermöglichen.

# 1. Introduction

Food, plastic, paint, pharmaceutical, cosmetic, paper-pulp, ceramic, metal, crude oil, and chemical industries encounter concentrated suspensions (or emulsions), which are non-transparent complex multiphase systems of particles (or drops) dispersed in a continuous phase containing emulsifiers and polymers. The macroscopic quality of these products depends on their microstructure, and concentration and physico-chemical nature of the constituents. The microstructure includes the particle and agglomerate size and shape distributions, their spatial orientation, interaction between particles, emulsifiers, polymers and continuous phase, and formation of three-dimensional networks. The processing conditions involving different flow fields such as shear and elongation affect the microstructure and hence the rheology (flow behaviour) of such multiphase systems. The various aspects of the interrelationship between the processing conditions, microstructure, rheology and product quality have been extensively investigated by Windhab and his co-workers for different industrial processes involving food and other multiphase systems (Birkhofer *et al.*, 2005; Windhab *et al.*, 2005; Müller-Fischer and Windhab, 2005).

The product quality is usually controlled based on the rheological information such as the shear rate dependent viscosity obtained using conventional commercial Off-Line Rheometers (OLR) as there exists no in-line rheometer for opaque suspensions. This method is not reliable, since the flow field in OLR can be significantly different to that in the actual flow process. In addition, OLR cannot be used for in-line purpose because of the lack of suitability of their geometry and invasive nature. Furthermore, OLR are sometimes difficult to use for suspensions with extreme rheological properties. The use of optical methods for flow visualisation and in-line rheometry is limited since most of the industrial suspensions are not transparent.

The pulsed Doppler ultrasound velocity measurement technique was developed from the 1970ies onwards (Baker, 1970) for blood flow measurements. Pipe flows measurements outside the medical field were reported by Fowles (1973), Kowalewski (1980) and Takeda (1986). A method for in-line rheometry involving the measurement of Ultrasonic Velocity Profiles (UVP) and Pressure Difference (PD) in a pipe section was developed and tested at our laboratory and other research groups for laminar flow of a wide variety of suspensions. For some systems

results from the in-line UVP-PD measurements were compared with OLR (Müller *et al.*, 1997; Wunderlich and Brunn, 1999; Ouriev, 2000; Ouriev and Windhab, 2002; Brunn *et al.*, 2004; Wiklund *et al.*, 2002; Dogan *et al.*, 2005a; Choi *et al.*, 2006; Pfund *et al.*, 2006; Wiklund, 2007). Our laboratory used the UVP-PD technique for measurements of model and industrial suspension systems such as corn starch in silicon oil and glucose syrup; chocolate, and aqueous suspensions of surfactants and cellulose fibers.

However, there are limited publications on the systematic investigation of the effect of size distribution and concentration of particles on the rheological properties of suspensions measured using both in-line UVP-PD and off-line rheometers. The investigations of the in-line concentration dependent acoustic properties such as sound velocity are also limited (Birkhofer *et al.*, 2004; Choi *et al.*, 2006; Wiklund, 2007).

Currently the applicability of the in-line UVP-PD technique has to be tested for specific individual food process applications as for food materials there is virtually no information available on acoustic properties such as attenuation and echogenicity. The latter affect the quality or even the feasibility of the flow profile measurement in such highly concentrated systems as chocolate with a solid content up to 60%.

The time domain analysis of the Doppler signal is constrained in the sense that it does not provide an information on the signal to noise ratio (SNR) and the signal amplitude and hence quality of the measured flow velocity is not known. In contrast, the spectral analysis of the Doppler signal results in the distribution of the flow velocity instead of a single value at a given measurement position.

In addition, none of the UVP-PD publications seem to have considered the influence of inherent distortions of the pipe flow velocity profiles due to the finite sampling volume and other factors (which are well known in the medical field) or the effect of spatial resolution on the rheological calculations using fluid models (power law, Herschel-Bulkley, etc.).

### 1.1. Aims of the work

The following were the objectives:

1. Integration of the measurement of the ultrasound Doppler based velocity profiles (UVP), the pressure drop (PD) and the acoustic properties into one single software application, which also allows for the preconditioning and spectral analysis of the Doppler shift signal, and calculates the rheological parameters from the acquired data.

2. Evaluate the UVP-PD technique for in-line rheological characterization of model suspensions of particles dispersed in oil with simultaneous measurement of the sound velocity. Investigate the effect of concentration and particle unimodal and bimodal size distributions on the in-line shear rate dependent viscosity of suspensions. Compare these results with those measured using an off-line rheometer.
3. Monitor the temporal variation in rheological properties of cocoa butter crystal suspension produced in a shear crystallization process due to a step change in process parameters using the in-line UVP-PD technique. Investigate the dynamic acoustic properties of cocoa butter crystal suspension to determine the time dependent solid fat content.
4. Investigate the applicability of the in-line UVP-PD technique for highly concentrated and attenuating suspension systems such as milk chocolate seeded with a small percentage of precrystallized cocoa butter.
5. Check the accuracy and precision of velocities measured using UVP technique by determining the velocity of a dilute suspension of particles rotating as a rigid body in a cylinder for different ultrasound parameters.
6. Examine the effect of concentration of ultrasound reflectors in open channel flow relevant to suspension flows in food process engineering and other applications such as hydraulic engineering.



## 2. Ultrasound Doppler velocimetry

Historically the development of the Doppler velocimetry started in the medical field in the 1950s (Satomura, 1957) with continuous wave devices, the first pulsed range gate systems being introduced at the beginning of the 1970s (Wells, 1969; Baker, 1970; Peronneau, 1992). Outside the medical field the UVP was applied to measurements of liquid metal flow by Fowles (1973) using continuous wave ultrasound, while Pinkel (1979) utilized pulsed ultrasound at low frequencies to measure ocean currents. Kowalewski (1980) used pulsed ultrasound for pipe flow measurements of suspensions and Garbini *et al.* (1982a,b) characterized turbulence using the spectral broadening of the echo signal. Takeda (1986) investigated pipe and Taylor vortex flows. He also applied the UVP technique for flow mapping in mercury (Takeda, 1987).

A short and good overview of the UVP method including the signal processing for the Doppler shift frequency estimation and application was given by Lemmin and Rolland (1997). An extensive coverage of Doppler ultrasound can be found in three textbooks (Jensen, 1996; Evans and McDicken, 2000; Hill, 2004) from the medical field which describe many aspects also relevant for engineering applications of ultrasonic measurements.

### 2.1. Blood flow measurement

With the availability of commercial UVP devices which feature user friendly software for the monitoring, it is relatively simple to make velocity profile measurements. But to be able to interpret the results acquired under non optimal conditions (e. g. in highly attenuating fluid) or to obtain the best possible accuracy and precision an understanding of the physics of ultrasound and the signal processing are beneficial. This also implies that it is advantageous to have access to the RF signal<sup>1</sup> and the baseband signal<sup>2</sup> as well as to know the characteristics of

---

<sup>1</sup>In ultrasonics the RF (Radio Frequency) signal is usually refers to the received signal which has a frequency close to the emission frequency, thus in our case 2, 4 or 8 MHz.

<sup>2</sup>The baseband signal denotes the Doppler shift frequency as it is obtained from demodulating and filtering the RF signal which is distributed around zero. Sometimes also the term “demodulated echo amplitude” (DMEA) is used.

the transducers and the analog electronics. The application of ultrasound Doppler techniques in fluid dynamics or generally engineering is a relatively new field. In contrast, the researchers in the medical field spent more than the last 40 decades to develop and improve every single aspect of ultrasonic measurements from the transducer design over the knowledge of the pressure field and the interaction of the ultrasound with the scatterers to the the analog and digital signal processing. While the instruments used for engineering applications were derived from medical devices it seems that only few groups applying the UVP technology were aware of the relevance of some of the findings made in the medical research. Blood is also a highly concentrated suspension and the aim of the medical research is also to measure the flow profiles with the best possible temporal and spatial resolution. Compared to the measurements in a conventional laminar pipe flow the challenges for measurements in the human body are (i) the penetration of the attenuating tissue, (ii) the movement of the vessel wall due to (iii) pulsation of the flow (iv) complicated vessel geometry (compared to a straight pipe) such as the arch of the aorta, (v) the not very well defined Doppler angle and (vi) data visualization for the medical personnel who does not necessarily have a high level of expertise in ultrasound.

In the following an overview on the literature on Doppler ultrasound of relevance for engineering applications is given. References to articles dealing with backscattering from blood and tissue are given in section 3.3.4.

### 2.2. Influence of the sample volume

Two interesting papers from the research group of Jorgensen (Jorgensen *et al.*, 1973; Jorgensen and Garbini, 1974) investigated the influence of the measurement sample volume (which depends on the pulse length and beam diameter) on the measured velocity profile for large ratios ( $> 0.1$ ) of pulse length to pipe diameter. An example of the approximate shape of the ultrasonic pulse which partly depends on the transducer characteristics is given in figure 2.1 on the left. For a short pulse the intensity increases exponentially until the end of the electrical pulse and in the following ringing phase (gradual decay of the stored energy) the intensity decays also exponentially. This results in a drop like shaped measurement volume (fig. 2.1, on the right). In addition, there is also the pressure distribution (assumed to be parabolic) in the lateral plane of the sampling volume. So the distortion of the Doppler profile is caused by the averaging which takes place over the sample volume with the described shape. Hence the resulting velocity for one channel is proportional to the average velocities within the sample volume weighted by the



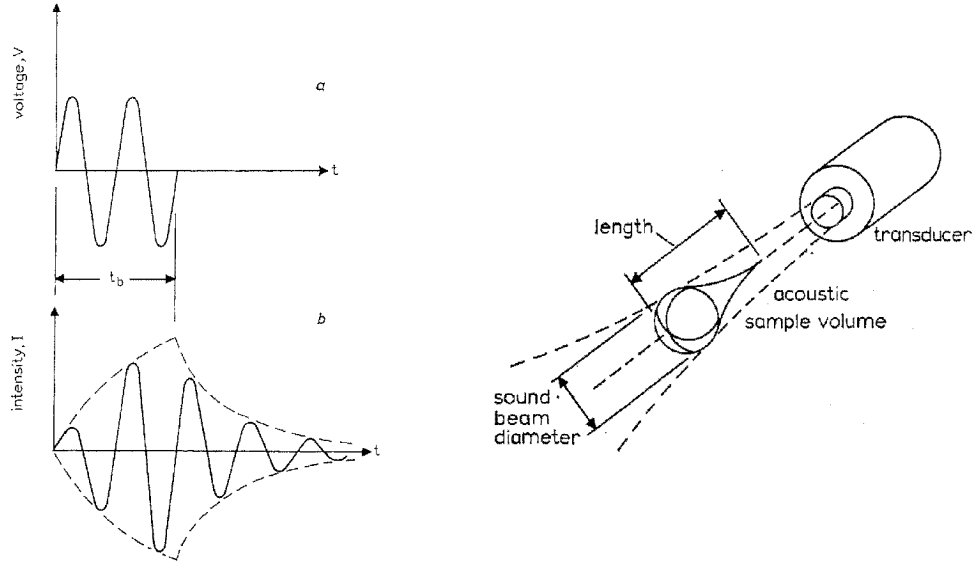


**Figure 2.1.:** On the left side: piezocrystal transducer response: (a) driving burst, (b) acoustic burst. On the right side: Schematic of the sample volume geometry. (Both figures reproduced from Jorgensen *et al.* (1973) with permission from Springer.)

associated intensity distribution, thus

$$v(r) = \frac{\int_0^r \int_{y_1}^{y_2} \int_{z_1}^{z_2} v_t(x, y, z) I(r - x, y, z) dx dy dz}{\int_{x_1}^{x_2} \int_{y_1}^{y_2} \int_{z_1}^{z_2} I(x, y, z) dx dy dz} \quad (2.1)$$

with the velocity along the path of propagation  $v(r)$ , the true velocity distribution  $v_t$ , the intensity distribution of the sample volume  $I$ , and the geometric limits and position of the sample volume  $x_1, x_2, y_1, y_2, z_1, z_2$ .

The true profile can then be calculated applying the convolution theorem, which states that the Fourier transform of the convolution (\*) of two functions is equal to the product of the two Fourier transforms ( $\mathcal{F}(f_1(t) * f_2(t)) = F_1(\omega)F_2(\omega)$  where  $\mathcal{F}$ : Fourier transform and  $F_1(\omega)$  and  $F_2(\omega)$  are the Fourier transforms of  $f_1(t)$  and  $f_2(t)$  respectively). Thus after a few more transformations we get

$$v_t(r, x, t) = \mathcal{F}^{-1} \left( \frac{\mathcal{F}(v_w(x, y, z))}{\mathcal{F}(I(x, y, z))} \right) \quad (2.2)$$

with  $v_w$  being the product of the one-dimensional function of the true velocity profile  $v_t$  and the volume integral of that portion of the sample volume within the flow field.

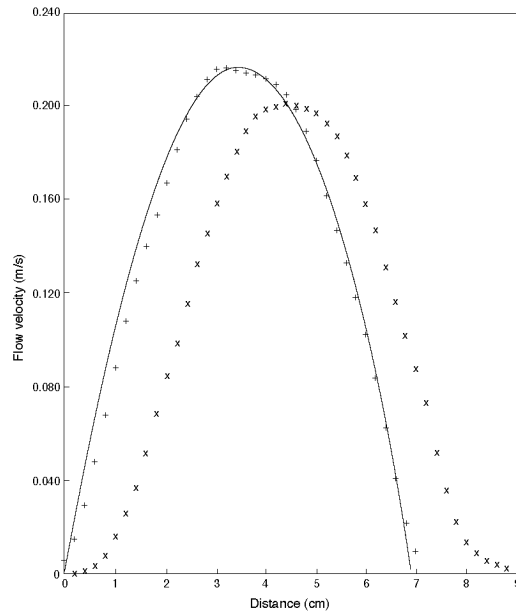


**Figure 2.2.:** Deconvolution of a fully-developed laminar flow (results of Jorgensen and Garbini (1974)). x: Doppler image profile, +: deconvolved profile, full line: theoretical prediction

This could also be simplified from the three dimensional case to a one dimensional problem (Jorgensen and Garbini, 1974). An example of the application of the deconvolution is shown in figure 2.2.

A slightly modified version of this deconvolution was applied in Hughes and How (1993) for the estimation of wall shear rates in steady laminar flow and later in Hughes and How (1994) for pulsating flow. Flaud *et al.* (1997) also dealt with the convolution of the flow profile and measurement volume by proposing a method to calculate the sample volume from the assumed real profile and the measured profile (also by deconvolution). The influence of frequency dependent attenuation on the pulse shape was investigated by Fish and Cope (1991), where only simulated spectra were shown. They concluded that the effect could be significant for short pulses, where the attenuation of the high frequency part of the broadband signal increases the pulse length. The deconvolution was also used to improve the resolution of medical B-scan images (e. g. Jensen *et al.* (1993)), as in tissues there is also the problem of attenuation which deforms the pulse shape. There exists also an alternative approach to the deconvolution, which assumes the sampling volume to be cylindrical with the pulse length and beam diameter as dimensions (Wunderlich and Brunn, 1999; Nowak, 2002; Kikura *et al.*, 2004). However, this may be valid only for large pipe diameters or long pulses.

The deconvolution correction was not applied to the velocity profile measurements in the present work as no experimental installation for the measurement of the sample volume was set up. However, as the maximum pulse length to pipe diameter ratio used was less than 0.1 (4 cycle pulse in a 16mm diameter pipe), the deconvoluted velocity profile (figure 2.2) is shown to be similar (in terms of the shape and the velocity gradients) to the true velocity profile over most of the pipe radius excepting that close to the pipe wall. Consequently, the central region of radial velocity profile was used for calculation of rheological properties based on velocity gradient method. Nevertheless it will be important to investigate the shape of the sample volume in attenuating suspensions to allow the corresponding deconvolution of the velocity profile. The size of the sample volume is expected to be dependent on the measurement depth.

## 2.3. Test setups

The size of the sample volume can be investigated with a setup like the moving string test target used by Walker *et al.* (1982) or a single vibrating point as used by Hoeks *et al.* (1984), both being easier to implement than the original jet stream (Baker and Yates, 1973). Thijssen *et al.* (2002, 2007) described the objective performance testing of medical ultrasound equipment using various setups. The first paper described (besides tests of the imaging capabilities) the testing of Doppler flow metering with a 1 mm diameter rubber string, which could be seamlessly glued to make a ring, thus avoiding the problem of the knot that disturbs the measurement when using a silk string. A comparison of the different string materials (Nitrile O-ring, nylon and silks) is made by Hoskins (1994a,b), who also found the O-ring to be the most suitable material.

Once the sample volume is measured, it would be interesting to verify its functioning in a flow testing rig as reviewed by Law *et al.* (1989), who described the various setups and scattering systems published in the literature. Arnolds *et al.* (1989) considered the influence of gain settings on the measurement volume. Meagher *et al.* (2006) discussed the importance of the influence of acoustic properties of the wall material of pipe which the ultrasound beam and the backscattered echo have to cross. One can use very thin tubes such as cellulose dialysis tubes or heat-shrink sleeving (McDicken, 1986), which minimize the influence on the pressure field. But with such a duct material is not guaranteed that the tube is perfectly round. In contrast, tubes made of polyethylene, acrylic or pyrex glass have the advantage of a well defined round shape but the disadvantage of an impedance difference resulting in reflections at the interfaces. Teirlinck *et al.* (1998) described an effort to create an European norm for flow test objects. They proposed a measurement section made from tissue, blood and vessel mimicking materials with

similar acoustic impedances, the vessel mimicking tube was made from c-flex, a silicon copolymer with a velocity of sound of 1557 m/s. There were also descriptions (Rickey *et al.*, 1995) of wall-less vessel phantoms for testing purposes. The agar based tissue mimic was filled into the phantom box in liquid state and a thin metal rod (6.3mm diameter) was placed in the position of the vessel. After the tissue mimic hardened, the rod could be pulled out leaving the wall-less vessel.

### 2.4. Signal processing

There are many publications on the different algorithms for the velocity estimation. The first instruments used a fully analog signal processing with zero crossing counters for the frequency estimation of the baseband signal. Later the baseband signal was digitized which opened new possibilities. The algorithms for the frequency estimation from the baseband signal can be divided into spectral (FFT) and time domain algorithms. The time domain algorithms can be separated into (i) phase-shift estimators that use autocorrelation of the baseband signal to track the phase change at one measurement gate and (ii) time shift estimators that use frequently cross-correlation of the RF signal to track the movement of a scatterer from intensity of their echo (York and Kim, 1999).

Besides the textbooks on medical ultrasound referred in the introduction of this chapter on page 5, Lhermitte and Serafin (1984); Lhermitte and Lemmin (1994) gave a good introduction to the signal processing as they dealt with both theoretical and applied aspects of time domain and FFT based signal analysis while Jensen (2000) concentrated more on the theoretical aspects and Fish *et al.* (1997) describes only the spectral approach. Vaitkus and Cobbold (1988); Vaitkus *et al.* (1988) compared several different algorithms (FFT, autoregression, autoregression with moving average and maximum likelihood with subtypes) for continuous wave ultrasound. Markou and Ku (1991) also compared four different algorithms (zero crossing detector, FFT, autoregressive and minimum variance) for measurements of a pipe flow of an aqueous glycerin solution for Reynolds numbers between 500 and 8000. Under the ideal experimental conditions (good SNR) all algorithms performed similarly, the deviations were found to be the highest close to the pipe wall. Hein and O'Brien (1993) reviewed the time domain methods. Marasek and Nowicki (1994) compared three spectral techniques (FFT, autoregressive Burg and autoregressive moving average (ARMA)) and also three methods to extract the maximum frequency from the spectra. Guidi *et al.* (2000) compared FFT with the Burg algorithm (an autoregressive method) concluding that the availability of both algorithms (FFT for the analysis, Burg for the peak frequency respectively flow velocity) would be ideal.

One class of publications explores the possibilities of getting a higher spatial resolution from an interpretation of the RF signal partly using 2D-FFT: Newhouse and Amir (1983) (single particle tracking), Liu *et al.* (1991) (modified autocorrelation of the RF signal, comparison with autocorrelation, RF cross correlation and maximum entropy method), Loupas *et al.* (1995a,b) (2D autocorrelator, combining analysis of Doppler and RF signal), Allam and Greenleaf (1996); Allam *et al.* (1996) (direction of arrival) and Vaitkus and Cobbold (1998); Vaitkus *et al.* (1998) (using the root-MUSIC time-domain algorithm which was described by Barabell (1983)).

The most recent development for increasing the spatial resolution of Doppler ultrasound and thus to circumvent the distortion from the convolution with the sample volume is the use of coded (frequency or phase modulated) pulse excitation (Tsou *et al.*, 2006) which requires a relatively sophisticated processing of the RF signal.

### 2.4.1. Anti-aliasing

The so called aliasing occurs if the pulse repetition frequency is below the Nyquist frequency (double to frequency to be measured) for the Doppler shift frequency (respectively the flow velocity). There are different approaches to overcome this problem in order to be able to measure high flow velocities in combination with a low pulse repetition frequency which controls the maximum penetration depth.

Fischer *et al.* (2004) implemented a variation of the pulse repetition frequency as it is also used in radar in overcome the Nyquist limitation. Franca and Lemmin (2006) showed the implementation of a simple dealiasing algorithm capable to correct several degrees of data aliasing using the baseband signal and assuming a coherence between subsequent Doppler estimates. The dealiasing method of Tortoli (1989) used an assumption on the shape of the power spectrum respectively the location of the spectrum centroid.

### 2.4.2. Spectral broadening and signal to noise ratio

There are also many publications dealing with the spectral broadening of the RF signal. In general, the shorter is the pulse, the broader is its frequency distribution. When the pulse travels through an attenuating medium, the high frequency parts of the pulse are most attenuated. However, a subwavelength scatterer reflects rather the high frequency part of the spectrum of the incidence wave, thus acting as a high pass filter (Round and Bates, 1987).

The spectrum of the Doppler signal is also broadened from several sources as listed in the good overview article by Hoeks *et al.* (1991) and subsequently by Guidi *et al.* (1995): Sample volume size, velocity distribution and Doppler angle (the latter is treated in detail in McArdle and Newhouse (1996)). The random fluctuations in the power spectrum is caused by the random distribution of the scatterers (respectively the voxels they form) and thus random summation or cancelation of the phases (Hoskins *et al.*, 1990). One of the latest works on spectral broadening in pulsed wave measurements is from Bastos *et al.* (2000) who reviewed the existing literature on this topic and formulated a closed-form expression for a extended range of beam/flow conditions.

Alam and Parker (2003) wrote an interesting review article on flow imaging and its implementation issues. References for frequency/phase (Doppler), time-domain and multiple-burst (tracking) methods for the Doppler shift detection were given. The bias of the estimated Doppler frequency due to frequency dependent scattering and attenuation and different wall filtering strategies were discussed (details also in Fish and Cope (1991)). Fish (1992) also gave an overview of limitations of pulsed Doppler flow detectors and the spectral estimators. Gill (1985) described the sources of errors in the velocity estimation. Also to mention is an extensive review by Jones (1993) on the topic.

Law *et al.* (1991) investigated the Doppler spectra in terms of maximum, mean and mode frequencies and spectral broadening index as a function of position in the pipe and sample volume in a stationary laminar flow field in a pipe with 9.5 mm radius. The spectral broadening index and other quality indicators showed that the quality of the measurement increases from the wall to the center of the pipe.

Regarding the actual implementation Fischer *et al.* (2006) presented a method for noise reduction in the Doppler signal, further details on the work being given by Fischer (2004).

Another aspect related to attenuation and scattering is the broadening of the pressure field, which was observed for liver and skin tissue by den Aarsen *et al.* (1989). This is also an interesting point regarding the development of the sample volume inside a highly concentrated suspension such as chocolate.

## 2.5. Instruments

There are many descriptions of Doppler ultrasound measurement instruments with a varying degree of given details given in the literature. Following a selection of interesting articles describing single UVP instruments. Brandestini (1978): the

first multigate flow meter with digital zero crossing counter; Tortoli and Andreuccetti (1988): 128 point complex FFT calculated on a DSP; Black and How (1989): base frequency of 20 MHz, comparison of zero crossing detector with FFT and deconvolution of the sample volume; Tortoli *et al.* (1996, 1997): display of 64 point spectra at 64 gates with a rate of up to 50 images per second using a specialized Fourier transform processor; Lombardi *et al.* (2001): using cross correlation; Bambi *et al.* (2003): analog electronics for amplification and quadrature demodulation and DSP on a PCI card. An especially interesting device was presented by Ricci *et al.* (2004, 2006). This flexible system was designed for the development and testing of new algorithms with two channels for transmission and reception, emission frequency between 1 and 16 MHz, maximum 100 Vpp output voltage for low and high impedance elements. The RF signal is sampled at 64 MHz with 14 bit and the gain is programmable between 20 and 60 dB. Arbitrary waveforms can be transmitted and also the time between two pulses can be freely adjusted. There are four demodulators implemented digitally in a FPGA (field-programmable gate array) which can be operated at different frequencies and the consecutive low pass filters is also programmable. The digital signal (RF or baseband) processing is conducted on the mentioned FPGAs and a DSP (digital signal processor) which are all fully programmable. There is 64 MB memory available to buffer the RF or baseband data. The board is connected via an USB 2.0 interface to a computer where the data is visualized.





## 3. Particulate Suspensions

This chapter gives the background on the rheological, ultrasonic and other characteristics of suspensions relevant to the present work entitled “Ultrasonic In-Line Characterization of Suspensions”. In addition, it introduces the concept of UVP-PD, which involves the combination of ultrasonic velocity profiles and pressure drop measurements in pipe flow for the in-line rheological characterization of fluids.

### 3.1. Rheology

Suspensions of solid particles dispersed in a liquid medium are ubiquitous in food pharmaceutical and other industries. In many cases, as for example ketchup, fruit yoghurt or toothpaste, the rheology of the product is an important functional property for the customer satisfaction.

For the characterization of suspensions, including the rheology one can distinguish between colloidal systems with particle sizes between 1 nm and 1  $\mu\text{m}$  and suspensions with a disperse phase of a larger particle size. In colloidal systems, Brownian motion of the particles has to be considered as the surface area to volume ratio is high.

At very low concentrations (volume fraction of disperse phase  $\phi < 0.03$  (Larson, 1999) to  $\phi < 0.1$  (Hiemenz and Rajagopalan, 1997)) where no particle-particle interactions influence the system, the viscosity of a suspension  $\eta$  increases due to particles disturbing the flow streamlines and take up energy for rotation. This can be predicted based on the viscosity of the suspending fluid  $\eta_s$  with the simple formula  $\eta = \eta_s(1 + 2.5\phi)$  proposed by Einstein (1906, 1911). The equation can also be written as relative viscosity:

$$\eta_r = \frac{\eta}{\eta_s} = 1 + 2.5\phi \quad (3.1)$$

Considering two-body interaction, the equation was expanded by Batchelor (1977) for systems with Brownian motion to:

$$\eta_r = 1 + 2.5\phi + 6.2\phi^2 \quad (3.2)$$

For suspensions with a higher concentration, the following empirical equation was proposed by Krieger and Dougherty (1959):

$$\eta = \eta_s \left(1 - \frac{\phi}{\phi_m}\right)^{-[\eta]\phi_m} \quad (3.3)$$

with the maximum-packing volume fraction  $\phi_m$  and  $[\eta]$  as the intrinsic viscosity also described as shape factor (2.5 for spherical particles) given by  $[\eta] = \lim_{\phi \rightarrow 0} \frac{\eta - \eta_s}{\phi \eta_s}$ .

The maximum-packing density  $\phi_m$  depends on size and shape of the particles. If the size distribution of the particles is not monodisperse, the maximum-packing density is increased as the small particles are packed into the interstices between the large ones and thus the viscosity is lowered. In a bidisperse system, the minimum viscosity is reached at a volume fraction of 0.6 of the larger particles, which is known as ‘‘Farris effect’’ (Larson, 1999).

The viscosity becomes sensitive to the shear rate  $\dot{\gamma}$  if the shear rate is high enough to disturb the equilibrium distribution of the interparticle spacings. There are several possible types of behavior for suspensions under shear. Shear thickening can occur in highly concentrated suspensions at particle volume fractions  $\phi \geq 0.4$  under high shear stresses above the range where shear thinning occurs. This is explained with the disruption of the particle alignment, which causes the shear thinning behavior at lower shear rates (Larson, 1999) and the increase of the hydrodynamic stress due the formation of large clusters (Brady, 1996). Viscoelastic properties can be found even in hard-sphere suspensions. The slight elasticity is explained by Brownian motion, which tends to restore to equilibrium the shear-distorted particle configurations. Of course the viscoelasticity is much more important in polymer melts, doughs and similar fluids. Highly concentrated suspensions can also show an apparent yield stress  $\sigma_y$  below which there is no flow as the particles arrange in a network structure. This behavior can be modeled as Bingham plastic ( $\sigma = \sigma_y + \eta_{pl}\dot{\gamma}$  with the ‘‘plastic viscosity’’  $\eta_{pl}$ ) or the Casson equation ( $\sqrt{\sigma} = \sqrt{\sigma_y} + C\sqrt{\dot{\gamma}}$ ). However, the most important effect in the suspensions used in the present work is the shear thinning which is explained in detail in the next section.

#### 3.1.1. Shear thinning

For low shear rates with negligible hydrodynamic forces and structural forces dominating, suspensions exhibit either a Newtonian plateau or a yield value if the particles form a network. If the shear rate (or shear stress) is high enough to disturb the equilibrium distribution of the interparticle spacings, a concentrated

suspension exhibits a shear thinning behavior. This can be described by the dimensionless Péclet number  $Pe$ , which is the ratio of the shear time scale to the time required for diffusion.

$$Pe = \frac{\eta_s \dot{\gamma} a^3}{k_B T} \propto \dot{\gamma} t_D \quad (3.4)$$

where  $\dot{\gamma}$  is the shear rate,  $a$  the particle radius,  $k_B$  the Boltzmann's constant,  $T$  the temperature and  $t_D$  the time for a particle to diffuse a distance equal to its radius  $a$ . If  $Pe > 1$ , the time scale in which the system restores is longer than the time of shear and therefore the structure is changed and shear thinning behavior can be expected. For monodisperse suspensions the particles align threadlike in the direction of the shear field. This is explained with repeated collisions between particles, the repulsion and the subsequent separation of the particles (Phung *et al.*, 1996).

Windhab (2000) explained the non-Newtonian shear thinning effect with hydrodynamic fluid immobilization by the particles. According to that, a particle or agglomerate moves within the flowing continuous fluid phase in such a way (e. g. by rotation) that a certain fluid portion is excluded from contributing to the continuous fluid phase flow. Shear thinning and shear thickening behavior changes, e. g. after a particle size distribution change by milling, are explained with an effective volume fraction  $\phi_{\text{eff}}$  which is the sum of the volumes occupied by the solid particles, fluid directly on their surface, in the volume of porous aggregates and the hydrodynamical induced fluid immobilization. The rheological function is based on Krieger-Dougherty equation:

$$\eta(\phi, \dot{\gamma}, t, \delta) = \eta_F \left[ 1 - \frac{\phi_{\text{eff}}(\phi, \dot{\gamma}, t, \delta)}{\phi_m(\dot{\gamma}, t, \delta)} \right]^{[\eta](\delta)\phi_m(\dot{\gamma}, t, \delta)} \quad (3.5)$$

with  $\delta$  being the degree of orientation in the case non-spherical or non cube-like particle shapes such as rods or disks in a manner that facilitates the flow.

### 3.1.2. Aggregation and flocculation

There are several forces that can lead to particle collisions and subsequently to aggregation, flocculation or clumping which influence the viscosity because of the increase of the size distribution of the disperse phase. There are gravitational collisions and viscous drag due to the continuous phase as hydrodynamic forces. From thermodynamic considerations there are the following possible interactions influencing the aggregation between particles: (i) Brownian collisions (Péclet number), (ii) presence of polymers, surfactant micelles and colloidal particles (depletion aggregation at low concentrations and inhibition due to layered colloidal particle structures at high concentrations), (iii) van der Waals forces of attraction, (iv)

adhesion due to partial coalescence of semi-solid particles and (v) electrostatic repulsion due to surface charge which also causes an augmentation of the intrinsic viscosity of the suspension because of increased energy dissipation in the electrical double layer surrounding the particle. At the same time the systems are highly shear thinning as the charged particles arrange easily in sliding layer structures in non-colloidal suspensions.

There exists numerous literature investigating the effects listed above for dilute suspensions. However, there is no quantitative information on inter-particle collision rates and efficiencies available for concentrated suspensions. The experimental data on concentrated suspensions were summarized by Jeelani *et al.* (2005).

#### 3.1.3. Creaming or sedimentation

The Péclet number  $Pe$  can also be expressed as the ratio of gravitational to Brownian forces:

$$Pe = \frac{a^4 \Delta \rho g}{k_B T} \quad (3.6)$$

with  $\Delta \rho$  as the density difference between particle and liquid medium and  $g$  as the acceleration due to gravity.

If  $Pe$  is larger than unity, particles tend to cream or settle. Jeelani *et al.* (2005) found the following equation of Garside and Al-Dibouni (1977) to predict reasonably well extensive published creaming velocity  $v$  data covering a wide range of radii  $a$  and volume fractions  $\phi$  of mono-disperse particles and physical properties:

$$v = v_S (1 - \phi)^{5.1} \quad (3.7)$$

where

$$v_S = \frac{2 \Delta \rho g a^2}{9 \eta_s} \quad (3.8)$$

is the Stokes creaming or sedimentation velocity of a single particle in a Newtonian liquid of viscosity  $\eta_s$ . Jeelani *et al.* (2005) modeled the creaming velocity of suspensions considering particle aggregation. The results were in good agreement with experimental data.

#### 3.1.4. Particle migration

There are many published articles on measurements and models for the particle migration relative to the streamlines during the flow of suspensions. The particle sizes, geometries (pressure driven channel and pipe flow and Couette flow), flow

rates, and ratio of particle to pipe radii ( $a/R$ ) respectively channel width ( $a/h$ ) are distributed over a wide range. Also different measurement techniques such as microscopy, laser Doppler anemometry (LDA), nuclear magnetic resonance (NMR) are used. An overview of the existing models and measurements can be found in a review article from Lareo *et al.* (1997b).

As a summary one can state that it was shown that the particles migrate and increase their concentration at the central region of the pipe or channel where the velocity gradient is the lowest. For low Reynolds numbers, larger the size ratio  $a/R$  or  $a/h$  for monodisperse particles (Lyon and Leal, 1998a), higher is the tendency of migration towards the central region. The concentration of larger particles in a bidisperse system (Lyon and Leal, 1998b) is higher at the centre of the pipe due to migration and segregation resulting in negligible radial concentration gradient of smaller particles.

The effect of particle migration relative to the flow streamlines was first described in detail in the work of Segré and Silberberg (1963) and subsequently in another important contribution of Ho and Leal (1974). Karnis *et al.* (1966) investigated the pipe flow behavior of spheres, rods and discs of different sizes and concentrations for Couette and Poiseuille flow using tracer particles, microscopy and analog motion picture. Also quite interesting are three articles from Koh *et al.* (1994) and Lyon and Leal (1998a,b) with modeled and experimental data of flow profiles, particle concentration, particle velocity fluctuation and local particle size distributions for mono- and bidisperse systems in channel flow measured with LDA. The experimental data of Lyon and Leal (1998a,b) were compared with the results from a simplified model by Buyevich and Kapbsov (1999). Butler and Bonnecaze (1999); Butler *et al.* (1999) used electrical impedance tomography to measure particle (size 125 to 180  $\mu\text{m}$ ) concentration ( $\phi$  up to 0.4) profiles in pipe (diameter 20.4 mm) flow. Compared to the other known publications on particle migration, that of Butler and Bonnecaze (1999) is an exception as it uses a relatively small  $a/R$  ratio of 0.0064. NMR technique was used by Hampton *et al.* (1997) to measure velocity profiles and concentration in pipe flow with an  $a/R$  ratio of 0.0256 and 0.0625. The same method was used by Norman and Bonnecaze (2005); Norman *et al.* (2005) to measure the migration of buoyant particles in pipe flow. In those measurements the density differences were quite important with densities of 2500 and 725  $\text{kg}/\text{m}^3$  for the disperse phase, and 1080 and 1100  $\text{kg}/\text{m}^3$  for the continuous phase with particle sizes of 30 and 110  $\mu\text{m}$ .

Kowalewski (1980), who was the second author to publish on velocity profile measurements in pipe flow using UVP technique, already mentioned the nonuniform concentration distribution possibly contributing to the “tubular pinch effect” besides the alignment of the particles. Regarding food processing, two articles from Lareo *et al.* (1997a,c) are interesting as they show experimental results from the

pipe flow of carrot cubes and their migration during flow. The latest work on particle migration in pipe flow are from Shapley *et al.* (2004) and Miller and Morris (2006).

The main reason for migration of a spherical particle across a streamline in a prolonged shearing flow is given as a jump in the Bernoulli stress across the particle, which is larger than the Brownian stress. If the ratio

$$\frac{\rho_p \bar{v}^2 a^4}{2Rk_B T} \quad (3.9)$$

(where  $\rho_p$  is the particle density,  $\bar{v} = (2/3)v_{\max}$  is the mean velocity for Poiseuille flow and  $R$  is the pipe radius) is smaller than 0.01 (for Poiseuille flow), the migration can be neglected (Ho and Leal, 1974; Macosko, 1994).

There are phenomenological models (Leighton and Acrivos, 1987; Phillips *et al.*, 1992) based on particle migration, which is driven by gradients in the shear rate. In an alternative group of granular flow-based models (Nott and Brady, 1994), the migration is driven by gradients in “suspension temperature”, defined as the average kinetic energy of particle velocity fluctuation due to interparticle collisions.

## 3.2. Ultrasound based in-line rheometry

The UVP-PD method allows the determination of rheological parameters for the laminar pipe flow of Newtonian and Non-Newtonian liquids or suspensions by combining ultrasonic velocity profile (UVP) and pressure difference (PD) measurements, and use of a rheological flow model. The latter can be e. g. power law ( $\tau = K\dot{\gamma}^n$ ) or Hershel-Bulkley ( $\tau = \tau_0 + K\dot{\gamma}^n$ ). Alternatively, direct calculation of the rheological parameters can also be carried out using the flow velocity profile (gradient method for shear rate) and the pressure drop. If a fluid model is used, the parameters  $K$ ,  $n$  and  $\tau_0$  are obtained by minimizing difference between measured and fitted velocity profiles using non-linear regression. Further details on the technique can be found in the literature referred below, especially Ouriev (2000).

As mentioned in the previous section, the rheology of concentrated suspensions of particles is important to several industrial applications such as food, pharmaceuticals, ceramics, cosmetics, electronic materials and paper. Usually the suspensions encountered in many applications are not only opaque but also involve process conditions like high pressure or high temperature. These complicate the experimental investigation of their rheological behavior using off-line rheometry.

### 3.2.1. Existing literature on UVP-PD

The non-invasive technique of measurement of ultrasound Doppler based velocity profiles (UVP) and pressure drop (PD) has been investigated by many authors for in-line rheological characterization of suspensions of particles or fibers or colloidal polymers dispersed in a continuous phase flowing through pipes. An overview of the investigations on UVP-PD measurements carried out by various research groups is given in the text below and tables 3.1 and 3.2.

**P. Brunn, University Erlangen-Nürnberg, Germany:** The UVP-PD principle was first mentioned by Brunn *et al.* (1993) although no experimental results were presented. Then Müller *et al.* (1997) calculated shear rate dependent viscosities from simultaneous measurements of velocity profiles and pressure drop in a Newtonian glycerin/water solution, a non-Newtonian aqueous polyacrylamide solution, and a non-Newtonian hydroxypropyl guar gum solution. The in-line flow curves were compared with those measured using an off-line rheometer and good agreements were found. Later Wunderlich and Brunn (1999) measured also a polyacrylamide solution and fitted the measured profiles with polynomial, power law and an “Ellis-fluid” functions. Brunn *et al.* (2004) presented results of UVP-PD measurements of a body lotion (concentrated surfactant solution).

**E. Windhab, ETH Zurich:** The UVP-PD technique was first used for a semester work (Cantz, 1994) and a diploma work (Drost, 1995), the latter containing rheological calculations. Results were also presented by Windhab (1994) including power law fits. B. Ouriev published numerous articles from his PhD work (Ouriev, 2000). Ouriev and Windhab (2002) applied power law and Herschel-Bulkley models to a shear thinning suspension of corn starch in silicon oil and a shear thickening suspension of corn starch in glucose syrup. Ouriev (2002) gave details on the wall slip measurements of shear thickening suspension. UVP-PD measurements in chocolate suspension and the influence of seeding with pre-crystallized cocoa butter were presented by Ouriev *et al.* (2003). Ouriev and Windhab (2003) carried out flow mapping in the entrance flow of a shear-thickening suspension and they (Ouriev and Windhab, 2004) investigated transient flows of non-Newtonian model suspensions. Ouriev *et al.* (2004) presented results on measurements in partly pulsating chocolate flow and corresponding power law fits. In their diploma work at ETH Zurich, Johansson and Wiklund (2001) made measurements in shear thinning surfactant solutions and cellulose suspension and fitted the results to power law and Herschel-Bulkley models. The results were also compared with off-line rheometer measurements. A part of the findings were presented by Wiklund *et al.* (2001) and Wiklund *et al.* (2002). In the course of the PhD work, Birkhofer *et al.*

(2004) presented in-line measurements of the acoustic properties of cocoa butter and subsequently Birkhofer *et al.* (2006a) concentrated on the in-line rheology measurements of cocoa butter crystal suspension.

**J. Wiklund and M. Stading, SIK Gothenburg:** After his above mentioned diploma work at ETH Zurich, Wiklund continued with a PhD work at SIK and reviewed (Wiklund, 2003) the literature on in-line rheology and ultrasound Doppler methods related to the food industry. Wiklund *et al.* (2004) and Wiklund *et al.* (2006) presented a comparative LDA-UVP study where the UVP-PD method was applied to measure velocity profiles and rheology of highly concentrated cellulose fiber suspensions. Results showed that the UVP-PD method can be used to determine the yield stress of such suspensions, directly in-line and that an important concentration gradient exists close to the wall. Wiklund *et al.* (2007) presented results of the UVP-PD measurements of various food systems such as cheese sauce, fruit yoghurt and a vegetable sauce. The aim of these trials was to test the applicability of the UVP-PD method to highly concentrated polydisperse suspensions containing anisotropic particles of various shapes and sizes up to several cm in length. Rheological and structural changes due to increasing processing were also studied. This article contains also an overview on the UVP-PD methodology in addition to details of the signal processing and statistical methods such as low pass filtering of the velocity information obtained by the time domain algorithm and singular value decomposition methods to determine the wall position by channel correlation. Regner *et al.* (2007) presents data on the modelling of the displacement of yoghurt by water in a pipe using CFD (computational fluid dynamics), UVP and ERT (electrical resistance tomography). The results showed that UVP-PD can be used to monitor liquid displacements in pipes in real-time, with good agreement with modelled data. The collection of the research carried out during his PhD thesis is now available (Wiklund, 2007).

**R. Powell, K. McCarthy and M. McCarthy, UC Davis, USA:** Arola *et al.* (1997) used flow velocity profiles measured with magnetic resonance imaging (MRI) in combination with the pressure drop to measure rheological properties. Choi *et al.* (2002) compared this technique with UVP-PD method<sup>1</sup> for corn syrup solution and tomato juice flow. Dogan *et al.* (2002) presented results on measured properties of diced tomatoes suspended in tomato juice including yield stress, consistency index and apparent wall slip. Dogan *et al.* (2003b) investigated the flow of tomato concentrates with different solid content, the shear thinning behavior with a yield stress being fitted to power law and Casson models. Subsequently, they

---

<sup>1</sup>Similar comparisons were also made earlier at the ETH Zurich (Vieli *et al.*, 1989; Maier *et al.*, 1989)



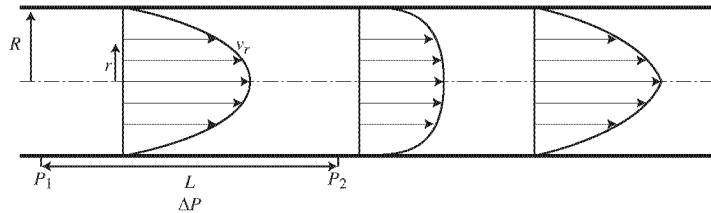


**Figure 3.1.:** Pipe flow profiles with the geometric sizes used in equations 3.10 and 3.11. In addition the typical profiles for the three fluid types Newtonian ( $n = 1$ ), shear thinning ( $n < 1$ ) and shear thickening ( $n > 1$ ) shown from left to right.

(Dogan *et al.*, 2005a,b) investigated chemically modified and native corn starch and polymer melt flows. Choi *et al.* (2005) described the data processing procedure for the UVP-PD measurements. The first steps (removing the DC offset and apply a complex FFT on the baseband signal) are conventional, but then it seems that the power spectra are saved as image data and then read in again to determine the velocities based on image analysis. However, the flow model was fitted using the velocity profile obtained by a polynomial fit of the actual measured profile rather than the measured data itself. Choi *et al.* (2006) described the in-line monitoring of tomato concentrate during evaporation by measuring velocity profiles and sound velocity, the latter being used for the determination of the concentration. Powell and Pfund (2005) applied the UVP-PD method to the flow of slurry suspensions. Pfund *et al.* (2006) investigated the flow of a non-Newtonian solution of Carbopol EZ-1 with sodium hydroxide, which forms a gel. They claimed that a patent of their group (Shekarriz and Sheen, 1998b) covers the combination of profile measurements with pressure drop for in-line rheometry. However, the actual patent does not seem to mention pressure or pressure drop measurements.

An alternative method for the in-line determination of the viscosity was proposed by Bachelet *et al.* (2003) for Newtonian fluids and Bachelet *et al.* (2004) for non-Newtonian fluids respectively, which involved a convergent-divergent tube instead of pressure difference measurement. The method is based on the measurement of the flow profile (UVP) at several positions in the converging and diverging sections in combination with numerical modeling of the flow profile. As this method requires certain assumptions regarding the flow behavior of the system, it is not evident that it would also work for complex fluids.

### 3. Particulate Suspensions

**Table 3.1:** Fluids and suspensions used for UVP-PD measurements. Abbreviated rheological models: gradient method (gr), Herschel-Bulkley (HB) and power law (pl).

Reference	Fluid	Shape	Particle size	$\lambda$ $\mu\text{m}$	$c$ $\text{m/s}$	Conc.	Shear rate $1/\text{s}$	Viscosity $\text{Pa}\cdot\text{s}$	Model
Müller <i>et al.</i> (1997)	glycerin and water						1 – 100	3	gr
"	polyacrylamide					4000 ppm	1 – 100	0.01 – 0.1	gr
"	hydroxypropyl guar gum					8000 ppm	1 – 100	0.2 – 2	gr
Wunderlich and Brunn (1999)	polyacrylamide					4000 wppm	0.1 – 10	0.01 – 0.06	polynomial, Ellis, pl
Brunn <i>et al.</i> (2004)	surfactant solution						5 – 20	20 – 110	gr
Ourlev and Windhab (2002)	silicon oil AK10 and native corn starch					$\leq 40\%$ wt	1 – 2000	0.1 – 1	pl, HB
"	glucose syrup (50%), starch particles and water					$\leq 40\%$ wt	1 – 2000	0.1 – 1	pl, HB
Ourlev (2002)	glucose syrup (50%), starch particles and water					30 and 40% wt	0.1 – 200	0.1 – 1	
Ourlev <i>et al.</i> (2003)	starch particles and water						0.1 – 30	1 – 100	pl, HB
Ourlev <i>et al.</i> (2002)	chocolate								pl, HB
Wiklund <i>et al.</i> (2007)	surfactant solution								pl, HB
"	cellulose fibre suspension					1, 2, 3%			pl, HB
Wiklund (2007)	PEC400								pl
"	xanthan gum solution						0.1 – 1000	0.01 – 100	pl
"	yoghurt ( $< 0.2\%$ fat)						0.1 – 1000	0.01 – 100	pl
"	cheese sauce (8% fat)						0.1 – 100	0.01 – 100	pl
"	pasta sauce						0.1 – 1000	0.01 – 100	pl
"	vegetable sauce						0.1 – 1000	0.01 – 100	pl
"	mayonnaise						0.1 – 1000	0.01 – 100	pl
Wiklund (2007)	pulp suspension					0.74 – 7.8% wt			HB
Wiklund (2007)	diary products					8% wt			HB
"	glycerol and glass beads					5% wt			HB
"	slurries					20% wt			HB
"	rapeseed oil and polyamide particles					25% wt			HB
"	syrup and starch particles								HB
"	tomato sauce					30% wt			HB
"	strawberry yoghurt					30% wt			HB
"	marmelades, fruit soup					8% wt			HB
"	fruit jams					35% wt			HB
"	pasta sauce					35% wt			HB
"	cellulose pulp								HB
"	cheese sauce and carrots					8% wt			HB
"	seafood chowder					1% wt			HB
"	vegetable sauces								HB
Choi <i>et al.</i> (2002)	corn syrup solution						0.1 – 500		gr
"	tomato juice suspension								gr
Dogan <i>et al.</i> (2002)	diced tomatoes in juice	complex	1 – 3 mm			65.7 °Brix	1 – 5	4 – 8	gr
Dogan <i>et al.</i> (2003a)	xanthan gum solution					8.15% wt	0.1 – 100	0.01 – 10	HB, pl, Casson
Dogan <i>et al.</i> (2003b)	tomato concentrate					3.5% vol	0.25 – 5	0.1 – 10	gr
Dogan <i>et al.</i> (2005a)	acid-thinned and native corn starch		4 – 17 $\mu\text{m}$ (avg)			8.75 – 17.10 %	0.5 – 50	0.1 – 10	pl, Casson
Dogan <i>et al.</i> (2005b)	polydimethylsiloxane		11.4 $\mu\text{m}$			6% vol	1 – 50	0.1 – 10	pl
Choi <i>et al.</i> (2006)	tomato concentrate						1 – 30	100 – 120	gr, Eyring
Phund <i>et al.</i> (2006)	carbopol, sodium hydrox- ide and glass beads		40 – 90 $\mu\text{m}$			5 – 24 °Brix	0.1 – 50	0.1 – 200	gr
						0.1% wt/ 0.032%vol	0 – 50		gr

**Table 3.2.:** Measurement parameters. #Prof is the number of profiles averaged used for processing. The Angle is the Doppler Angle between the flow and beam direction.  $v_{\max}$  is the maximum velocity in the profile.

Reference	Instrument	Transducer type	Transd. pos	Freq. Pulse	$N_{\text{rpt}}$	#Prof	Angle	Pipe diam.	Flow rate	$v_{\max}$
Müller <i>et al.</i> (1997)	DOP 1000		wall	4	4	128	1024	16.6	1 - 7	500
Wunderlich and Brunn (1999)	DOP 1000			4				16.6		900
Brunn <i>et al.</i> (2004)	DOP 1000			4		512		16.6		50 - 350
Ouriev and Windhab (2002)	UVP X3	Imasonic TN	contact/flush	4		25 - 50	70	23	7.3 - 30	500 - 1200
Ouriev (2002)	UVP X3	Imasonic TN	contact/flush	4		25		23	7.3 - 30	500 - 1800
Ouriev <i>et al.</i> (2003)	UVP X3	Imasonic TN	contact/flush	4		25	70	32	230	120
Wiklund <i>et al.</i> (2002)	UVP X3	Imasonic TN	contact	4	4	88	70	23	8.4 - 44	400 - 1800
Wiklund (2007)	Duo/FFT			4	2 - 4	128 - 512	10 - 300	65 - 71	10 - 70	
Wiklund (2007)	Duo			2	2	90	1024	69 - 73		
Wiklund (2007)	Duo							40	19	
Choi <i>et al.</i> (2002)		Xactex IM-HP-1/4-5	contact/flush	5	5	512 - 2048	8	50.8	0.78 - 4.1 <sup>a</sup>	40 - 68
Dogan <i>et al.</i> (2002)	custom/FFT						8	53.2	8 - 25	128 - 298
Dogan <i>et al.</i> (2003a)	custom/FFT							20/53		
Dogan <i>et al.</i> (2003b)	custom/FFT	Xactex IM-HP-1/4		5	10			53.2		40-120
Dogan <i>et al.</i> (2005a)	custom/FFT			5		4096		20.4		100
Dogan <i>et al.</i> (2005b)	custom/FFT		wall	5	10	4096		20.4	0.25 - 0.77 <sup>a</sup>	160
Choi <i>et al.</i> (2006)	Duo	Xactex IM-HP-1/4-2 <sup>b</sup>	contact/flush	4	5 - 20	200	256	45		
Pfund <i>et al.</i> (2006)	custom/FFT	Xactex IM-HP-1/4-5	contact/non-flush/bottom	5	5 - 20	1024	16	53.2		8 - 33
		XIM 1055-27								

<sup>a</sup>Flow rates, pipe diameter and maximum velocity given in the article seem to be inconsistent.

<sup>b</sup>According to the naming scheme of Xactex this would be a 2 MHz transducer, according to the text it is a 4 MHz transducer.

### 3.2.2. Power law fluid model

Equations for the variation in viscosity  $\eta$  with the shear rate  $\dot{\gamma}$  for laminar flow of fluids in a pipe section of length  $L$  (figure 3.1) have been derived in literature, which are based on the fact that the shear stress  $\tau$  along the radius  $r$  is given by

$$\tau = \frac{\Delta P r}{2L} \quad (3.10)$$

where  $\Delta P$  is the pressure drop. The corresponding variation in shear rate is given by

$$\dot{\gamma} = -\frac{dv}{dr} \quad (3.11)$$

where  $v$  is the fluid velocity at any radius  $r$ . The apparent viscosity is then given by  $\eta = \tau/\dot{\gamma}$ . The variation in shear stress with shear rate depends on the type of the fluid. The power law model

$$\tau = K\dot{\gamma}^n \quad (3.12)$$

represents the shear thinning ( $n < 1$ ) or shear thickening ( $n > 1$ ) non-Newtonian fluids (see also figure 3.1), where  $K$  is the consistency index and  $n$  the flow exponent. Combination of the above equations and integration results (Wiklund *et al.*, 2002) in an equation for the radial velocity profile:

$$v = \frac{R}{(1 + 1/n)} \left( \frac{R\Delta P}{2LK} \right)^{1/n} \left[ 1 - \left( \frac{r}{R} \right)^{1+1/n} \right] \quad (3.13)$$

while the shear rate and viscosity are respectively given by

$$\dot{\gamma} = \left( \frac{\Delta P r}{2LK} \right)^{1/n} \quad (3.14)$$

$$\eta = K \left( \frac{\Delta P r}{2LK} \right)^{1-1/n} \quad (3.15)$$

### 3.2.3. Herschel-Bulkley fluid model

The analysis in the previous section can be extended Wiklund *et al.* (2002) to other rheological models such as Herschel-Bulkley with the yield stress  $\tau_0$ :

$$\tau = \tau_0 + K\dot{\gamma}^n \quad (3.16)$$

The corresponding equations for the velocity, shear rate and viscosity are respectively given by

$$v = \frac{nR}{1+n} \left( \frac{R\Delta P}{2LK} \right)^{\frac{1}{n}} \left[ \left( 1 - \frac{R_*}{R} \right)^{1+\frac{1}{n}} - \left( \frac{r}{R} - \frac{R_*}{R} \right)^{1+\frac{1}{n}} \right] \quad (3.17)$$

in which  $r > R_*$  and  $R_* = 2L\tau_0/\Delta P$  is the radius of the plug.

$$\dot{\gamma} = \left( \frac{\Delta P}{2LK} \right)^{\frac{1}{n}} (r - R_*)^{\frac{1}{n}} \quad (3.18)$$

$$\eta = \frac{\tau}{\dot{\gamma}} = K \left( \frac{\Delta P}{2LK} \right)^{1-\frac{1}{n}} \frac{r}{(r - R_*)^{\frac{1}{n}}} \quad (3.19)$$

The models can be used to describe the velocity profile and rheological properties using the measured pressure drop. The parameters  $K$ ,  $n$  and  $\tau_0$  are then determined by a nonlinear optimization, which is an integral part of the software described in section 4.4.

### 3.2.4. Gradient method

An alternative method for the determination of the the shear rate  $\dot{\gamma}$  along the radius  $r$  of the pipe during the flow of the suspension was proposed by Müller *et al.* (1997). It uses directly the gradient  $-dv/dr = \dot{\gamma}$  of the velocity profiles at different radial positions. The corresponding shear stress  $\tau$  was obtained using the pressure drop  $\Delta P$  so that  $\tau = \Delta Pr/2L$ . The apparent viscosity is then given by  $\eta = \tau/\dot{\gamma} = \Delta Pr/2L\dot{\gamma}$ . This approach will be utilized to characterize the in-line rheology of flowing suspensions in section 5.1 which also compares this method with that one described in the previous section.

### 3.2.5. Direct ultrasonic measurement of viscoelasticity

Kulmyrzaev and McClements (2000) used the complex shear wave reflected from the surface to measure the high frequency shear rheology of pure and water diluted honey. The same method was used by Saggin and Coupland (2001b) for viscosity measurements in different oils. Gladwell *et al.* (1985) measured velocity of sound and attenuation in castor, olive, groundnut, safflower and rapeseed oils at frequencies between 2 and 95 MHz and tried to derive the viscoelastic properties, which depend on the molecular structure (triglyceride composition). Also Saggin

and Coupland (2004a) tried to derive the dynamic viscosity of xanthan (0% and 0.5%) and sucrose (74 to 78%) solutions over a range of temperatures. The quantitative agreement with measurements from oscillatory viscometry was reported to be poor, the xanthan solution without sucrose being not distinguishable from water. Saggin and Coupland (2004b) characterized coating fat in corn oil dispersions of different concentrations (2.5 to 12.5%) and different crystal sizes (30  $\mu\text{m}$  and  $< 1 \mu\text{m}$ ) by measuring shear and longitudinal ultrasound properties. For both size groups, the crystals aggregated to structures of about 80  $\mu\text{m}$ . For the longitudinal measurements, sound velocity and reflectance were only sensitive to the solid fat contents while the attenuation was also sensitive to the microstructure. With the shear ultrasonic reflectance and the oscillatory viscometry, the systems with the smaller crystals had higher viscosity. Again the two latter methods were in qualitative but not in quantitative agreement. The measurement method (shear and longitudinal waves) was also proposed as an in-line sensor for the determination of SFC, density and rheological properties of fat crystal suspensions.

#### 3.2.6. Ultrasonic blood viscosity estimation

Brands *et al.* (1995) bridged medical Doppler ultrasound with rheology by proposing a method to estimate the wall shear rate of blood vessels in vivo. A RF time domain (cross correlation) estimator was used with a vessel wall filter which was adaptive to get an optimal discrimination between the slowly moving structures, like vessel walls, and the slowly moving blood near the vessel wall. Other measurement methods of wall shear stress for medical application were reviewed by Shaaban and Duerinckx (2000). Flaud and Bensalah (2005) presented a method for the measurement of the blood viscosity, which assumed that blood is a Newtonian fluid and finally Tortoli *et al.* (2006) used a second transducer perpendicular to the vessel to determine the wall movement.

### 3.3. Acoustic properties

The measurement of the acoustic properties of particulate suspensions and other food systems has been investigated by many researchers in the past decades. The acoustic properties comprise mainly of ultrasonic velocity, attenuation coefficient and acoustic impedance (McClements, 1997).

There are different forms of sound propagation, the three most important being compression, shear and surface waves. For practical use in measurements, compression waves are most often used as they are physically the simplest sort of waves, which are least attenuated. In general, sound frequencies above 16 kHz,

the average threshold for human hearing, are called ultrasound frequencies (Povey and Mason, 1998, chap. 3). Ultrasound measurements are assumed to be non-destructive as power levels are small enough to leave the physical and chemical properties of the material where it passes unaltered.

In the following mostly particles larger than 1  $\mu\text{m}$  are considered. The acoustics of colloidal systems is more or less a separate topic, on which detailed information was given by Dukhin and Goetz (2002) and Challis *et al.* (2005).

### 3.3.1. Propagation

An ultrasonic wave is usually characterized by frequency ( $f = \omega/2\pi$ ), attenuation ( $\alpha$ ), velocity ( $c$ ), wavelength ( $\lambda = v/f$ ) and characteristic impedance ( $Z = \rho c$ ). The attenuation is a measure of the decrease in signal amplitude ( $\xi$ ) of a compression wave with distance  $z$ . The variation in the signal amplitude  $\xi$  along the distance  $z$  in the beam direction with time  $t$  is then given by:

$$\xi = \xi_0 e^{i(\omega t + kz)} \quad (3.20)$$

in which  $\xi_0$  is the original signal amplitude at  $z = 0$ ,  $i = \sqrt{-1}$  and  $\omega = 2\pi f$  is the angular velocity. The wave vector is  $k = k' + ik''$  where  $k' = \omega/c$  and  $k'' = i\alpha$ .

The relationship between the ultrasonic and physical properties of a material has been derived by a mathematical analysis of the propagation of an ultrasonic wave through a material and is expressed in the so called dispersion relation with  $E$  as the complex elastic modulus:

$$\frac{\omega}{k} = \sqrt{\frac{E}{\rho}} \quad (3.21)$$

in which both  $k$  and  $E$  are frequency dependent. For most ultrasound measurements  $k' \gg k''$  as otherwise measurements are nearly impossible.

### 3.3.2. Attenuation

Ultrasound transducers are phase sensitive, thus a low measured signal is not certainly due to attenuation but possibly scattering. This is one of the reasons why the measurement of the attenuation is less reliable than the sound velocity measurement. In addition there are diffraction, losses at interfaces and relaxation effects. The attenuation coefficient can be calculated by fitting the data from a measurement of the amplitude as a function of the distance from the transducer to the following equation.

$$\xi = \xi_0 e^{-\alpha z} \quad (3.22)$$

More theoretical details are given by Allegra and Hawley (1972).

### 3.3.3. Sound velocity

The velocity of sound depends on the density and the adiabatic compressibility of the medium. For most materials the velocity of sound decreases with increase in temperature. In contrast, in water it increases with increase in temperature (3 m/s/K).<sup>2</sup>

As the pressure waves propagates through the medium the volume and density fluctuate locally about the normal values. This can be expressed as dilation  $D$

$$D = \frac{\Delta V}{V_0} \quad (3.23)$$

and condensation  $s$

$$s = \frac{\Delta \rho}{\rho_0} \quad (3.24)$$

The adiabatic compressibility  $\kappa$  is then defined as

$$\kappa = -\frac{1}{V} \frac{\partial V}{\partial p} \cong \frac{D}{\Delta p} \quad (3.25)$$

The bulk modulus of elasticity is then

$$B = -\frac{\Delta p}{D} = \frac{1}{\kappa} \quad (3.26)$$

Wood (1964) showed that the velocity of sound  $c$  in *homogeneous* liquids and gases is independent of frequency and is given by the Wood equation

$$c = \sqrt{\frac{B}{\rho}} = \sqrt{\frac{1}{\kappa \rho}} \quad (3.27)$$

A simple approach to calculate the velocity of sound in a suspension is the Urick equation (Urick, 1947) in which  $\kappa$  and  $\rho$  in the Wood equation (3.27) are replaced by

$$\kappa = \sum \phi_i \kappa_i \quad \rho = \sum \phi_i \rho_i \quad (3.28)$$

---

<sup>2</sup>The velocity of sound in water increases with temperature until 74°C and decreases for higher temperatures (Kell, 1975). The reason for this unexpected behavior is the temperature dependent compressibility which is different from usual liquids. At lower temperatures the water molecules are ordered in a more ordered structure (expanded) which features a higher compressibility as the more packed structure at higher temperatures (Chaplin, 2007).



where  $i$  is the  $i$ th component of the mixture. This is called a homogeneous description because the properties of each phase contribute independently to the properties of the system (Povey and Mason, 1998, chap. 3).

In order to consider scattering effects, Pinfield and Povey (1997) proposed a modified Wood equation. The Urick equation and the following extensions of it were reviewed by McClements and Povey (1987b).

### 3.3.4. Scattering

The following considerations on ultrasound scattering are valid if the wavelength is much greater than the size of the particles. There are two different physical phenomena, namely thermal and visco-inertial effects, which lead to scattering of ultrasound as explained below.

#### 3.3.4.1. Thermal scattering

As the sound wave travels through the medium, there is an adiabatic compression and expansion. In an inhomogeneous medium, there are differences in thermal expansion and heat capacity resulting in a temperature difference at the boundary between particles and continuous medium, which leads to a heat flow. This causes a differential expansion and contraction of the boundary region that acts as a source of scattering (Pinfield and Povey, 1997).

#### 3.3.4.2. Visco-inertial scattering

The more frequently used explanation for the source of scattering is the density difference between particles and their continuous phase. Particles excited by the ultrasound wave may move relative to the suspending continuous medium due to their different inertia. Both the density difference and viscosity of continuous phase affect the relative motion and hence the scattering. If the viscosity is high, the particle moves with the continuous phase and the visco-inertial scattering will be small. If the viscosity is very low, the reaction between the particle and the displaced fluid volume will be small and once again the visco-inertial scattering will be small. Therefore, the visco-inertial scattering depends on ultrasound frequency, density difference, and continuous phase viscosity in a complicated way (Povey and Mason, 1998, chap. 3).

### 3.3.4.3. Scattering in suspensions and emulsions

There are basically two mathematical models describing the propagation in scattering media. An overview was given by Adjadj *et al.* (2006).

The scattering models based on the wave equation are described by Epstein and Carhart (1953) and Allegra and Hawley (1972) (thus also called ECAH theory). They are based on the interaction with single particles with thermal and visco-inertial scattering. Waterman and Truell (1961) and Lloyd and Berry (1967) also considered multiple scattering. McClements and Povey (1989) derived following approximate expressions for the effective compressibility and density which are used in the Urlick equation to calculate the sound velocity in scattering media.

$$\kappa_{\text{eff}} = \kappa \Re \left( 1 - \frac{3i\Phi\alpha_0}{k_c^3 a^3} \right) \quad (3.29)$$

$$\rho_{\text{eff}} = \rho \Re \left( 1 - \frac{9i\Phi\alpha_1}{k_c^3 a^3} \right) \quad (3.30)$$

$\alpha_0$  and  $\alpha_1$  are the attenuation coefficients related to thermal and visco-inertial scattering respectively.  $k_c$  is the wavenumber of the compressional wave.

Another approach was chosen by Harker and Temple (1988), Gibson and Toksöz (1989), Atkinson and Kytömaa (1992) and Evans and Attenborough (1997) as they used coupled phase models. The further work of Atkinson and Kytömaa seems interesting as in the next publication Atkinson and Kytömaa (1993) they investigated the development of the ultrasonic pressure field generated by the transducer, attenuation and sound velocity in suspensions of different concentrations (up to the maximum packing density). This article also described in detail an UVP device that exists yet at MIT in the Center for Nanofluids Technology. Kytömaa and Atkinson (1993) measured attenuation and backscattering in function of particle concentration and particle size while Kytömaa (1995) summarized the information that is extractable from sound velocity and attenuation measurements regarding particle size, concentration and mechanical properties of the constituents.

### 3.3.4.4. Ultrasound spectroscopy

In ultrasonic spectroscopy, the acoustic properties (in most cases, velocity of sound and attenuation) of particulate suspensions or emulsions are measured as a function of the frequency. The acoustic properties depend on the scattering, the latter itself depending on the interaction between the ultrasonic wave and the disperse phase. Thus, it is possible to derive information on the structure of the system. In

an ideal case, mostly only for very well defined simple systems, it is even possible to derive particle size distributions via the ultrasound spectroscopy. The following few articles are useful for understanding the fundamentals of the topic: Harker and Temple (1988); Riebel and Löffler (1989); Holmes *et al.* (1993, 1994); Storti *et al.* (2000).

An interesting application of measurement of particle size dependent scattering characteristics was used by Haider *et al.* (2002) to determine the shear rate as function of disaggregation in polymer melt.

#### 3.3.4.5. Backscattering of Ultrasound from blood and tissue

All the papers dealing with conventional suspensions discussed scattering in relation with simple attenuation or spectroscopy for particle sizing or other system characterization measurements. Only articles from the medical field investigated the (back) scattering and its relation with the received signal, which is used for the Doppler shift estimation. In blood flow, it is assumed that the red blood cells (erythrocytes) outnumber the other possible scatterers far both by quantity and volume (Shung *et al.*, 1976) and are therefore the main source of scattering in blood. Red blood cells are disk-like structures with a diameter of about  $7.5\ \mu\text{m}$  and a thickness of 1 to  $3\ \mu\text{m}$ . If several red blood cells aggregate stacked one above another, the resulting structure is called rouleau. Besides the acoustic properties of blood also the attenuation and scattering of tissues are of interest in the medical field for two different aspects: (i) it is in-between the transducer and the blood vessels if the measurement is made non-invasive and (ii) it can also be used to characterize the tissue itself, which is, for instance, applied to the liver (Thijssen, 2003).

Theoretical analysis of scattering by Angelsen (1980) was based on the assumption that blood is an isotropic continuum and that the scattering arises from fluctuations in the compressibility and mass density of the continuum. This explains the development of the backscattering coefficient as a function of the hematocrit<sup>3</sup> shown in figure 3.2. Until about 20% hematocrit, the backscattering coefficient increases with the concentration of the scatterers. Above this, if the concentration is high enough, the waves scattered by the individual particles will interfere which leads to phase cancelation. The overall scattering depends therefore on the configuration of the set of scatterers. The more regular is the distribution and thus the higher is the isotropy, the lower is the backscattering coefficient. Thus towards the maximum packing density the backscattering coefficient reaches its minimum.

---

<sup>3</sup>A hematocrit of 100% corresponds to the concentration of red blood cells in the pellet after centrifugation of blood.

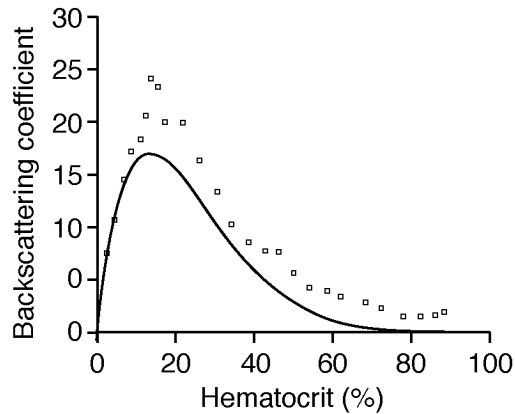


**Figure 3.2.:** Plot of the backscattering coefficient (BSC) versus hematocrit for porcine red blood cells suspended in saline (symbols). The smooth curve represents the Percus-Yevick theory for the packing of hard spheres. Results from Mo *et al.* (1994).

The anisotropy of the blood and tissue is also causing the typical speckle patterns in the ultrasonic imaging. The effect was also be used for an alternative to conventional ultrasound Doppler measurements. Bohs *et al.* (1995); Sandrin *et al.* (2001); Carlson and Ing (2002) used a transducer array to record B-Mode scans of the pipe flow. The velocity was then extracted from a cross correlation of the speckle patterns of two consecutive scans (up to 5000 per second).

#### 3.3.4.6. Backscattering theories

The mentioned models of Angelsen (1980) and Twersky (1988) were further developed independently by Mo *et al.* (1994) and Bascom and Cobbold (1995) by combining them with the voxel model. A voxel refers to an elemental volume that is small enough so that the incident ultrasonic wave may be assumed to arrive with the same phase at every scatterer located within it. Yet another model for the scattering in tissues was developed by Jensen (1991) in which effects of flow disturbance and hematocrit on the backscattered Doppler signal were explained by means of a backing dimension and a particle dimension.

#### 3.3.4.7. Backscattering measurement techniques

The acoustic backscattering coefficient  $\beta(\omega)$  is defined in ultrasound measurements as the differential scattering cross section per unit volume for a scattering angle of  $180^\circ$ . One of the first methods for the quantification of the backscattering from

randomly distributed scatterers was presented by Sigelmann and Reid (1973). The amplitude of backscattering is compared to the reflection from a target of known coefficient of reflection. Madsen *et al.* (1984) and Insana *et al.* (1986) presented a method of data reduction to determine the backscattering coefficient as

$$\beta(\omega_0) = \overline{N} \|\Psi(\omega_0)\|^2 = \frac{\overline{\|V_s(\omega_0)\|^2}}{(\tau/2\pi)(a'(\omega_0) + \overline{N}b'(\omega_0))} \quad (3.31)$$

Where  $\overline{N}$  is the average number of scatterers per unit volume,  $\Psi(\omega_0)$ ,  $a'$  and  $b'$  are transducer characteristics which could be determined with the echo from a reference reflector.  $\overline{\|V_s(\omega_0)\|^2}$  is measured as part of the experimental procedure, it is the mean value of the square of the moduli of the Fourier transforms of the time gated (duration  $\tau$ ) narrow-band pulse echo from the sample averaged over several measurements at different positions. Chen *et al.* (1993), also in the group of Madsen, measured backscattering coefficients as a function of the frequency and gate duration using broadband pulses. A different method based on the ratio of the spectra from a plane reflector and the random medium was proposed by Ueda and Ozawa (1985).

#### 3.3.4.8. Backscattering data analysis

Shung *et al.* (1984) showed that the backscattering coefficient was higher in turbulent flow compared to laminar flow. This was explained with macroscopic local variation of the elastic properties induced by the turbulent behavior of the medium, which decreased the correlation between two particles due to the presence of a flow disturbance. Mo *et al.* (1994) measured backscattering from blood with hematocrit values up to 100% (figure 3.2). In another interesting article, Chen and Zagzebski (1996) described measurements of the backscattering coefficient as a function of frequency and scatterer volume fraction for narrow- and broad-band pulses. The scattering system consisted of a volume fraction between 5 and 50% Sephadex particles with a mean diameter of 42  $\mu\text{m}$  in a gel matrix. The frequency was varied in the range from 2.5 to 9 MHz. The volume fraction with the maximum backscattering coefficient increased with the frequency. Also the frequency dependence of the backscattering increased with the particle concentration. This was explained with the continuum scattering models as their spatial autocorrelation function depends on the scatterer volume fraction. Lin and Shung (1999) measured backscattering as a function of hematocrit and shear rate at different pulsation rates and found it to vary during the flow pulse cycle (only for 20 BPM but not for 60 BPM) and increase with flow rate. Berger *et al.* (1991) compared results from the polydisperse scattering theory by Twersky (1988) with

measured data from red blood cells. The backscattering coefficient was found to increase with variance of the size distribution of the scatterers.

The backscattering from focused transducers was investigated by Wang and Shung (1997) for frequencies from 5 to 30 MHz for different concentrations. There was a difference to conventional transducers at higher concentrations. The backscatter from blood at 30 MHz was investigated by van der Heiden *et al.* (1995) concentrating on the influence of rouleau size. The measurement setup was similar to that described by Manneville *et al.* (2003) as the measurement was made in the gap of a Couette viscometer. The backscattering was found to decrease with increase in shear rate, which was explained with the reduction of rouleaux. Also the spectral slope (The backscatter coefficient is linearly proportional to the  $n$ th power of the frequency and this parameter  $n$  is referred to as the spectral slope of the backscatter.) was found to be related to the rouleau size and was close to the theoretical value (Rayleigh scattering) of 4 at the lowest rouleau concentration. Even higher frequencies (35 to 65 MHz) were used by Lockwood *et al.* (1991). In this frequency range the wavelength becomes similar to the size of the red blood cells, thus Rayleigh scattering is not any more valid. The spectral slope was therefore decreased to 1.4. An article on the cyclic variation of the power of the backscattered signal by Cloutier and Shung (1993) is interesting as it used a dilute suspension of polystyrene microspheres with a diameter between 20 and 130  $\mu\text{m}$  besides porcine blood as model scatterers. The backscattering power changes during the pulsating flow if the flow rate is high enough, which is explained with the flow disturbance. Further there are two review articles to be mentioned. Cloutier and Qin (1997) summarized the models, influencing factors, blood aggregation and in vivo measurements. Shung and Paeng (2003) proposed ultrasonic scattering from blood as a method to measure hematological and hemodynamic properties. Two hemodynamic phenomena, the black hole (a low echogenic zone in the center stream of a blood vessel) and the collapsing ring (an hyperechogenic ring converging from the vessel periphery toward the center and eventually collapsing during pulsatile flow) are shown. Sleaf and Lele (1988) described a model and corresponding measurement that allowed the estimation of the number density of random scatterers from the backscattered acoustic signals by characterization of the statistical nature of the signal including frequency-dependent attenuation, spatially varying media statistics and beam shape. Measurements were made with a phantom containing glass coated polystyrene beads with an average size of 120  $\mu\text{m}$  at a density between 10 and 800 scatterers per  $\text{cm}^3$ .

Rouffiac *et al.* (2004) related the shear rate with the echogenicity, which were measured independently and in vivo. The echogenicity was related to the aggregation of the red blood cells, which depended on the shear rate in the blood vessel. Wang and Shung (2001) also measured the backscattering coefficient in vivo.

#### 3.3.4.9. Spectral analysis of backscattered signal

Not directly dealing with backscattering coefficients but nevertheless relevant is the work of Fink and Cardoso (1984) on diffraction effects in pulse-echo measurements. Fink *et al.* (1983) (and also Cloostermans and Thijssen (1983)) described a method for the estimation of the frequency dependent attenuation from the backscattered signal. The short time Fourier analysis revealed the time evolution of the running spectral centroid. In the referred article a base frequency of 2.5 MHz and a Hamming window size of 2  $\mu$ s and 4  $\mu$ s was used while sampling with 10 bit at 20 MHz. The resulting development of the frequency as a function of time respectively depth was described to be well correlated to the frequency dependent medium attenuation. A more recent article (Kim and Varghese, 2007) used the cross-correlation of the short time Fourier analysis to derive the attenuation from the diffraction compensated RF signals.

#### 3.3.4.10. Backscattering in hydraulic engineering

Besides the medical field, the backscattering was also used in hydraulics to measure the concentration of sediment particles in flows. Thorne *et al.* (1993) was one of the first to publish an approach to the problem via the scattering theory instead of a simple calibration. The backscattering was measured by the RMS (Root Mean Square) of the received signal averaged over 100 observations as the phase of the backscattered waves was randomly distributed. Then the spatial distribution along the beam axis of the particle concentration can be expressed as function of received amplitude, attenuation coefficient (which also depends on the concentration and the location) and several other parameters. The measured concentrations (up to 1 kg/m<sup>3</sup> of marine sediment) agreed well with the actual concentrations. In a later publication by Thorne and Buckingham (2004), the influence of the size (45 to 380  $\mu$ m) and shape factor of sand on the backscattered signal was investigated. In the Rayleigh scattering regime (small particle size compared to wavelength) the scattering from glass spheres and sand grains of comparable size was similar. For larger particle sizes, the backscattering from the sand grains was higher than that from the spheres, which was explained with the difference in surface area between the two geometries. A comparable method by Shen and Lemmin (1996) used the signal transmitted and backscattered to compensate for the depth dependent integrated attenuation. The method was tested for concentrations of 1.1, 2.9 and 4.7 %wt of glass spheres of 115  $\mu$ m diameter with a distance between the transducers of 38.6 cm. The particle shape influence on frequency dependent attenuation was investigated by Schaafsma and Hay (1997) also for lead-glass spheres and different sediment particles (mean diameters between 30 and 212  $\mu$ m). The attenuation spectrum of the irregular shaped particles

was found to depend on the diameter of a circle with equal projected area and the diameter of the equal volume sphere.

#### 3.3.5. Fat crystallization and ultrasonic monitoring

When considering the Urlick equation, it is evident that the velocity of ultrasound in solid fat is greater than that in oil because of the difference in density and compressibility. Consequently, a measurement of the ultrasonic velocity in a fat/oil mixture can be used to determine the solid fat content (SFC). The velocity increases by about 3 m/s per % increase in solid fat content (McClements and Povey, 1992). During the phase transition, often the fractional changes in compressibility are much greater than the fractional changes in density (Povey, 1997).

When monitoring the crystallization process, one has to consider that the small energy input from the ultrasound measurement in the range of millikelvins can disturb the equilibrium. This results in an increased attenuation and a frequency dependent velocity of sound (Dobromyslov and Koshkin, 1970; Akulichev and Bulanov, 1981; McClements *et al.*, 1993b) because of the relation of relaxation time and the period (Povey, 1997).

According to Miles *et al.* (1985) and Pinfield *et al.* (1995), the volume fraction  $\phi$  of solid in an emulsion (with sound velocity  $c$ ) of dispersed phase with volume fraction  $\Phi$  can be calculated by

$$\phi = \frac{\frac{1}{c^2} - \frac{1}{c_l^2}}{\frac{1}{c_s^2} - \frac{1}{c_l^2}} \Phi \quad (3.32)$$

in which  $c_s$  and  $c_l$  are the extrapolated velocities of sound of emulsions containing wholly solid droplets and wholly liquid droplets respectively.

For pure oil/fat mixtures the equation can be simplified to

$$\phi = \frac{1 - \left(\frac{c_l}{c}\right)^2}{1 - \left(\frac{c_l}{c_s}\right)^2} \quad (3.33)$$

In order to calculate the SFC with equation (3.32) or (3.33), it is necessary to know the ultrasonic velocities of the liquid oil (no solid fat) and the solid fat at the same temperature. These values can be obtained by extrapolating ultrasonic velocity measurements made at low or high temperatures to the region of interest (Hussin and Povey, 1984; McClements and Povey, 1992, 1988b).



There are many articles dealing with ultrasound for the monitoring of fat crystallization, a summary of the measured systems being given in table 3.3. The Nuclear Magnetic Resonance (NMR) method, frequently used in our laboratory for the SFC measurements in cocoa butter and other fats, was compared with ultrasonic velocimetry by McClements and Povey (1988a) and Singh *et al.* (2004). The first article described measurements of SFC values up to 20% at a constant temperature of rapidly cooled tristearin in paraffin oil, tristearin in sunflower oil and tripalmitin in paraffin oil. The newer article is more relevant for our cocoa butter crystallization as it investigated the crystallization process of cocoa butter and anhydrous milk fat, both pure and blended with canola oil<sup>4</sup>. It was shown for pure cocoa butter that the onset of the crystallization resulted in a discontinuity in the ultrasonic velocity-temperature profile. For cocoa butter diluted with canola oil, this effect was not visible in the measurement. The NMR and velocity measurements agreed in most cases. For the cocoa butter canola oil mixtures, the sound velocities were higher than those in pure cocoa butter at the same temperature. This was explained with the polymorphism of the cocoa butter crystals and thus different microstructures. The modified Urick equation (velocity of sound as a function of SFC) was found to be not valid for cocoa butter (in contrast to the anhydrous milk fat) but there were only two sampling points in the region between 0 and 20%, which was interesting for the application in the shear crystallization process. Further it was not possible to clearly relate the SFC and microstructure of the cocoa butter to the velocity of sound, but it seems to be an interesting approach. This work in the group of A. Marangoni in Guelph was continued using spectroscopy methods. Martini *et al.* (2005) reported high attenuation around a low SFC (5%) due to large crystals, an SFC dependent attenuation around 10% SFC and a crystal size dependent attenuation around 20% SFC. For the measurements, the cocoa butter samples were cooled under shear in a temperature controlled cell.

Garbolino *et al.* (2000) presented another experimental setup involving a rheometer equipped with a pulse-echo reflectometer, which was used to monitor the velocity of sound and echo amplitude during the shear crystallization of a coating fat (hydrogenated and fractionated mixture of soybean and cottonseed oils). Both parameters showed a clear change at the melting point. Thus, as expected, onset of the crystallization was found with increase in the shear rate.

Kloek *et al.* (2000) speculated that an intermediate maximum of the sound velocity during the melting process of hydrogenated palm oil in water was due to the conversion from the  $\alpha$  to the  $\beta$  and  $\beta'$  polymorph form arguing with the lower compressibility of the more stable  $\beta$  variant. But there was no further information on reproducibility of this peak or any comparison with DSC (Differential Scanning Calorimetry) measurements.

---

<sup>4</sup>Canola is a variant of rapeseed, the oil has a melting point of  $-10^{\circ}\text{C}$

In a work comparable to Singh *et al.* (2004), Saggin and Coupland (2002) carried out ultrasound measurements in dispersions of cocoa butter and coating fat in corn oil. In contrast to Singh *et al.* (2004), the reflection index measured by the latter authors showed a linear dependence on the SFC measured by NMR, thus being independent to the polymorphic form. But the solid content used by Saggin and Coupland (2002) was only reaching a maximum of 36%, while that used by the former authors was 70 to 100%. The reflectance index method was also tried for an on-line monitoring of a chocolate tempering process. It was hypothesized that it was possible to monitor the point of the onset of the crystallization by measurements with a temper meter and molding of samples before and after this certain point, where the reflectivity drops at a constant temperature.

#### 3.3.6. Application in food systems

One of the first applications of ultrasound in food systems was the measurement of fat content of meat by Miles and Fursey (1977). Since then the use of ultrasonic systems in the food industry was further developed but is still not yet wide spread. Javanaud (1988) wrote an early review article on the application of ultrasound to food systems. Povey and McClements (1988); Povey (1989); McClements (1997) reviewed extensively the application of ultrasound in food engineering. Later Povey and Mason (1998) presented a few interesting chapters on analytical use of ultrasound. McClements (1998) dealt specifically with the characterization of food emulsions. Povey (1998) briefly gave examples of applications of ultrasound in food systems and the corresponding measurement devices. Coupland and Saggin (2003) presented extensively on ultrasound sensors for the food industry. Coupland (2004) described various applications of low intensity ultrasound for food systems. Elmehdi *et al.* (2003) measured the sound velocity, attenuation and density of dough during fermentation and found two distinct effects influencing the velocity of sound. During the first phase of fermentation, CO<sub>2</sub> was dissolved and caused a reduction of the pH and thus a weakening of the intermolecular interactions, likely due to charge repulsion effects on the proteins. Of course, the gas content also influences the velocity of sound. In a very recent publication, Álava *et al.* (2007) measured velocity of sound and attenuation in dough from different flours. The flours were characterized by the ratio of attenuation to velocity of sound.

##### 3.3.6.1. Characterization of edible oils and fats

McClements and Povey (1992) gave a brief overview of the ultrasound methods to analyze different aspects of edible fats and oils including triglyceride composition

Table 3.3.: Articles on fat crystallization. —: not applicable, n/a: information not available.

Author	Type	Dispersed	Continuous	Emulsifier	Drop diam. $\mu\text{m}$	Freq. MHz	Technique
Dobromyslov and Koshkin (1970)	pure	—	n-tricosane	—	—	0.7 – 7.5	n/a
Povey (1984); Hussin and Povey (1984)	dispersion	palm oil, coconut oil, tristearin, vegetable fat	triolein	—	—	5	pulse-echo
Miles <i>et al.</i> (1985)	pure	olive oil, corn oil, lard, dripping	—	—	—	2.5	transmission
McClements and Povey (1987a)	dispersion	tristearin, tripalmitin, trilaurin, 1-oleodipalmitin	paraffin oil (80 – 100%)	—	—	1	transmission
McClements and Povey (1988c)	dispersion	glyceride (SSS, PPP, LLL, SS, POP, SOS, PSP, POS)	paraffin oil	—	—	n/a	n/a
Dickinson <i>et al.</i> (1990, 1991, 1993)	emulsion	n-hexadecane (20%)	water	Tween 20 (2%)	0.8	1.25	pulse-echo
Dickinson <i>et al.</i> (1993)	emulsion	n-hexadecane	water	Tween 20, octaethylene glycol n-dodecyl ether ( $\text{C}_{12}\text{E}_8$ ), SDS	0.35	1.25	pulse-echo
McClements <i>et al.</i> (1993b)	emulsion	n-hexadecane	water	—	0.4 – 1	0.3 – 4	pulse-echo
McClements <i>et al.</i> (1993a)	emulsion	n-hexadecane (20%)	water	Tween 20, SDS, $\beta$ -lactoglobulin, $\beta$ -casein	< 1	1.25	pulse-echo
Archer <i>et al.</i> (1996)	emulsion	lanolin, light white mineral oil	water (20%)	—	8	2.25	pulse-echo
Hodate <i>et al.</i> (1997)	emulsion	palm oil (30%)	water	sodium caseinate, hydrophilic sucrose polyesters	—	—	—
Garbolino <i>et al.</i> (2000)	pure	—	confectionary coating fat	—	—	2.25	pulse-echo
Hindle <i>et al.</i> (2000)	emulsion	cocoa butter	water	Tween 20	0.14	n/a	pulse-echo
Kloek <i>et al.</i> (2000)	emulsion	sunflower oil, hydrogenated palm oil	water	sodium caseinate, Tween 20	0.4 – 3	—	pulse-echo
Saggin and Coupland (2002)	dispersion	confectionary coating fat (5 to 15%), cocoa butter (26 to 36%), dark chocolate	corn oil	—	—	2.25	pulse-echo
Singh <i>et al.</i> (2004)	pure and emulsion	anhydrous milk fat, cocoa butter	canola oil (0 – 30%)	—	—	3.5	pulse-echo
Awad (2004)	emulsion	palm mid-fraction, palm kernel oil	water (80%)	sucrose oligoesters, polyglycerine ester, Tween 20	0.8	2	pulse-echo
Martini <i>et al.</i> (2005)	pure	—	cocoa butter	—	—	0 – 2.5	transmission

and spectroscopy. A table with the acoustic properties of various edible oils at 20°C was given. McClements and Povey (1988c) tabulated the temperature dependency of the sound velocity for many different triglycerides in solid and liquid state (see also table 3.3). McClements *et al.* (1990) measured sunflower oil content (0 to 35%) and tried to characterize the droplet size (0.55 to 10.2  $\mu\text{m}$ ) in salad cream by measuring the velocity of sound as a function of the frequency (1.25 to 10 MHz). Bamberger and Greenwood (2004) described an ultrasound sensor that could be clamped on a steel pipe to monitor fluid density from the echo amplitude of multiple reflections from the wall, which depended on the impedance of the medium in the pipe and solids concentration from the velocity of sound in the medium.

#### 3.3.6.2. Measurement methods

McClements and Fairley (1991) showed an ultrasonic pulse echo reflectometer, which consisted of a transducer, a buffer rod, sample cell and reflector plate. This allowed the simultaneous measurement of velocity of sound, attenuation coefficient and impedance. A similar setup was also used by Saggin and Coupland (2001a) to measure the velocity of sound and reflection coefficient of sucrose, glycerol, sodium chloride and tomato ketchup. In all cases, the two measured sizes were found to depend linearly on the concentration.

## 4. Materials and Methods

### 4.1. Suspensions

The following two different categories of suspensions were investigated: (1) model suspensions of particles with well defined parameters such as their concentration and size distribution dispersed in an oil or water as continuous phase with known viscosity; (2) cocoa butter crystal and chocolate suspensions relevant to industrial applications.

#### 4.1.1. Model suspensions of polyamide particles in rapeseed oil

The disperse phase of the model suspensions for the presented pipe flow measurements (see section 5.1) consisted of 11 and 90  $\mu\text{m}$  mean diameter polyamide particles (with trade name Vestosint manufactured by Degussa AG, High Performance Polymers, Marl, Germany) with a density of 1016  $\text{kg}/\text{m}^3$  at 23  $^\circ\text{C}$ . Purified commercial rapeseed oil (called Lobra) supplied by Karlshamns AB (Karlshamn, Sweden) was used as continuous phase. The rapeseed oil is a Newtonian fluid with a viscosity of 66  $\text{mPa}\cdot\text{s}$  at 20  $^\circ\text{C}$  and a density of 910  $\text{kg}/\text{m}^3$  at 30  $^\circ\text{C}$ . The polyamide particles exhibit a chemical resistance for more than 6 months to the Lobra oil according to the manufacturer. The suspensions were prepared directly in a vessel (20  $\ell$  volume) fitted with a propeller agitator, which was connected to the flow loop.

#### 4.1.2. Model suspensions of polyamide particles in water

For the experiments in the rotating cylinder (see section 4.2.4), different materials such as corn starch (C\*Gel 03402, Blattman Cerestar AG, Switzerland), Gril-tex 5P1 (EMS-GRILTECH, Switzerland) and SASOALWax Spray30 (Sasol Wax, South Africa) were tested as reflectors. Finally polyamide particles obtained from Dantec Dynamics (Skovlunde, Denmark) were found to be the most suitable material. These particles have a density of 1.03  $\text{g}/\text{cm}^3$  and a diameter of 20  $\mu\text{m}$ . At

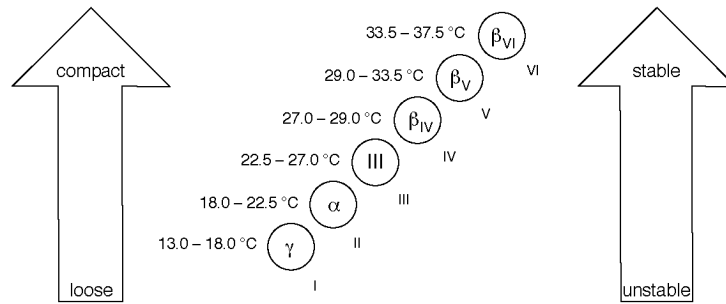


**Figure 4.1.:** The different cocoa butter crystal conformations, their stability and packing.

high concentrations a mixture with water results in a very stable foam but at low concentrations around 0.1 % the polyamide particles proved to be good reflectors for the ultrasound measurements.

### 4.1.3. Cocoa butter suspension

Cocoa butter used for chocolate production is a mixture of triglycerides with a polymorphic crystallization behavior due to different possible arrangements of the triglycerides that has a melting temperature between 29 and 34 °C. The hydroxyl groups of the glycerin are mainly oleic acid (C18:1), stearic acid (C18:0) and palmitic acid (C16:0). The triglyceride composition depends on the geographical origin of the cocoa butter.

The six different crystal conformations with different melting points are shown in figure 4.1. There are two different naming schemes for the different conformations, both shown in figure 4.1. The chocolate industry uses the definition from Wille and Lutton (1966), which numbers the different conformations from I to VI. In contrast, the fat industry uses greek characters  $\gamma$ ,  $\alpha$  and  $\beta$  with subgroups according to Larsson (1966). The conformations built depend on the crystallization conditions such as temperature, magnitude and time duration of applied stress. For the chocolate production the stable  $\beta$  forms are the desired ones.

X-ray diffraction spectroscopy for the investigation of the polymorphism of cocoa butter was described by deMan (1992) and van Malssen *et al.* (1996b,c,a, 1999). Hernqvist (1990) used Raman spectroscopy in addition to X-ray diffraction. Marangoni and McGauley (2003) investigated the microstructure of cocoa butter crystallized under static conditions at different temperatures showing some microscopic pictures of the structures and their relation to the polymorphic forms. Padar (2003) investigated the morphology of cocoa butter crystals produced under different static and shear crystallization conditions using microscopy, DSC

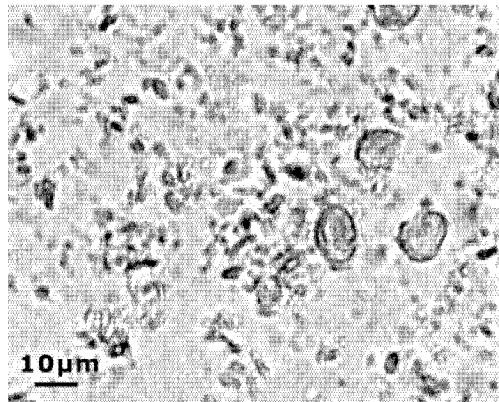


**Figure 4.2.:** Microscopy picture of a diluted sample of the suspension produced in the shear crystallization process. There are single, spherical to rod like particles below  $10\ \mu\text{m}$  in diameter and a few larger aggregates with a diameter larger than  $10\ \mu\text{m}$ .

and NMR. One example of the microscopy pictures of the suspension produced in the shear crystallization process is shown in figure 4.2. Literature on ultrasonic measurements of the cocoa butter crystallization can be found in section 3.3.5.

#### 4.1.4. Chocolate suspension

The molten chocolate suspension used was dark milk chocolate consisting of 41 % sugar, 18 % cocoa mass, 16 % cocoa butter, 0.5 % soya lecithin, 23 % whole milk powder and 1 % skimmed milk powder. Thus solid content was around 70 % (weight) and 65 % (volume). The density of the molten chocolate mass was  $1237\ \text{kg}/\text{m}^3$ .

Fryer and Pinschower (2000) gave an overview on the material science of chocolate including the polymorphism of the cocoa butter.

## 4.2. Analytical techniques

### 4.2.1. Off-line rheometry

The flow behavior of the model suspensions (section 4.1.1) of polyamide particles in rapeseed oil were analyzed off-line by Johan Wiklund at SIK in a stress controlled rheometer, Rheologica Stresstech (Rheologica Instruments, Lund Sweden).

The viscometric measurements were performed using concentric cylinder geometries with a bob diameter of 20 mm (CC20). The viscosity was measured over a wide range of shear rates, which corresponded to the conditions in the flow loop experiments at 20, 22, 24 and 26 °C. The measurements at room temperature (20 °C) were used for the comparisons with the in-line results.

#### 4.2.2. Nuclear Magnetic Resonance Technique (NMR)

The Solid Fat Content (SFC) of the cocoa butter crystal suspension was determined using Nuclear Magnetic Resonance (NMR) spectroscopy. The Minispec NMS 120 (Bruker BioSpin GmbH, Rheinstetten, Germany) with a magnetic flux density of 0.47 T of the permanent magnet and an impulse frequency of 20 MHz recorded the time evolution of the NMR response. The resulting signal contained the analytical information from which the fractions of hydrogen in solid and liquid state may be deduced. In solid matter, oscillations of the angular momentum of the nuclei are heavily damped, and the signal decays relatively quickly. In contrast, in the liquid, the surroundings are more mobile, thus causing less dampening and a slower decay of the signal. The relaxation time of molten fat is about 100 ms while that for the fat crystals is 40 ms. The device calculates the SFC from the total signal the percentage of protons in a liquid and solid environment.

#### 4.2.3. Laser Diffraction Particle Size Analyzer

The size distributions of particles in the model suspensions were determined using a laser diffraction particle size analyzer (Beckman Coulter instruments, Fullerton, USA; model LS 13320). The instrument can measure particles as small as 40 nm due to the Polarization Intensity Differential Scattering (PIDS) technology. PIDS uses the combined data from the polarization effect of light scattering with the wavelength dependence at high angles to analyze particles much smaller than the wavelength of the laser light (780 nm) used. The size distribution the polyamide particles was determined in dry powder form.

#### 4.2.4. Rotating cylinder

In order to obtain reference data for measuring the flow velocity under stationary flow conditions, a series of experiments were carried out. A rotating cylinder (fig. 4.3 on the left side) comparable to the one used by Takeda and Haefeli (1991) made of Plexiglas GS (Degussa, Darmstadt, Germany) with density 1.19 g/cm<sup>3</sup> was set up in a water tank of square cross-section. Two sizes of acrylic glass



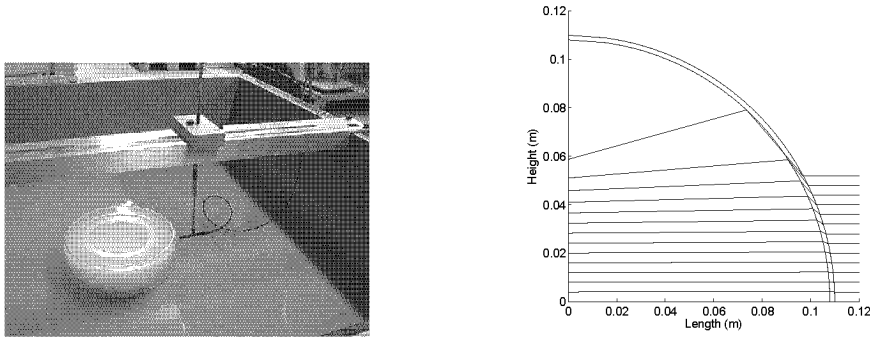


**Figure 4.3.:** Left side: rotating cylinder (large) with transducer position system. Right side: calculated beam path considering the refraction at the cylinder wall and longitudinal wave propagation for the small rotating cylinder.

cylinders were used to compare the effect of size and geometry on the ultrasound propagation through the medium. The volume of small cylinder is  $3\ell$  while that of the big cylinder is  $10\ell$ . The big cylinder is 30 cm in diameter and 14 cm in height with a wall thickness of 5 mm. The small cylinder is 15 cm in diameter and 7 cm in height. The outer wall of both cylinders is grooved at mid-height at about 2 mm to reduce the influence of the wall on the propagation of the ultrasound beam. The cylinder is placed in the center of a 1 m by 1 m by 50 cm water container to ensure the coupling between the transducer and the cylinder, which is rotated by a motor (Type F71K-4, Replec SA, Lutry/Lausanne, Switzerland). The speed of the motor was calibrated to the value displayed by the controller (Altivar 28, Schneider Electric, Rueil-Malmaison, France) using a tachometer. The rotation speeds written in the text refer to the nominal values displayed by the transformer from 1 to a maximum value of 50 rather than the calculated rotation speed in rotations per minute (rpm).

The water container was scaled in  $x$  and  $y$  axis direction. The position of transducer can be fixed and the scale is readable from the  $y$ -axis. The distance of transducer from the cylinder can be defined from  $x$ -axis as well. The container was filled until the upper edge of the cylinder, which was closed with a lid to avoid air bubbles inside the cylinder. Depending on the measurement system, the cylinder was filled with different suspensions. The results presented in section 5.5 were obtained with a suspension of 0.1 % polyamide particles (20  $\mu\text{m}$  diameter) in deionized water.

As the velocity of suspension in the rotating cylinder projected to the transducer is known from the rotation speed which is constant over the whole secant (fig. 4.4), it is possible to compare the UVP measurements with the actual velocity. Many experiments were carried out by varying (1) system parameters: (i) different model suspensions; (ii) influence of sedimentation velocity on reproducibility of

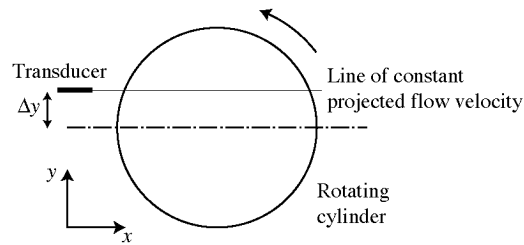


**Figure 4.4.:** Scheme of rotating cylinder.

measurements; (iii) concentration of particles in suspension; (iv) two cylinders with different diameters; (v) rotational speed of the cylinder; (vi) position of transducer and distance to the cylinder; (vii) effect of reflections from the opposite tank wall and (2) UVP parameters: (i) number of profile repetitions; (ii) number of cycles per pulse.

The pulse emitted from the transducer travels through three media: from (i) water to (ii) Plexiglas, from Plexiglas to (iii) suspension and its echo comes back in the reverse direction. The theoretical path, considering only the longitudinal propagation (Thompson *et al.*, 2000), is shown in figure 4.3 (right side). The transducer position was kept inside the range where the influence from the curvature of the cylinder was negligible.

The distance of transducer to the cylinder was kept constant at 17 mm in order to have the focal point at the cylinder wall. The measurements were carried out at different transducer positions, by shifting the transducer position from the center of cylinder towards the edge ( $\Delta y$ , see figure 4.4). The resulting velocity  $v$  at the angular velocity  $\omega$  is  $v = \Delta y\omega$ .

## 4.3. Instrumentation

### 4.3.1. UVP

The UVP-Duo (Met-Flow SA, Lausanne, Switzerland) is a pulsed wave Doppler system, which uses a quadrature phase detection as directional demodulation to get the Doppler shift (baseband) signal. This principle is described e.g. Baker (1970), Jensen (1996, chap. 6), Evans and McDicken (2000, chap. 4.2.2.) and in particular, by Durst *et al.* (1992). The instrument uses an autocorrelation (time domain) algorithm described by Barber *et al.* (1985) for the frequency estimation. During the work, the firmware of the instrument was customized to allow direct access to the digitized baseband signal. From this data, the power density spectra

(Lee and Waag, 1978; Hoeks *et al.*, 1991; Tortoli *et al.*, 1996) of one set of profiles (usually between 20 and 100) were averaged (the variability was shown by Cloutier *et al.* (1992) to decrease exponentially with the number of profiles). The Doppler shift frequency (flow velocity) was then determined by taking the geometric mean from the spectra above an offset, which is a fraction of the maximum power density. Further details on the ultrasound Doppler technique and implementation can be found in sections 2 and 3.2.

The UVP-Duo can emit pulses of a variable length (1 to 32 cycles) with a base frequency of 0.5, 1, 2, 4 or 8 MHz with an emission voltage of 30, 60, 90 or 150 V peak-peak. There is a voltage controlled amplifier, which is programmable with a simple ramp using a start and end value defined by the user. The minimum pulse repetition frequency is 244 Hz. The minimum channel distance is 500 ns as the two 14 bit Analog to Digital Converters (ADC) for the baseband signal have a maximum sampling rate of 2 MS/s. There is no mechanical switch between the sending and receiving unit, which has the advantage that there is no minimum depth for the start of the measurement window. However, the receiving unit is over-steered by the high voltage signal of the emitted pulse and it takes a few  $\mu$ s until the full sensitivity is reestablished. In addition to the ADCs for the baseband signal, there is also a separate 2 MHz ADC recording the RF signal from the voltage controlled amplifier (therefore also the name “Duo”).

The instrument has an integrated multiplexer with 20 BNC connectors, which allows to emit signals with one of the given base frequencies on any of the connectors. Thus the instrument is also capable of vector flow velocity measurements. In addition to the multiplexer there are four connectors. Two of them emitting a trigger signal for the pulses and the measurement window respectively. Also the analog RF signal after the voltage controlled amplifier, going to the additional ADC mentioned above, can be simultaneously monitored on an oscilloscope. Finally there is a connector to trigger data acquisition externally.

The communication with the instrument works via a proprietary TCP/IP protocol over an ethernet connection. On the client PC side there are basically two options to interact with the instrument. One use an application called “UVP Monitor” from Met-Flow which provides a Graphical User Interface (GUI) to set the parameters and view respectively save the flow profiles. As alternative way there is also an ActiveX library from Met-Flow which allows any 3rd party application to communicate with the UVP-Duo.

This ActiveX library (“UVPAX”), which was improved considerably in close collaboration with Met-Flow, was used for most the measurements in the presented work using a MATLAB based application (see section 4.4) as client. The UVPAX library allows access to all the features of the UVP. It provides an Application

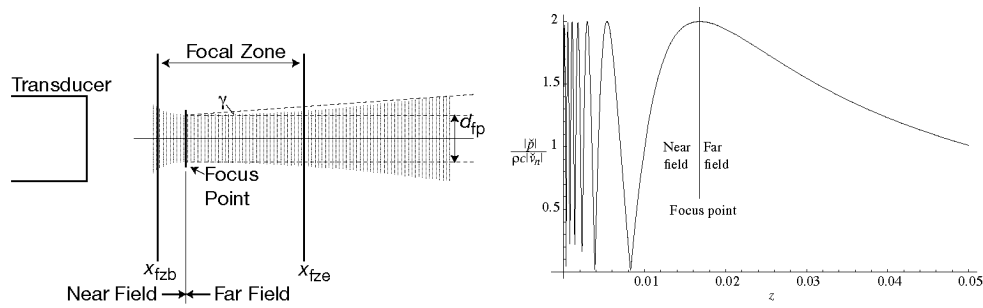


**Figure 4.5.:** Left side: Scheme of the focal zone ( $x_{fzb}$ ,  $x_{fze}$ : focal zone begin and end,  $d_{fp}$ : diameter of the beam at the focus point) with the divergence half angle  $\gamma$ . Right side: Pressure distribution in the center of the beam according equation (A.5) on page 116 for a 4 MHz transducer with an active diameter of 4 mm.

Programming Interface (API) to get the hardware limits, read and write the measurement parameters, define multiplexer items for velocity vector measurements and finally acquire either the flow profiles calculated on the DSP (Digital Signal Processor) on the instrument together with the RF signal or the baseband signal (in-phase and co-phase). There are two different schemes to get the measurement values. One can either get them directly calling a function, which returns the data or install an event handler which is called every time data is available. Later option is more efficient and is also working directly with MATLAB since the latest UVPAX library versions.

### 4.3.2. Ultrasound Transducer

For all the measurements, transducers with base frequencies of 2, 4 and 8 MHz from the TN and TX series from Met-Flow SA (developed by Imasonic, Besançon, France) were used. The acoustic energy emitted by those 4 MHz transducers is around  $1 \text{ W/cm}^2$ .

For velocity profile measurements in the rapeseed oil based model suspensions (see sections 4.1.1 and 5.1), an additional transducer from Signal Processing SA (Lausanne, Switzerland) was used besides a TX transducer. As receiver for the sound velocity measurements, also TN series transducers were used. All those transducers have a transmission frequency of 4 MHz, and an active and outer diameters of 5 mm and 8 mm respectively. These parameters result in water ( $c = 1480 \text{ m/s}$ ) in a near field length of 16.9 mm and a divergence half angle of  $2.2^\circ$  (see also figure 4.5).

Also the 8 MHz transducers of the TN and TX lines were tested. Compared to the 4 MHz transducers the sensitivity and penetration depths did not match the

expectations. The 2 MHz transducer was not used for in-line measurements as the housing has a larger diameter (13 mm). For highly concentrated model and molten chocolate suspensions, measurements with the 4 MHz transducers with an excitation frequency of 2 MHz worked well.

A good overview of problems and paradoxes of transducer design was given by Hunt *et al.* (1983). Szabo *et al.* (2004) published recently on the calibration of focused transducers. An interesting transducer design was presented by Murakawa *et al.* (2005) who used a so called multi-wave concentric transducer, which had a 2 MHz element in the center and an 8 MHz element in the outer area. The two different frequencies were used to measure a two phase flow of air bubbles (2 to 4 mm) in a suspension of nylon micro-particles (80  $\mu\text{m}$ ). The lower frequency was used to detect the flow of the larger structures (bubbles) and the higher frequency for the solid particles.

### 4.3.3. Flow adapters

The flow adapters were used to fix the transducers enabling the pipe flow measurements with as little interference with the actual flow as possible. There are several possibilities to position the transducer. Direct contact of the transducers were described by several authors (Shekarriz and Sheen, 1998a; Choi *et al.*, 2002; Ouriev and Windhab, 2003). Other setups were shown by Lemmin and Rolland (1997); Wiklund and Stading (2006) involving a film in front of the cavity to minimize influences on the pipe flow stream lines. It is also possible to measure through the pipe wall especially for materials such as Plexiglas (Yamanaka *et al.*, 2002). As steel pipes (Kishiro *et al.*, 2004; Wada *et al.*, 2004) are quite difficult to penetrate, many authors used e. g. a wedge transducer Tezuka *et al.* (2006) to improve the measurements.

The following articles deal with the measurements through a non-metallic pipe wall. The effects of a layer of Plexiglas or polyethylene on the ultrasound beam as a function of the incidence angle for longitudinal and shear waves were investigated in detail theoretically and experimentally by Thompson *et al.* (2000). Power spectra from a string phantom measurement were compared for the cases with and without transmission through a 2 mm plexiglass sheet. Around the critical angle (in the case of water and Plexiglas  $33^\circ$ ) the frequency distribution was very sensitive on the angle. The influence of the curvature of the pipe on the pressure field was modeled by Thompson and Aldis (1996) but was not verified with experimental data. One finding was that the ratio of the sound velocity in the two materials was quite important, and that the influence of a diverging interface (sound velocity in the tube material higher than inside the pipe) was smaller than from a converging interface. Tortoli *et al.* (1999) described the effects of the pipe

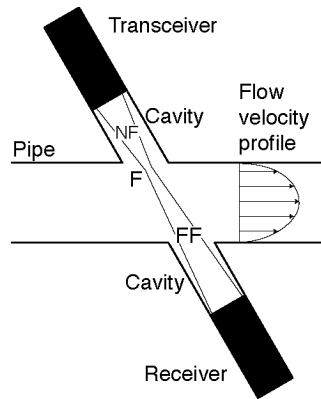


**Figure 4.6.:** Flow adapter with two ultrasound transducers (NF: near field; F: focal point; FF: far field).

curvature on the dual mode propagation (longitudinal and shear waves) when the ultrasound beam was incident on the plastic tube off-axis as it was the case for the rotating cylinder. Regarding flow adapter material selection, Nowak (2002) is of interest as it gives the velocity of sound and densities for various relevant materials (PEHD, PVC, PET (Mylar), PMMA). Hung and Goldstein (1983) presented the density, sound velocity, impedance, reflectance and attenuation coefficients for Plexiglas, nylon, Teflon, Delrin and various polyethylene amongst others. Further information on the acoustic properties of pipe wall materials and their influence on the pressure field can be found in section 2.3 on flow phantoms used in the medical field.

During this project, various flow adapters made from hard PVC were manufactured and tested. It was not possible to measure the flow velocity profiles in cocoa butter system through the pipe wall, probably due to a weak reflectivity and a high attenuation in the pipe wall material. A setup with a film between the cavity for the sensor and the pipe could not be achieved without entrapping air bubbles in the line of the ultrasound beam, which affect the measurement. Temperature sensitive cocoa butter suspension cannot be used to fill the closed cavity. If another liquid or gel is filled in the cavity, impedance difference between these two media affect the Doppler angle. Consequently, the whole adapter was submerged in liquid cocoa butter respectively water in order to avoid suction of air into the system. In the case of the cocoa butter this setup also enabled a heating of adapter avoiding solidification of fat on the pipe wall inside the flow adapter.

As described by Lemmin and Rolland (1997), the transducer was usually positioned such that the flow profile measurement begins at the end of the near field (figure 4.6). Under these conditions, the focal point and hence the smallest sampling volume diameter is located at the pipe wall, where the velocity gradient

is maximum. Thus the spatial resolution should be as good as possible. In addition, as mentioned by Hoeks *et al.* (1991), measurements inside the near field have disadvantages of inhomogenous pressure distribution and variation in the Doppler angle (Bascom *et al.*, 1986). On the other hand, the cavities in front of the transducers containing the near field had the disadvantage to contribute to the accumulation of large sized particles over a period of time as observed by an increase of velocity of sound for the model suspension (see section 5.1.2) even if the transducers were positioned in a horizontal plane. In the cocoa butter there is the possibility of fat crystallization inside the cavities. Consequently, both processes could affect the accuracy of determination of wall position in the measured flow velocity profile. In addition, as a flow field exists in the region connecting the cavity and the pipe, the shear stress at the pipe wall cannot be determined precisely.

In order to measure velocity of sound and attenuation simultaneously with the profiles, a second transducer facing the one measuring the profiles was fixed in the flow adapter. This setup was described by Shekarriz and Sheen (1998a), Birkhofer *et al.* (2004), Wiklund and Stading (2006) and Choi *et al.* (2006). As it is possible to measure the flow profiles with both transducers it is also possible to check the symmetry of the flow even if the profile is distorted e. g. by echoes from the distal wall.

The Doppler angle (the angle between the flow and the beam directions) was chosen between  $60^\circ$  and  $70^\circ$  (respectively  $250^\circ$  and  $240^\circ$ ) for all the flow adapters. When choosing the angle, one has to consider maximum and minimum measurable flow velocities (small angles for slow flow velocities, steep angles for high flow velocities) and the averaging, which decreases with the Doppler angle (McArdle and Newhouse, 1996).

#### 4.3.4. Oscilloscope

In order to monitor the transmitted pulse (second transducer connected directly to the oscilloscope) or the RF signal (from the corresponding connector of the UVP), a Yokogawa (Tokyo, Japan) Digital Oscilloscope (DL1520L, two channels, 150 MHz bandwidth, 8 bit, 200 MS/s) was used. This oscilloscope was connected via serial port (RS-232, only 9600 baud) to the PC. A part of the MATLAB software described in section 4.4 acquires the whole waveform data periodically to calculate the velocity of sound from the distance of the PRF-Trigger from the UVP and the reception of the pulse in a similar way as described in da Silva *et al.* (1992) with the difference that a linear instead of a quadratic fit of one cycle was used to determine the point of the zero crossing of the signal. Further the *y*-scaling (volts per division) and the horizontal time shift are automatically

adjusted to keep the pulse in the center of the region of interest acquired from the oscilloscope in case the velocity of sound respectively the attenuation changes during a measurement.

### 4.3.5. Pressure sensors

For the measurements of absolute pressures at upstream and downstream of the flow adapter during the flow of model and cocoa butter suspensions, two different pairs of pressure sensors were used. It would be preferable to measure directly the pressure difference but this is technically very difficult because of the distance of at least one meter between the two measurement points and additional problems with the fluids, e. g. the crystallization of cocoa butter at room temperature. For the cocoa butter, two Kulite (Leonia, NJ, USA) XTM-190M-3.5BARVG pressure transducers were used. These sensors have a diameter of only 3.8 mm of the diaphragm. For the model suspensions, two sensors from Svenska Industri Instrument AB Gothenburg Sweden of the type S-10, 0-4 Bar were used.

### 4.3.6. Temperature sensors

Conventional Pt100 resistance temperature sensors were used for the cocoa butter while thermo elements (Pentronic, Gunnebo, Sweden) were installed in the model suspension flow loop.

## 4.4. Data acquisition software

A MATLAB (MathWorks, Natick, MA, USA) based application with a Graphical User Interface (GUI) was developed for (i) data acquisition (UVP-Duo, Oscilloscope, pressure and temperature sensors) automation, (ii) flow profile estimation, (iii) calculation of rheological parameters from profile shape and pressure drop, (iv) data post processing and (v) data visualization. The corresponding data flow chart is given in figure 4.7.

During the data acquisition, the software modules controlling the data acquisition from the hardware run in independent threads using timers. After the data acquisition (typically 20 to 100 profiles), the acquired data are saved in a compressed MATLAB file and visualized. Alternatively to the data acquisition, it is also possible to read a saved MATLAB file, mfprof files saved with the Met-Flow UVP Monitor application or raw binary data files. So the application is suited for



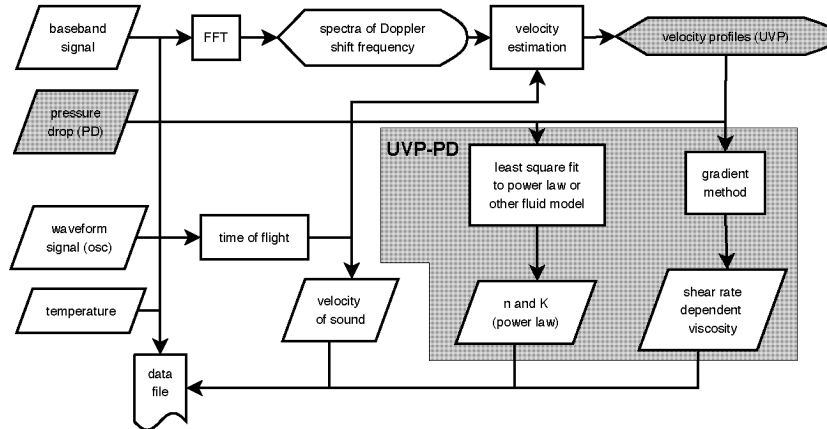


**Figure 4.7.:** Data flow chart with the data inputs on the left side and the processing resulting in the rheological parameters.

in-line monitoring (making repeated acquisitions) as well as for post-processing of measured data.

When the data is available in memory, the flow velocity is estimated from the power spectra of the baseband signal and it is possible to either fit the flow profiles and the pressure drop to a fluid model such as power law or calculate the rheological parameters using the gradient method proposed in section 3.2.

The following data visualizations are possible: (i) arbitrary channels and repetitions of the baseband signal (in- and co-phase) and the power spectra of a single channel of a single profile or the average over several profiles including a visualization of the velocity estimation; (ii) channel wise data such as velocity profile (from spectral analysis or time domain), RMS and peak-peak amplitude of the baseband signal, the amplitude of the RF signal, the signal to noise ratio from the power spectra, the first and the second derivative of the velocity profile; (iii) results of the rheological calculations such as  $\dot{\gamma}$ ,  $\eta$ ,  $\tau$ , plug radius and the profile resulting from the fit to a fluid model; (iv) temporal variation of pressure, pressure drop, temperatures, velocity of sound, transmitted signal amplitude, maximum flow velocity and the rheological parameters from the fluid model fitting such as  $n$  and  $K$ ; (v) animations of the development of the profile over time; (vi) surface plots of the amplitude of the baseband signal (either individual pulse echoes or the RMS over time) and the flow velocity profiles over time; (vii) comparison of features such as simply the flow profiles from several data files.

The whole application consists of approximately 12 000 lines of MATLAB code, which were written over more than two years with over 300 commits to the revision control system. MATLAB proved to be a very suitable environment for data processing as its base data type is a matrix. A similar application also using

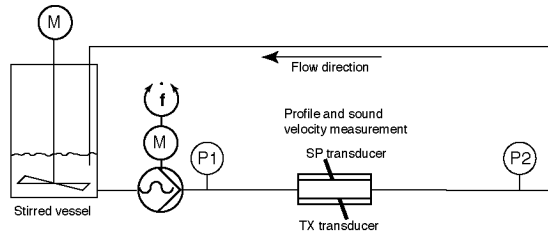


**Figure 4.8.:** Flow loop for the model suspension.

the combination of MATLAB and the UVPAX ActiveX library from Met-Flow was developed by Wiklund (2007). Also Choi *et al.* (2005) presented a MATLAB based application for the velocity estimation from the baseband signal with FFT and the calculation of the rheological parameters. Tortoli (Fidanzati *et al.*, 2005; Guidi *et al.*, 2000) and Jensen (Pedersen *et al.*, 2003) also based some of their data processing applications on MATLAB.

## 4.5. Process flow loops

### 4.5.1. Model suspension

The flow loop (figure 4.8) consisted of a stirred vessel, a pump (positive displacement pump, Model No. 75NDM, AB Record Material, Sollentuna, Sweden) a straight pipe with an inner diameter of 22.5 mm and length of 2.7 m containing the two pressure sensors separated by the length  $L = 1.85$  m and the flow adapter for the ultrasound transducers. Thermo elements were installed in the vessel and after the pump. The Reynolds Number  $Re = \rho \bar{v} 2R / \eta$  was kept below a value of 100 thus in a laminar regime. According to Durst *et al.* (2005) the maximum development length is then only 0.12 m.

**Experimental procedure** The suspension of a known concentration was allowed to circulate at a certain volume flow rate through the flow loop by the pump until steady-state was reached before measurements were made. The experiments were repeated at different flow rates and particle concentrations with different size distributions at room temperature (about 20 °C).

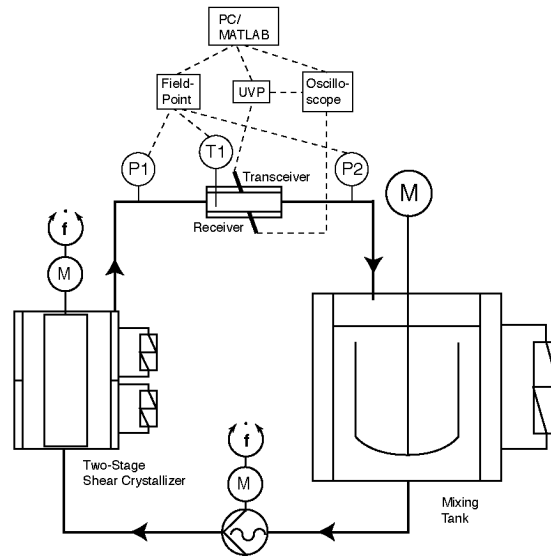


**Figure 4.9.:** Scheme of the shear crystallizer flow loop, its instrumentation and data acquisition devices. P1, P2: pressure transducers; T1: thermocouple; M: motor; f: frequency transformer.

#### 4.5.2. Cocoa butter shear crystallization

As described in section 4.1.3 the crystal conformation depends on the crystallization conditions. A shear crystallization process developed by Yuantong Zeng at our laboratory (Zeng, 2000) creates a crystal suspension with a high amount of  $\beta_{VI}$  crystals (nomenclature according to Larsson Larsson (1966)) which are desired in the chocolate production described in the subsequent section.

Experiments were carried out at Bühler AG in Uzwil (Switzerland) using the fully temperature controlled flow loop shown in figure 4.9. It consists of a stirred cocoa butter feed tank, a two stage shear crystallizer and the measurement pipe section with an inner diameter of 16 mm. The two pressure sensors P1 and P2 are 1 m apart from each other. The shear crystallizer is a scraped heat exchanger. Molten cocoa butter is super cooled at the wall temperature of 15 °C in the first stage and 26 °C in the second stage. First the  $\alpha$  crystal form is built. As the solid fat content rises, the shear stress  $\tau$  is increasing accordingly. Thereby the transformation from  $\alpha$  to the  $\beta_V$  crystal form is promoted. In the 2nd stage of the shear crystallizer the suspension is conditioned and a partial transformation from  $\beta_V$  to the most stable  $\beta_{VI}$  takes place. The details of the shear crystallization process can be found in Zeng (2000).

### 4.5.3. Seeded chocolate suspension

Measurements in chocolate were carried out in a compact shear crystallizer from Bühler AG (Uzwil, Switzerland). This contained two independent flow loops for chocolate and one cocoa butter shear crystallization unit described in the previous section. A small quantity (0.2 to 2%) of the pre-crystallized cocoa butter was added to the flowing chocolate using a dosage pump followed by a static mixer. This seeding process with preconditioned cocoa butter crystals of the desired conformation replaces the tempering process used in conventional chocolate production.

With a mass flow rate of 380 kg/h, a pipe diameter of 16 mm, a density of 1200 kg/m<sup>3</sup> and viscosity of 3.5 Pas of the chocolate, the Reynolds number  $Re$  was 2.4 for the measurements. Thus the flow was laminar and the entry lengths for a fully developed flow after a change in the diameter of the pipe is rather short (in the order of a few millimeters).

The flow adapter, which was used for the cocoa butter, was placed in the flow loop after the end of the static mixer. As chocolate was highly attenuating, a part of the measurements were made with one of the transducer edges in flush with the inner pipe wall as also shown by Markou and Ku (1991). If the transducer was pulled back 17 mm to avoid measurements in the near field, the penetration depth inside the pipe did not even reach the center of the pipe. In addition, for the seeding experiments the static chocolate in the cavity in front of the transducer would not have correspond to the dynamically changing chocolate in the pipe volume.

# 5. Results and Discussion

The two major series of measurements presented in this work are the ones in the model suspensions conducted together with J. Wiklund at SIK in Gothenburg, Sweden (section 5.1) and the ones monitoring the shear crystallization process of cocoa butter installed at Bühler AG in Uzwil (section 5.2). In addition to the cocoa butter crystal suspension the flow of molten chocolate was measured, too (section 5.3).

To support the mentioned measurements the influence of the concentration of gas bubbles on the quality of the measured profiles was investigated in an open channel flow at the Hydraulic Constructions Laboratory of EPFL (section 5.4). The interrelation of the measurement quality and measurement parameters was examined in a rotating cylinder (section 5.5).

## 5.1. Model suspensions

This section describes the evaluation of the UVP-PD in-line method to determine experimentally the influence of particle concentration and size distributions on the rheology of flowing suspensions of polyamide particles in rapeseed oil which were described in section 4.1.1.

### 5.1.1. Polyamide particle size distribution

Figure 5.1 shows microscopy pictures of two monodisperse suspensions while figure 5.2 shows the distributions of the volume mean diameters of the dry particles determined using Laser diffraction (see chapter 4.2.3). The smallest particles (full line) had an average diameter of 11  $\mu\text{m}$ , size ranging from about 1 to 20  $\mu\text{m}$ . The largest particles (broken line) had an average diameter of about 90  $\mu\text{m}$ , the size ranging from 40 to 250  $\mu\text{m}$ .

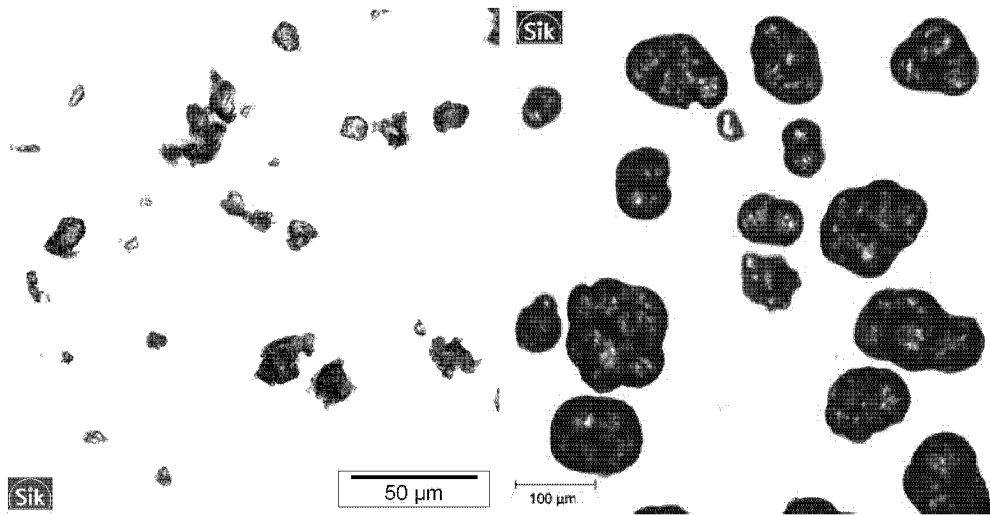


**Figure 5.1.:** Microscopic image of 11  $\mu\text{m}$  (left side) and 90  $\mu\text{m}$  (right side) polyamide particles in rapeseed oil. Pictures courtesy of SIK Gothenburg, Sweden.

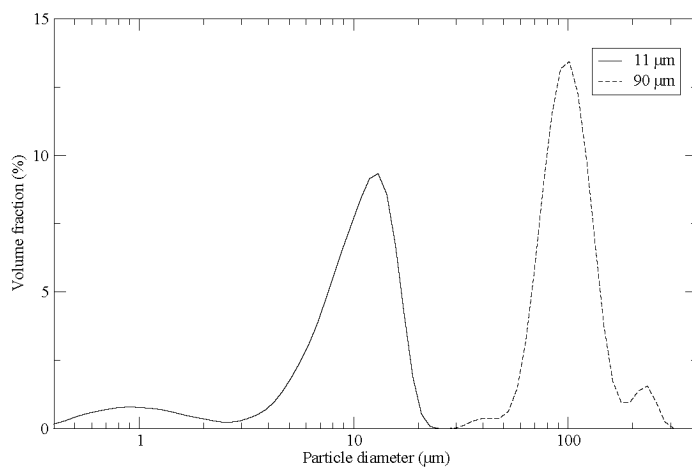


**Figure 5.2.:** Distributions of volume mean diameters for two mean diameter (11 and 90  $\mu\text{m}$ ) polyamide particles (dry powder) measured using Coulter particle size analyzer.

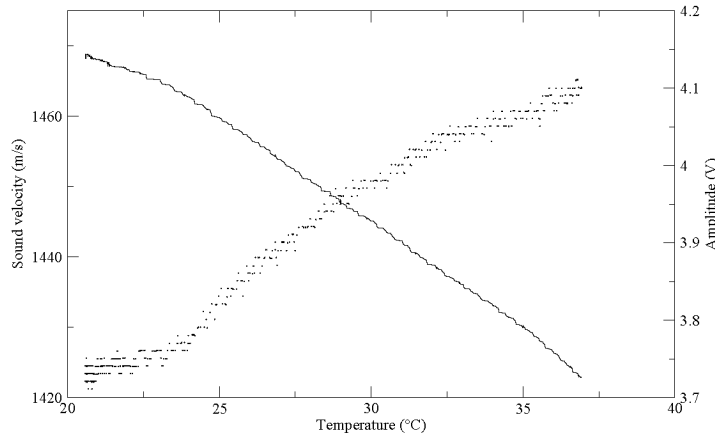


**Figure 5.3.:** Velocity of sound (full line) and throughput amplitude (dots) in function of temperature for rapeseed oil. (Rivara, 2004).

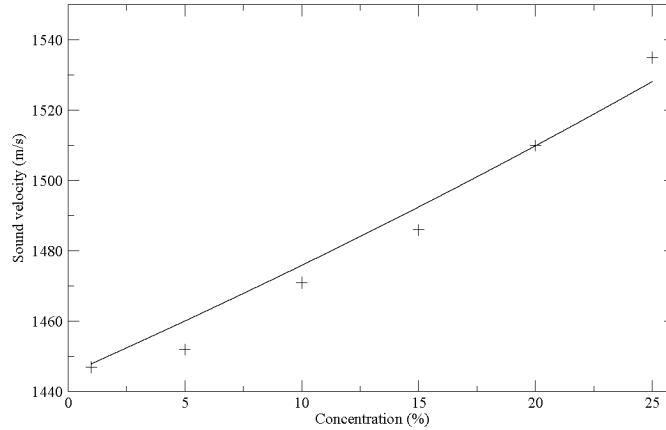
### 5.1.2. Velocity of sound

Figure 5.3 shows the acoustic properties of a rapeseed oil (from Florin AG, Muttenz, Switzerland, different from the one used for the polyamide suspension) in function of the temperature. The curve is not linear over the whole range, in the first part, approximately until 24°C, the temperature coefficient is  $-1.6 \text{ m/s/K}$  and for the remaining part it is  $-3.0 \text{ m/s/K}$ .

The velocity of sound in function of the concentration of the  $11 \mu\text{m}$  polyamide particles is shown in figure 5.4. With the Wood (3.27) and the Urick equation (3.28) on page 30 it is possible to calculate the compressibility of the rapeseed oil ( $0.526 \times 10^{-9} \text{ 1/Pa}$ ) and then fit the Urick equation into the measured dependency of velocity of sound on particle concentration resulting in a compressibility of  $0.253 \times 10^{-9} \text{ 1/Pa}$  for the polyamide.

With increasing concentration the velocity of sound increases faster for the suspension with the  $11 \mu\text{m}$  particles compared to the  $90 \mu\text{m}$  particles (see tables 5.1, 5.2 and 5.3). As the two particle sizes are at the border of the long and intermediate wavelength regime it is difficult to apply any of the models mentioned in section 3.3.4.3.

The the sedimentation of the  $90 \mu\text{m}$  particles in the cavities in front of the transducers (see also section 4.3.3) can be monitored by the development of the sound velocity over time. Figure 5.5 shows the sound velocity during a measurement in



**Figure 5.4.:** The measured velocity of sound (symbols) in function of the particle concentration and result from the fit to the Urlick equation (full line).

the highest concentrated system measured (25 %) starting several seconds after the cavities were cleaned manually. The sound velocity increases approximately 3 m/s per minute which corresponds to an increase of the concentration in the two cavities of 4.5 % per minute eventually reaching a concentration of 50 %. This value agrees with the nearly solid plug attached to the transducer front plate that was observed when the transducer was removed for cleaning.

### 5.1.3. Influence of particle migration

Particle migration due to velocity gradients during the flow of suspensions in pipes, channels and Couette geometries has been discussed in detail in section 3.1.4. The relevance of particle migration for the present measurements can be estimated from the article by Butler and Bonnecaze (1999) who used particles of acrylic glass with a density  $\rho = 1170 \text{ kg/m}^3$  and a size distribution between 125 and 180  $\mu\text{m}$  at a volume fraction of  $\phi = 0.25$ . The inner pipe diameter  $2R$  was 204 mm and the suspension viscosity  $\eta = 0.730 \text{ Pa}\cdot\text{s}$ . The concentration profiles were measured between 3 and 15 m after an in-line mixer. The value of the particle Reynolds number  $Re_p$  was given as  $2.2 \times 10^{-3}$ . The mean flow velocity (or flow rate), which was not given, can be determined from  $Re_p = Re(a/R)^2$  (Matas *et al.*, 2004) with the pipe flow Reynolds number  $Re = 2\rho\bar{v}R/\eta$  as  $\bar{v} = 1.7 \text{ m/s}$ . For the present work, 90  $\mu\text{m}$  polyamide particles in rapeseed oil ( $R = 11 \text{ mm}$ ,  $\eta = 0.3 \text{ Pa}\cdot\text{s}$ ,  $\rho = 910 \text{ kg/m}^3$ ,  $a = 45 \mu\text{m}$ ,  $\bar{v} = 300 \text{ mm/s}$ ) is the system most prone



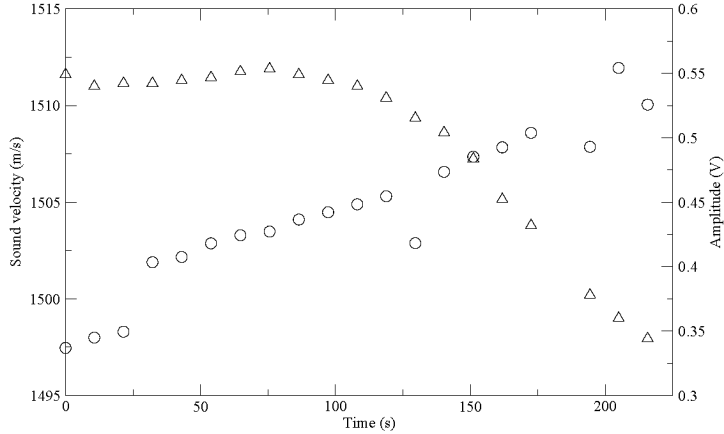


**Figure 5.5.:** The velocity of sound ( $\circ$ ) and throughput signal amplitude ( $\triangle$ ) in function of time during a measurement of the 25%/90  $\mu\text{m}$  suspension. The fluctuations in the sound velocity (which are not visible the amplitude) are due to the automatic scaling of the time resolution on the oscilloscope.

to particle migration. The particle Reynolds number  $Re_p$  is  $0.32 \times 10^{-3}$  which is about an order of magnitude lower than that of Butler and Bonnecaze. In one of the measurements of Butler and Bonnecaze,  $Re_p$  was varied from  $3.7 \times 10^{-3}$  to  $20 \times 10^{-3}$  and the resulting concentration in the center of the pipe after 15 m was increased from 0.34 to 0.41 for an average  $\phi$  of 0.25. Thus with the even much lower  $Re_p$  of  $0.32 \times 10^{-3}$  the effect should be further reduced. For  $Re_p = 2.2 \times 10^{-3}$ , the particle concentration measured by Butler and Bonnecaze 3 m after the mixer varied between 0.22 at the pipe wall and 0.29 at the center of the pipe. So for the present work, considering the lower  $Re_p$  and distance of only 1.5 m between pump and ultrasonic profile measurement, the concentration gradient over the pipe diameter should be rather small. Nevertheless one has to consider that the particle concentration in a thin layer at the wall, where the velocity gradient reaches its maximum, the concentration drops significantly.

The value of the Péclet number  $Pe$  (equation (3.6) on page 18) varies between 237 and  $1.06 \times 10^6$  for the particles of 11 and 90  $\mu\text{m}$  diameter respectively, thus Brownian motion is negligible compared with sedimentation. The corresponding Stokes sedimentation velocity  $v_s$  given in equation (3.8) varies between 0.10 and 7.0  $\mu\text{m/s}$  and thus the particles move 0.17 and 27  $\mu\text{m}$  respectively in vertical direction between the stirred tank and the profile measurement section as determined using equation (3.7) and the same flow parameters given in the previous paragraph. Thus the effect of particle sedimentation is negligible on the in-line

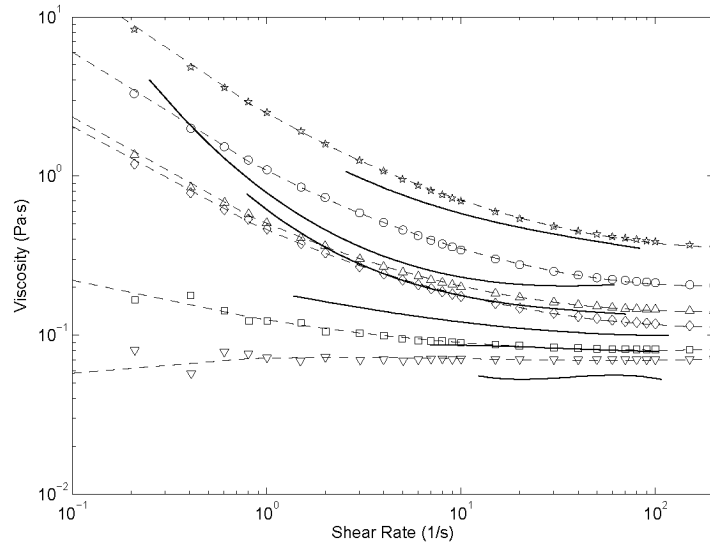


**Figure 5.6.:** Variation with shear rate  $\dot{\gamma}$  in the viscosity  $\eta$  of suspensions of 11  $\mu\text{m}$  diameter polyamide particles of different concentrations (% by volume) in rapeseed oil. Symbols: Data measured using off-line rheometer ( $\nabla$ : 1%;  $\square$ : 5%;  $\diamond$ : 10%;  $\triangle$ : 15%;  $\circ$ : 20%;  $\star$ : 25% joined by dashed lines). Full lines: Variation obtained by the in-line UVP-PD technique with gradient method.

rheological properties obtained.

#### 5.1.4. Off-line rheometry

The variations with shear rate in the viscosities of suspensions of 11  $\mu\text{m}$  diameter polyamide particles of different concentrations (% by volume) in rapeseed oil measured using an off-line rheometer are represented by symbols in Figure 5.6. The 1% particle suspension ( $\nabla$ ) can be seen to be Newtonian since its viscosity is independent of the shear rate and has a constant value of about 0.07 Pa·s. For each of the higher concentrations of the polyamide particles, the apparent viscosity can be seen to decrease by more than an order of magnitude as the shear rate is reduced by three orders of magnitude attaining a constant viscosity at higher shear rates indicating shear thinning behaviour. At lower shear rates such as 0.1 1/s, the viscosity of 25% particle suspension ( $\star$ ) is about an order of magnitude (1.5 Pa·s) larger than that (0.2 Pa·s) for the 5% suspension ( $\square$ ).

In contrast, the suspensions of the 90  $\mu\text{m}$  diameter polyamide particles even up to 20% concentration shown in figure 5.7 appear to be virtually Newtonian for shear

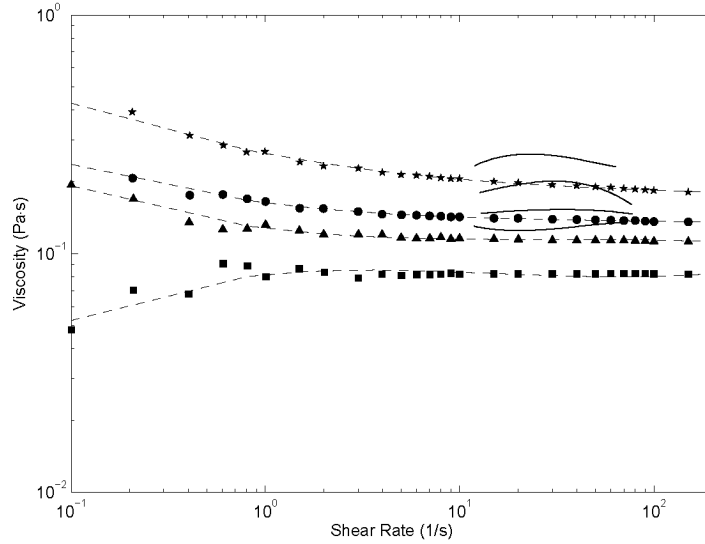


**Figure 5.7.:** Variation with shear rate  $\dot{\gamma}$  in the viscosity  $\eta$  of suspensions of 90  $\mu\text{m}$  diameter polyamide particles of different concentrations (% by volume) in rapeseed oil. Symbols: Data measured using off-line rheometer ( $\blacksquare$ : 5%;  $\blacktriangle$ : 15%;  $\bullet$ : 20%;  $\star$ : 25% joined by dashed lines). Full lines: Variation obtained by the in-line UVP-PD technique with gradient method.

rates larger than 1 1/s, although the absolute value of the viscosity increases with increase in the concentration.

Symbols in figure 5.8 show the variations in viscosity with shear rate for a total concentration of 25% for a bimodal mixture of particles of 11 and 90  $\mu\text{m}$  diameter measured using the off-line rheometer. At a given shear rate, the viscosity of the suspension is the highest for the unimodal particles of smallest diameter of 11  $\mu\text{m}$  ( $\star$ ). In contrast, the viscosity is the lowest for the unimodal particles of largest diameter of 90  $\mu\text{m}$  ( $\blackstar$ ). For instance, the viscosity of 11  $\mu\text{m}$  particle suspension at a shear rate of 1 1/s is about an order of magnitude larger than that for the 90  $\mu\text{m}$  particle suspension. This is due to the fact that in unit volume of suspension, the number of 11  $\mu\text{m}$  particles will be  $(90/11)^3 = 548$  times larger than that of 90  $\mu\text{m}$  particles. Thus the higher the number density of particles, higher is the resistance to flow not only due to immobilization of the fluid by particles in the suspension but also due to particle interactions (Krieger and Dougherty, 1959; Frankel and Acrivos, 1967; Farris, 1968; Chong *et al.*, 1971; Sengun and Probstein, 1989c; Hoffman, 1992; Stickel and Powell, 2005). Consequently, the viscosity of the suspension of bimodal particles decreases as the concentration of 11  $\mu\text{m}$  particles is reduced while the concentration of the 90  $\mu\text{m}$  particles is increased keeping the total concentration constant. This behaviour was also observed experimentally

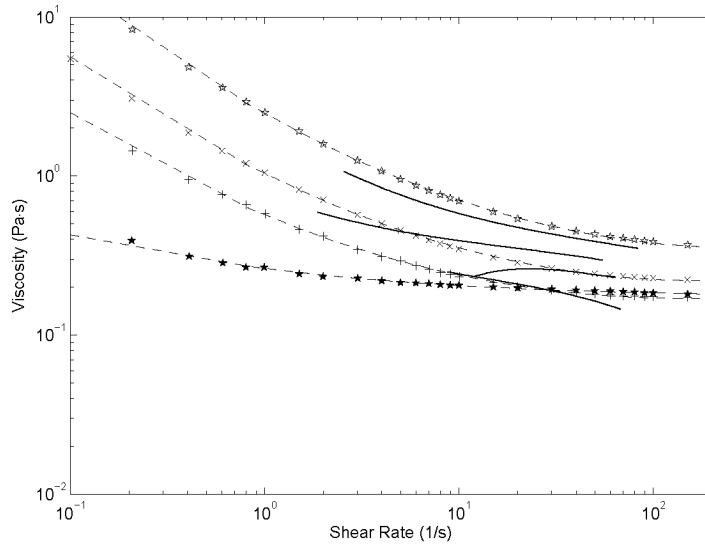


**Figure 5.8.:** Variation with shear rate in viscosity of suspensions of a constant total concentration of 25% by volume of a bimodal mixture of 11 and 90  $\mu\text{m}$  polyamide particles in rapeseed oil. Symbols: Data measured using off-line rheometer ( $\times$ : 15%;  $+$ : 20% joined by dashed lines correspond to 11  $\mu\text{m}$  particles.  $\star$  and  $\blackstar$  represent those in figures 5.6 and 5.7). Full lines: Variation obtained by the in-line UVP-PD technique with gradient method.

by Chang and Powell (1994), who compared with their (Chang and Powell, 1993) two-dimensional simulation results. Several authors investigated the rheology of bimodal suspensions (Gondret and Petit, 1997; Sengun and Probstein, 1997; Probstein *et al.*, 1994; Shapiro and Probstein, 1992; Poslinski *et al.*, 1988; Sengun and Probstein, 1989a,b).

### 5.1.5. Velocity profiles and in-line rheometry

Figures 5.9 and 5.10 respectively show two typical velocity profiles along the radius (channel distance  $d$  is given in table 5.1) of the pipe during the flow of suspensions of 5 and 25 % by volume of 11  $\mu\text{m}$  diameter polyamide particles in rapeseed oil measured using the UVP technique. The quality of these profiles can be seen to be good. The corresponding volume flow rates  $Q$  determined based on the first half of the velocity profiles are 6.76 and 8.23  $\ell/\text{min}$  respectively. The velocity profile for the 25% by volume of 90  $\mu\text{m}$  diameter polyamide particles in rapeseed oil suspension flowing at  $Q = 5.95 \ell/\text{min}$  is shown in figure 5.11. Similarly, figures 5.12 (6.00  $\ell/\text{min}$ ) and 5.13 (6.05  $\ell/\text{min}$ ) show two typical examples of the velocity

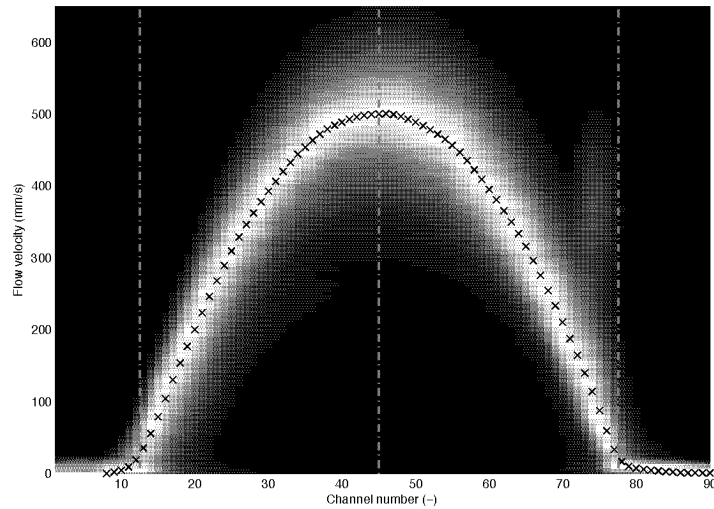


**Figure 5.9.:** Radial velocity profile in the pipe during the flow of a suspension of 5% by volume of 11  $\mu\text{m}$  diameter polyamide particles in rapeseed oil. For the measurement parameters see table 5.1.

profiles for a suspension of a constant total concentration of 25% by volume of a bimodal mixture of 20% 11  $\mu\text{m}$  and 5% 90  $\mu\text{m}$  polyamide particles. The quality of the velocity profiles shown in figures 5.11, 5.12 and 5.13 is not as good as that of the 11  $\mu\text{m}$  diameter particle suspensions (figures 5.9 and 5.10). The reduction in the quality of the former profiles could be due to the accumulation of large particles in the cavity before the transducers as mentioned in sections 4.3.3 and 5.1.2.

Tables 5.1, 5.2 and 5.3 give a summary of the values of measured flow ( $Q$ ,  $\Delta Q$  and  $\Delta P/L$ ), acoustic ( $c$ ) and UVP (number of profiles:  $N_p$ ; number of pulse repetitions:  $N_r$ ; channel distance:  $d$ ; emission frequency:  $f$  and pulse repetition frequency:  $f_{pr}$ ) parameters for suspensions of different concentrations  $\phi$  and size distributions of polyamide particles.  $\Delta Q$  is the difference in the volume flow rates determined using the first and second half of the velocity profile. It can be seen that the pressure drop  $\Delta P/L$  increases with increase in the volume flow rate  $Q$  and concentration of particles  $\phi$ , the highest being for the smallest diameter particles. The velocity of sound  $c$  also increases with increase in the concentration of the particles  $\phi$ , the highest being also for the smallest particles.

The precise locations of the pipe wall and pipe center from the actual position of the transducer (see section 4.3.2) could not be directly determined and so are obtained using the profile data. Because of the minimum channel distance of 360  $\mu\text{m}$  channel based methods as e.g. wall detection from the velocity variance over a series of individual profiles have the disadvantage of significant rounding

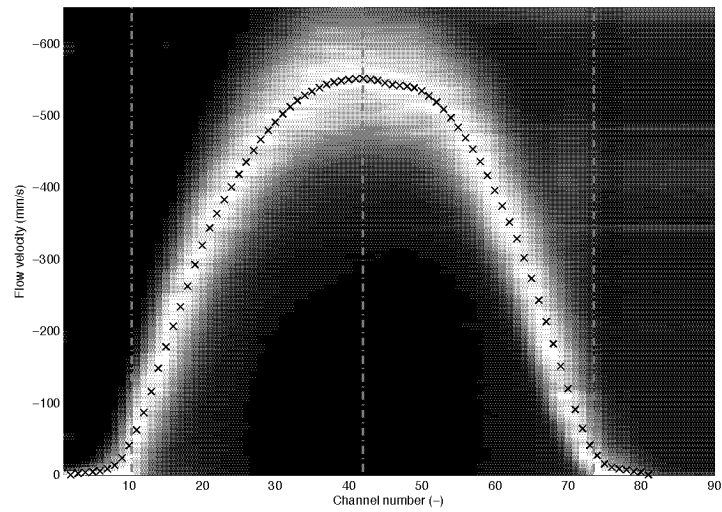


**Figure 5.10.:** Radial velocity profile in the pipe during the flow of a suspension of 25% by volume of 11  $\mu\text{m}$  diameter polyamide particles in rapeseed oil. For the measurement parameters see table 5.1.

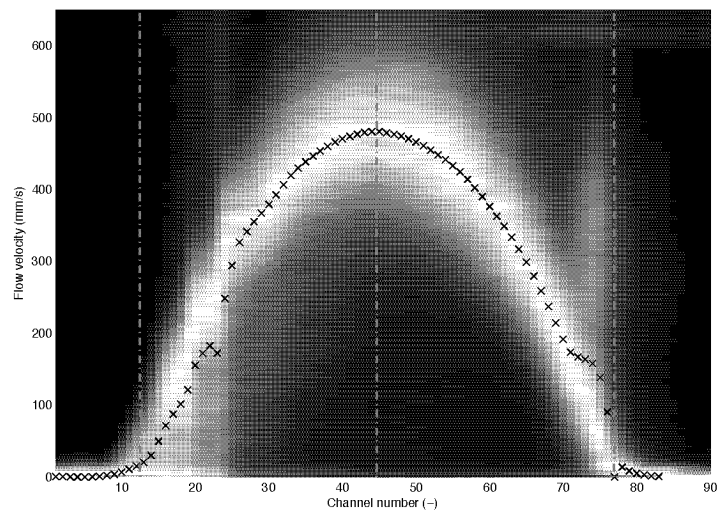


**Figure 5.11.:** Radial velocity profile in the pipe during the flow of a suspension of 25% by volume of 90  $\mu\text{m}$  diameter polyamide particles in rapeseed oil. For the measurement parameters see table 5.2.

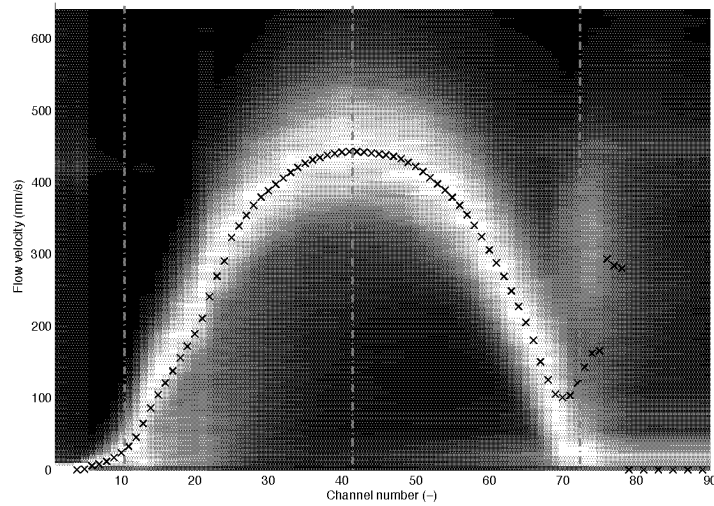


**Figure 5.12.:** Radial velocity profile in the pipe during the flow of a suspension of a constant total concentration of 25% by volume of a bimodal mixture of 20% 11  $\mu\text{m}$  and 5% 90  $\mu\text{m}$  polyamide particles in rapeseed oil. For the measurement parameters see table 5.3.

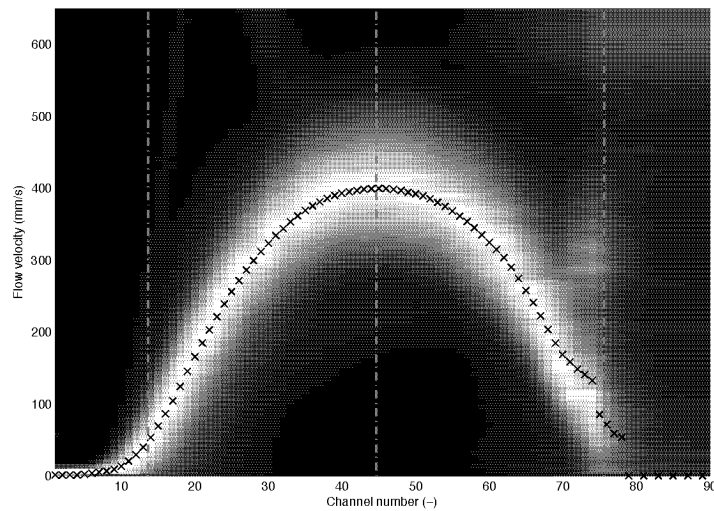


**Figure 5.13.:** Radial velocity profile in the pipe during the flow of a suspension of a constant total concentration of 25% by volume of a bimodal mixture of 20% 11  $\mu\text{m}$  and 5% 90  $\mu\text{m}$  polyamide particles in rapeseed oil. For the measurement parameters see table 5.3.

## 5. Results and Discussion

**Table 5.1.:** Values of measured flow ( $Q$ ,  $\Delta Q$  and  $\Delta P/L$ ), acoustic ( $c$ ) and UVP ( $N_p$ ,  $N_r$ ,  $d$  and  $f_{pr}$ ) parameters for suspensions of different concentrations  $\phi$  of 11  $\mu\text{m}$  diameter polyamide particles in rapeseed oil. The type (Td) of ultrasound transducers with a frequency  $f = 4$  MHz are also listed. The average of the ratio of wavelength to particle size is 32 for the listed measurements.

$Q$ $\ell/\text{min}$	$\Delta P/L$ $\text{Pa}/\text{m}$	$\Delta Q$ $\ell/\text{min}$	$c$ $\text{m}/\text{s}$	Td –	$N_p$ –	$N_r$ –	$d$ $\text{mm}$	$f_{pr}$ $\text{kHz}$	fig. –
$\phi = 25\%$									
7.62	6037	0.0691	1535	SP	100	256	0.374	2.4	
8.23	6585	0.0706	1535	SP	100	256	0.374	2.4	5.10
$\phi = 20\%$									
2.98	1161	0.0417	1510	SP	100	256	0.372	1.25	
3.26	1161	0.0148	1510	TX	100	256	0.377	1.23	
3.38	1134	0.1195	1510	TX	100	256	0.372	1.25	
6.08	3955	0.2060	1510	SP	100	256	0.373	2.93	
6.47	2914	0.3909	1510	TX	100	256	0.377	3.16	
6.93	2750	0.5755	1510	TX	100	256	0.376	3.17	
7.64	3353	1.0051	1510	TX	100	256	0.376	3.17	
$\phi = 15\%$									
6.85	2038	0.1348	1486	SP	100	256	0.371	3.26	
7.03	2257	0.0789	1486	SP	100	256	0.372	3.23	
7.21	2148	0.0494	1486	TX	100	256	0.372	3.24	
7.34	2038	0.1192	1486	SP	100	256	0.372	3.24	
$\phi = 10\%$									
3.69	887	0.0044	1471	TX	100	256	0.368	1.28	
3.85	887	0.1559	1471	SP	100	256	0.368	1.28	
6.92	1600	0.1279	1471	TX	100	256	0.368	2.5	
7.27	1654	0.2573	1471	SP	100	256	0.368	2.5	
10.02	2367	0.1804	1471	TX	100	256	0.368	3.53	
10.27	2257	0.1831	1471	SP	100	256	0.368	3.81	
11.07	2421	0.2490	1471	SP	100	256	0.368	3.81	
11.25	2148	0.1945	1471	SP	100	256	0.368	3.81	
$\phi = 5\%$									
4.07	778	0.0019	1452	TX	100	256	0.363	1.38	
4.11	778	0.0871	1452	SP	100	512	0.363	1.38	
6.76	1271	0.0447	1452	TX	100	256	0.363	2.75	5.9
6.91	1326	0.1030	1452	SP	100	256	0.363	2.75	
9.56	1819	0.1685	1452	TX	100	256	0.363	3.57	
9.86	1819	0.2200	1452	SP	100	256	0.363	3.57	
$\phi = 1\%$									
6.77	915	0.1068	1447	TX	50	256	0.362	2.54	
6.91	942	0.1262	1447	SP	50	256	0.362	2.54	
10.34	1326	0.1410	1447	TX	50	256	0.362	3.87	



**Table 5.2.:** Values of measured flow ( $Q$ ,  $\Delta Q$  and  $\Delta P/L$ ), acoustic ( $c$ ) and UVP ( $N_p$ ,  $d$ ,  $f$  and  $f_{pr}$ ) parameters for suspensions of different concentrations  $\phi$  of 90  $\mu\text{m}$  diameter polyamide particles in rapeseed oil. SP type of ultrasound transducer was used and  $N_r = 256$ . The ratio of wavelength to particle size is 8 and 4 for 2 respectively 4 MHz.

$Q$	$\Delta P/L$	$\Delta Q$	$c$	$N_p$	$d$	$f$	$f_{pr}$	fig.
$\ell/\text{min}$	$\text{Pa}/\text{m}$	$\ell/\text{min}$	$\text{m}/\text{s}$	–	$\text{mm}$	$\text{MHz}$	$\text{kHz}$	–
$\phi = 25\%$								
5.95	3681	0.4079	1500	200	0.367	2	1.42	5.11
$\phi = 20\%$								
6.24	2969	0.2703	1486	100	0.373	2	1.39	
6.46	2860	0.1279	1486	100	0.372	2	1.45	
9.73	3024	0.1443	1486	100	0.387	2	1.39	
$\phi = 15\%$								
6.77	2476	0.2029	1477	100	0.369	2	1.41	
7.70	2476	0.0399	1477	100	0.369	2	1.41	
$\phi = 5\%$								
6.20	2038	0.1261	1456	200	0.364	4	2.41	
6.38	2038	0.1394	1456	100	0.364	4	2.41	

**Table 5.3.:** Values of measured flow ( $Q$ ,  $\Delta Q$  and  $\Delta P/L$ ), acoustic ( $c$ ) and UVP ( $N_p$ ,  $d$ ,  $f$  and  $f_{pr}$ ) parameters for suspensions of different concentrations  $\phi$  of bimodal sized polyamide particles in rapeseed oil.  $N_r = 256$ .

$Q$	$\Delta P/L$	$\Delta Q$	$c$	Td	$N_p$	$d$	$f$	$f_{pr}$	fig.
$\ell/\text{min}$	$\text{Pa}/\text{m}$	$\ell/\text{min}$	$\text{m}/\text{s}$	–	–	$\text{mm}$	$\text{MHz}$	$\text{kHz}$	–
$\phi = 20\%$ of 11 $\mu\text{m}$ + 5% of 90 $\mu\text{m}$									
6.00	4229	0.0407	1525	SP	100	0.381	2	1.15	5.12
6.05	3901	0.1854	1525	SP	300	0.381	4	2.93	5.13
$\phi = 15\%$ of 11 $\mu\text{m}$ + 10% of 90 $\mu\text{m}$									
5.91	2148	0.2056	1520	SP	100	0.76	2	1.18	
6.66	2421	0.0705	1520	TX	100	0.76	2	2.31	
6.74	2312	0.0965	1520	SP	100	0.76	2	1.18	
8.03	2531	0.0475	1520	SP	100	0.76	2	1.57	
8.13	2586	0.2022	1520	SP	100	0.76	2	1.57	

off error as discussed later. The following method was, therefore, found to be the best suited. A fourth order polynomial was used to fit the measured profile data where from the second half of the profile only the monotonically decreasing part was used. The center was then determined from the apex of the polynomial fit. For the following two calculations a spline interpolation of the measured profile between the determined center and pipe wall position is used. The number of channels from the measurement is thereby not changed.

Next the gradients and viscosities are calculated according the equations given in section 3.2.4. For the shear rate, only the points between the first maximum from the pipe wall and the maximum viscosity towards the pipe center are used. For the power law rheological model, the experimental velocity profile data are least squares fitted to equation (3.13) using the measured flow profile and pressure drop  $\Delta P$  in the pipe section of length  $L$  to obtain the values of  $n$  and  $K$ . The radial variations in shear rate and the viscosity are then calculated using equations (3.14) and (3.15).

### 5.1.6. Comparison between in-line and off-line rheometry

Figure 5.14 compares the variation in viscosity with shear rate determined by the UVP-PD in-line rheometry (full and dashed lines correspond to velocity gradient and power law methods) with that measured using the off-line rheometer (dotted lines) for the suspensions of 5 and 25 % (lower and upper set of curves correspond to the velocity profile data shown in figures 5.9 and 5.10) particles of 11  $\mu\text{m}$  diameter in rapeseed oil. The three in-line curves (in each of the lower and upper set of curves) correspond to three values of the position of the pipe wall chosen in increments of 180  $\mu\text{m}$ , which is half of the minimum channel distance (numerical values of  $K$  and  $n$  are given in table 5.4). It is clear that the power law predicts viscosities much lower than those measured by off-line rheometer for shear rates (1 to 101/s). In contrast, the alternate gradient method predicts values of viscosities close to those measured by off-line rheometer. In addition, the off-line rheometric data show that the suspension of 5 % particles is Newtonian for shear rates larger than 101/s. However, the values of  $n$  determined by the power law model (see table 5.1) are greater than unity indicating shear thickening behaviour, which is unrealistic. The gradient method yielded virtually a constant viscosity. The variation in the in-line rheometric viscosity associated with the accuracy of the pipe wall position is insignificant for shear rates greater than about 20 1/s. These conclusions appear to be reasonable since the velocity profiles shown in figures 5.9 and 5.10 are virtually symmetric which is realistic and only data points between the inflection point of the velocity and the pipe center were used in order

**Table 5.4.:** Effect of wall position  $X$  (relative to the determined value) on the values of the power law parameters  $n$  and  $K$  for two different concentrations ( $\phi$ ) of 11  $\mu\text{m}$  diameter particles in rapeseed oil as shown in figure 5.14

$\phi$	$X$	$n$	$K$
–	$\mu\text{m}$	–	$\text{Pa}\cdot\text{s}^n$
5 %	–180	1.16	0.0410
5 %	0	1.03	0.0689
5 %	+180	0.91	0.1106
25 %	–180	0.83	0.740
25 %	0	0.74	1.075
25 %	+180	0.67	1.475

to minimize the influence from the convolution of flow velocity and measurement volume (see section 2.2).

Details of the influence of the location of the pipe wall position on the result of the power law fit are also shown in figure 5.15 for a different profile measured in the 5%/11  $\mu\text{m}$  polyamide suspension. For the fit the first 5 points from the pipe wall towards the center before the inflection point of the velocity were ignored to reduce the influence of the convolution close to the pipe wall. As in the previously described case a variation of the pipe wall position of only 300  $\mu\text{m}$  (which is less than the highest possible resolution) results in important differences of  $n$  and  $K$  while  $R^2$  is very close to 1.

Figure 5.6 compares the variation in viscosity with shear rate determined by the UVP-PD in-line rheometry (full lines) with that measured using the off-line rheometer (symbols) for the different concentrations of particles of 11  $\mu\text{m}$  diameter. In general, the agreement between viscosities at different shear rates measured using in-line and off-line rheometry is reasonably good indicating that the concentration of particles is uniform along the radius of the pipe and in the off-line rheometer.

As can be seen from figure 5.7, the shear rate dependent viscosities determined using in-line UVP-PD technique (full lines) are larger than those measured by off-line rheometer (symbols) for suspensions of different concentrations of 90  $\mu\text{m}$  polyamide particles in rapeseed oil. This could be due to the accumulation of large particles in the cavity before the transducers as discussed earlier. This is also true for the suspensions containing bimodal mixtures of 11 and 90  $\mu\text{m}$  particles (total concentration of 25 % by volume) in rapeseed oil as shown in figure 5.8.

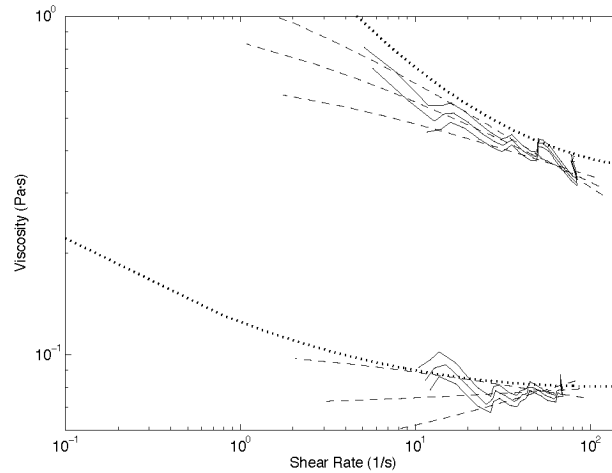


**Figure 5.14.:** Comparison of shear rate dependent viscosities of suspensions of 5 and 25% by volume of 11  $\mu\text{m}$  diameter polyamide particles in rapeseed oil measured using in-line UVP-PD (full and dashed lines represent values determined based on velocity gradient and power law methods for the velocity profile data shown in figures 5.9 and 5.10), and off-line (dotted lines) rheometers.

## 5.2. Cocoa butter crystallization

### 5.2.1. Crystal concentration and sound velocity

In an separate measurement in a one stage shear crystallizer described in Birkhofer *et al.* (2004) the solid fat content (SFC) was measured off-line with nuclear magnetic resonance (NMR) in parallel to the acoustic measurements. The measured values of temperature, sound velocity and SFC are shown in figure 5.16.

As shown in section 3.3.5 it is possible to determine the composition of a fat crystal suspension using the Urick equation when velocity of sound  $c$ , and the adiabatic compressibility  $\kappa$  and the density  $\rho$  of the solid and liquid phase are known. With a density  $\rho_l$  of  $890 \text{ kg/m}^3$  for the liquid cocoa butter and a  $\rho_s$  of  $975 \text{ kg/m}^3$  for the solid cocoa butter this results in compressibilities of  $\kappa_l = 0.62 \times 10^{-9} \text{ 1/Pa}$  and  $\kappa_s = 0.23 \times 10^{-9} \text{ 1/Pa}$  for the liquid and solid cocoa butter respectively. Figure 5.17 shows the velocity of sound in function of the SFC with the measured values and the results from the Urick equation (details also in Birkhofer *et al.* (2004)).

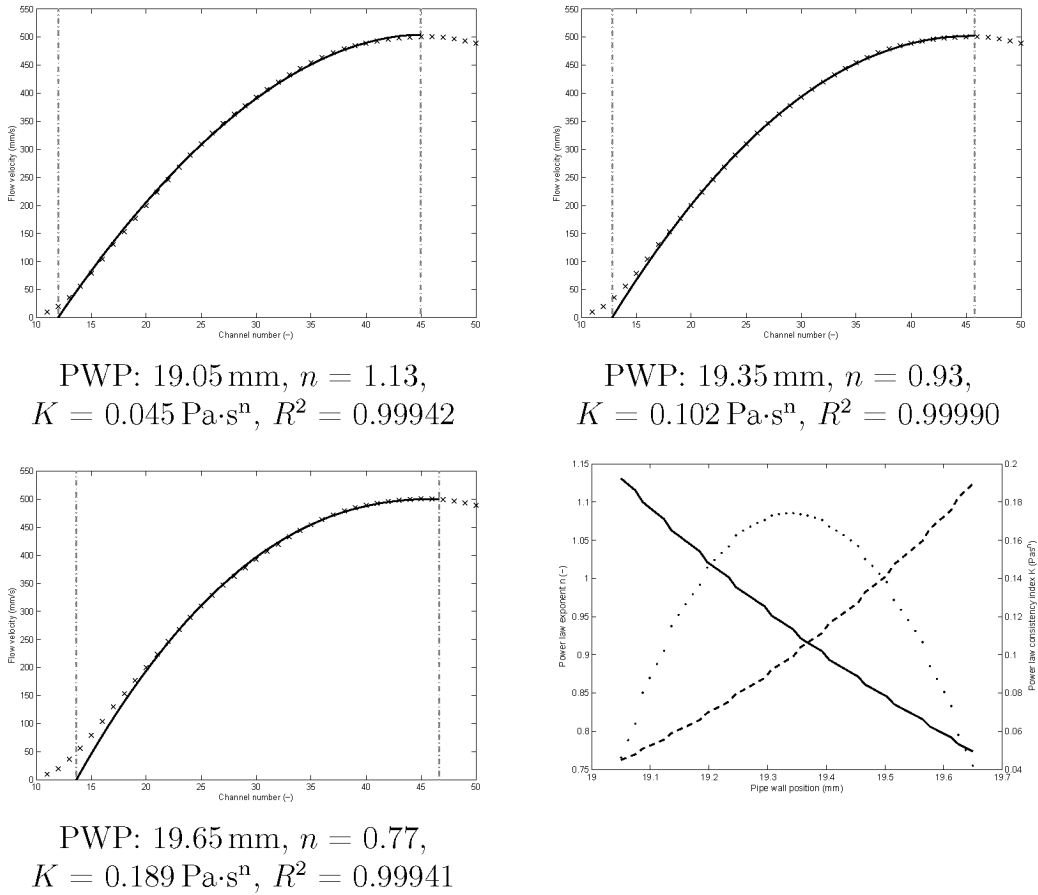


**Figure 5.15.:** The measured velocity profile in 5%/11  $\mu\text{m}$  polyamide suspension and the fitted power law velocity profiles for three different pipe wall positions 300  $\mu\text{m}$  apart from each other. The plot on the bottom right shows the variation of  $n$  (full line),  $K$  (dashed line) and the error  $R^2$  (dotted line; scale from 0.999 to 1) for the whole range covered by the shown profiles.

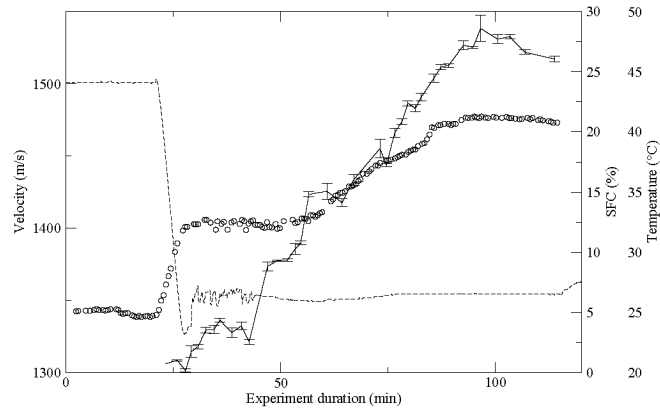


**Figure 5.16.:** Sound velocity (symbols), SFC (full line with error bars) and temperature (dashed line) during crystallization in the one stage shear crystallizer.

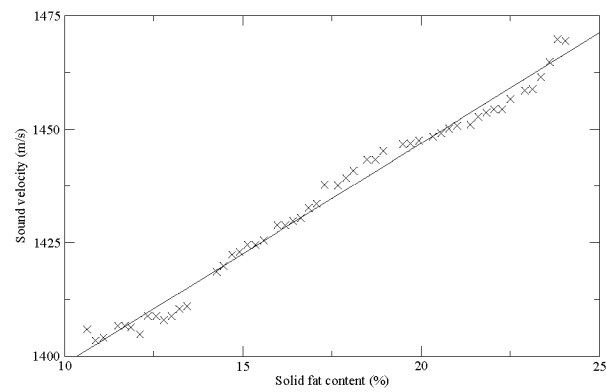


**Figure 5.17.:** Velocity of sound as a function of the solid fat content (both quantities originally measured as function of the time). Experimental:  $\times$ ; fitted: full line.

### 5.2.2. Crystallization process

Normally the two stage shear crystallizer described in chapter 4.5.2 operates at steady-state at a given flow rate of the cocoa butter crystal suspension with a constant concentration of the cocoa butter crystals. A small quantity of this crystal suspension is then added to the chocolate suspension for seed crystallization. As mentioned in section 4.5.2, the temperatures of the first and second stages of the shear crystallizer are usually 15°C and 26°C to produce the  $\beta V$  and  $\beta VI$  crystals respectively. Both the head of the spindle of the shear crystallizer and the double walled pipes after the shear crystallizer were maintained at 32°C to avoid solidification of cocoa butter at the internal surfaces. The concentration of the cocoa butter crystals in the suspension flowing at a constant flow rate through the ultrasound adapter (see Figure 4.9) will be constant under steady-state conditions. Consequently, the corresponding rheological properties such as the shear rate dependent viscosity of the suspension determined by the UVP-PD technique will also be constant.

The aim of the present work is to demonstrate that the influence of process parameters on fat crystallization process can be monitored using the in-line UVP-PD technique. This is performed under dynamic conditions during the start-up of the cocoa butter (fat) shear crystallization process with the two stage shear crystallizer shown in Figure 4.9 as explained below. Cocoa butter was melted in the tank, the rotor of the shear crystallizer was switched on and liquid cocoa butter was pumped through the flow loop at a constant flow rate of 13.9 kg/h and temperature of 41°C until steady-state was reached. The same temperature was maintained in all the units of the flow loop. Just 3 min after steady-state was attained, the temperatures of the first and second stages of the two stage shear crystallizer were set to 15°C and 26°C respectively. The temperatures of the head of the shear crystallizer spindle and double walled pipes were maintained at 32°C while that of the tank was increased to 43°C in order to re-melt the suspension produced by the crystallizer. The flow velocity profiles, velocity of sound, amplitude of attenuated ultrasound signal and temperature were continuously measured in the PVC flow adaptor together with the pressure drop to monitor the transformation of cocoa butter from liquid state to crystal suspension. These velocity profiles and pressure drop enable the determination of the temporal change in the rheological properties such as the variation in viscosity with shear rate.

### 5.2.3. Measured parameters

The temporal variation in measured parameters and evolution of velocity profiles are shown in figures 5.18 and 5.19 respectively. The parameters can be broadly

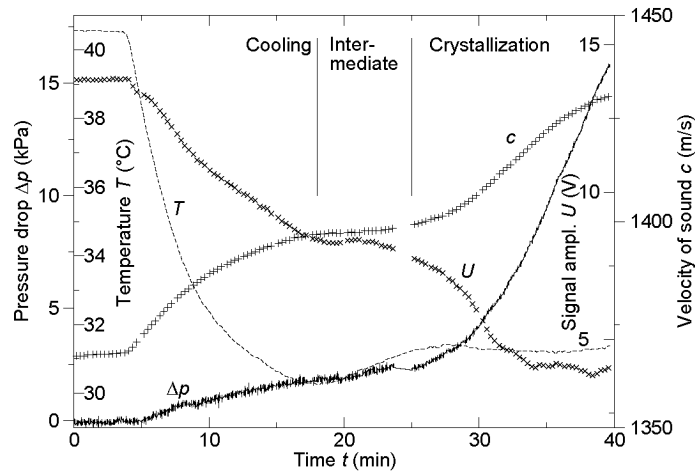


**Figure 5.18.:** Temporal variation in the measured values of the process and acoustic parameters in a pipe section after the shear crystallizer. Temperature: dashed line; pressure drop: full line; velocity of sound: +; amplitude of attenuated sound signal: ×.

classified into three categories: (i) process parameters such as the pressure drop and temperature in a pipe section after the shear crystallizer, (ii) acoustic parameters such as the velocity of sound and the amplitude of the transmitted ultrasound signal through the cocoa butter suspension in the pipe, and (iii) flow velocity profiles along the pipe diameter.

The dynamic period since the start up of the shear crystallizer (at about 3 min) shown in Figure 5.18 can be divided into three regions: (a) liquid cocoa butter cooling period (up to 18 min) during which shear induced nucleation may occur, (b) intermediate period during which the temperature slightly increased (18 min until 25 min), and (c) isothermal shear crystallization period during which the temperature was constant at 31.5°C and the concentration of the crystals increased in the cocoa butter suspension (after 25 min).

**(a) Liquid cocoa butter cooling period (up to 18 min):** Figure 5.18 shows that the temperature of the liquid cocoa butter flowing decreased from 41°C to 30°C in the cooling period. As expected, the corresponding pressure drop can be seen to increase due to increase in the viscosity of the liquid cocoa butter with decrease in temperature. The sound velocity increased as the compressibility of the liquid cocoa butter decreases by the temperature reduction due to the tighter arrangement of the triglycerides. The amplitude of the transmitted ultrasound signal was reduced due to attenuation associated with the increased viscous losses and also possibly the compression



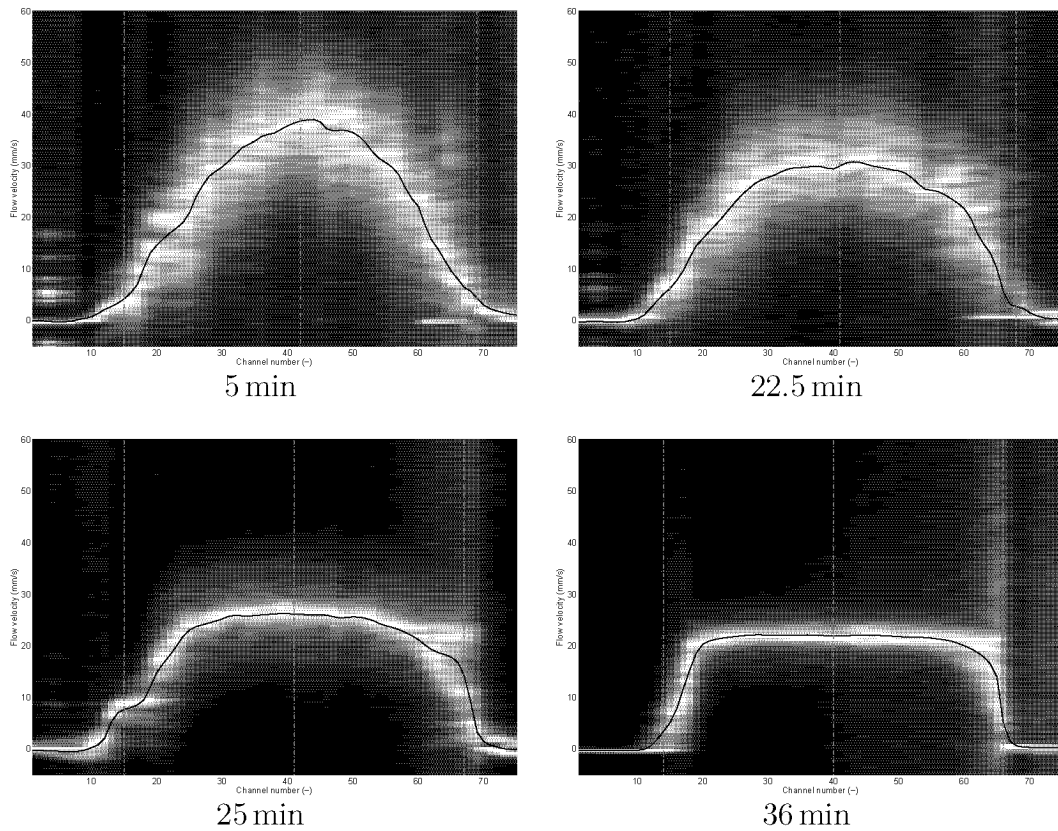


**Figure 5.19.:** Velocity profiles (average of 30 single profiles) given as channel-wise normalized baseband signal power spectra (grayscale background) and estimated velocity profiles (full lines) along the pipe diameter at different times after the start-up of shear crystallizer.

and relaxation of triglycerides.

- (b) Intermediate period (from 18 min until 25 min):** The response of the proportional-integral-differential (PID) temperature controller is the reason that the temperature slightly increased from 30°C to 31.5°C after which it remained constant. Thus the temperature was low enough for the beginning of increase in the concentration of the cocoa butter crystals. Consequently, both the pressure drop and velocity of sound continued to increase monotonically.
- (c) Isothermal shear crystallization period (after 25 min):** The temperature of the cocoa butter remained virtually constant and the concentration of cocoa butter crystals (referred as solid fat content SFC) in the suspension increased at a much faster rate due to higher rate of crystallization in the two stage shear crystallizer. This resulted in relatively larger increase in both the sound velocity (1400 to 1430 m/s) and the pressure drop (2.5 to 17 kPa). The SFC was not directly measured but according to measurements of SFC carried out (see figure 5.17) previously by Birkhofer et al. Birkhofer *et al.* (2004) under similar process conditions using nuclear magnetic resonance (NMR) technique, a value of around 20% was reached in this flow loop based on the measured velocity of sound. The attenuation increased with the increase of the SFC due to scattering and the increase in viscosity. Thus the amplitude of the transmitted signal received with the second transducer was further reduced to 4 V.

#### 5.2.4. Temporal evolution of velocity profiles

The evolution of the shape of the velocity profiles (full lines) during the above three (cooling, intermediate and isothermal shear crystallization) periods is shown in figure 5.19. The shear rate increases along the radius of a pipe during the laminar flow of a particulate suspension, the minimum being at the centre of the pipe. For shear thinning suspensions, the viscosity decreases with increase in shear rate at a given concentration of particles. The higher is the concentration of particles, higher will be the viscosity at a given shear rate. Since cocoa butter is a Newtonian liquid during the cooling period, the corresponding velocity profile at 5 min can be seen to be parabolic as expected. The velocity profile at 22.5 min, which corresponds to the intermediate period, is slightly flattened due to the formation of cocoa butter crystals indicating that the crystal suspension is shear thinning. As the concentration of cocoa butter crystals increases up to about 20% in the isothermal shear crystallization period mentioned above, the corresponding velocity profile at 36 min can be seen to be flatter and more shear thinning than that at 25 min.

### 5.2.5. Ultrasound scatterers in the cocoa butter

Against theoretical considerations assuming a pure oil it was possible to measure flow velocity profiles in the shear crystallizer flow loop even in the liquid cocoa butter at temperatures above 40°C. Thus the following two sections try to explain the echogenicity of liquid cocoa butter and the crystal suspension.

#### 5.2.5.1. Shear crystallizer start

Figure 5.20 shows the envelope of the baseband signal from liquid cocoa butter at 42°C of three consecutively acquired single profiles a few seconds after the shear crystallizer, which is installed upstream from the measurement location, was switched on (only the motor for the rotation, not the temperature control). The baseband signal amplitude shoots up from a very low level (maximum peak-peak amplitude at 10% of the ADC range) in the first envelope on the left to a complete saturation of the ADC in second and third envelope in the center region. From the second to the third envelope the region where the ADC is saturated increases from channels 35 – 50 to 30 – 53. This behavior can be explained with air in the head space of the shear crystallizer that was dispersed into small bubbles with the rotation of the spindle. Because of the parabolic flow profile the air bubble front is first visible in the center of the pipe and then broadening.

#### 5.2.5.2. Echo development during crystallization

Figure 5.21 gives an overview on the development of the amplitude of the baseband signal during the crystallization process (see also figure 5.18) which was started about 100 min after the start of the shear crystallizer rotation described in the previous section. The UVP parameters given in table 5.5 were used for the measurements during the crystallization. The first part until approximately 25 min shows single, randomly distributed spots with a high amplitude while the second part after 25 min, where the crystal content is assumed to increase significantly, shows a region of constantly high echo amplitude moving closer to the transducer over the time (this is also shown in figure 5.24). Assuming a crystal size around 10 µm (see figure 4.2) the ratio of wavelength to scatterer size is approximately 35.

An example of the baseband signal and the corresponding profile is shown in figure 5.22 for the case of the liquid cocoa butter. More than 100 min after the air bubbles were dispersed by the rotation of the shear crystallizer (section 5.2.5.1) the air bubbles were distributed in the cocoa butter. The structure looks quite similar to figure 5.43 on page 104 which shows the same data for an open channel

## 5. Results and Discussion

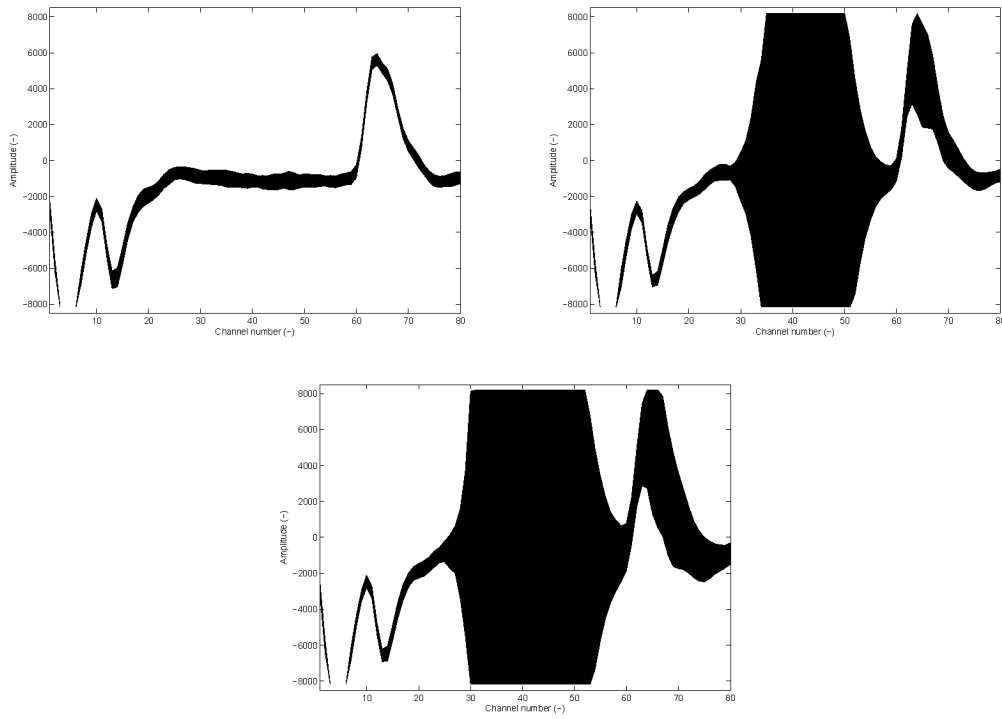


**Figure 5.20.:** Development of the baseband signal envelope in the liquid cocoa butter after switching on the shear crystallizer. The time between the profile measurements is 2.4 s, the duration of one measurement is 0.7 s.

**Table 5.5.:** UVP parameters for the measurement during the crystallization process.

Parameter	Value
Transducer type	TX
Active diameter	5 mm
Number of pulse repetitions	256
Pulse repetition frequency	0.36 kHz
Emission frequency	4 MHz
Voltage	150 V
Gain start	8
Gain end	9
Number of cycles	2
Sound velocity	1367 – 1428 m/s
Channel distance	0.342 – 0.357 mm
Window Start	17.0 mm

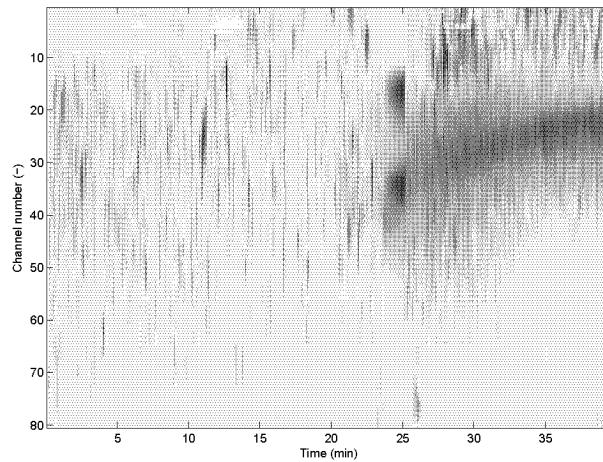


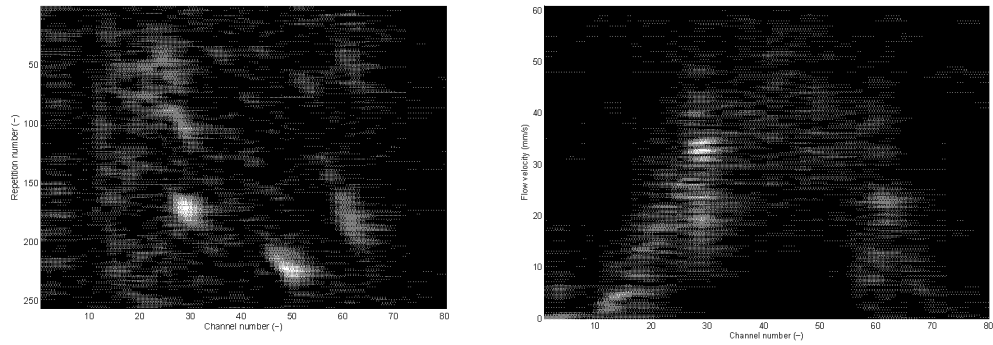
**Figure 5.21.:** Temporal (abscissa) and spatial (ordinate) distribution of the amplitude of the baseband signal. The higher the amplitude the darker the corresponding region in the plot. The tho half circle shaped structures around channel 25 are artifacts from the interpolation necessary for the visualization.

flow with gas bubbles generated by electrolysis (where it was shown that even a gas concentration in the range of several ppm is sufficient to measure a velocity profile).

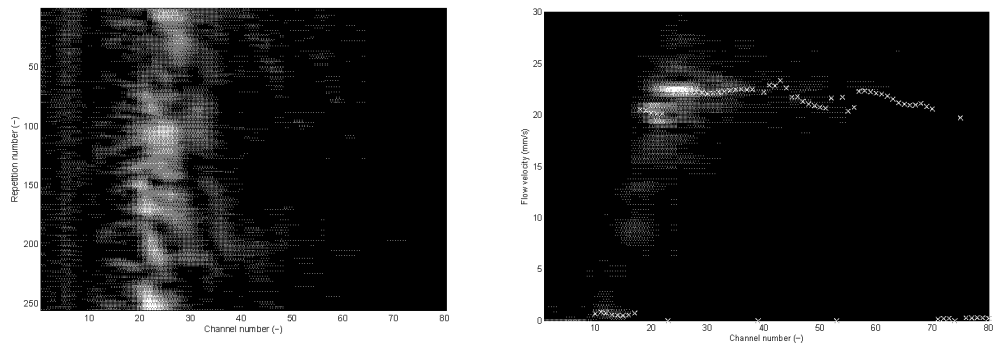
When the crystal content increases after 25 min the characteristics of the distribution of the baseband signal amplitude change significantly. Figure 5.23 shows a single profile at the end of the crystallization at 38 min. Most of the echo origins from the begin (seen from the transducer) of the flat region of the flow profile. The location of the maximum baseband signal amplitude for the whole measurement is shown in figure 5.24. Before 25 min the location is randomly distributed which agrees with the hypothesis that the main source of scattering are air bubbles. After 25 min the position stabilizes and moves towards the transducer with the increase in crystal content.

Figure 5.25 shows the direct comparison of the liquid cocoa butter and the crystal suspension. Unline the previous figures 5.22 and 5.23 which show single profiles, the average of 30 profiles is displayed. In the liquid cocoa butter the signal amplitude increases from close to the pipe wall (before channel 10) and has several local maxima due to the distribution of the scatterers passing by. Beyond channel 50 the amplitude only decreases. For the crystal suspension the signal has first a local minimum around channel 12 which is related with the DC offset<sup>1</sup> at the

<sup>1</sup>The baseband signal amplitude is expected to oscillate around zero. Thus the average of the pulse echo amplitudes at one channel is expected to be zero unless there is a DC offset. The



**Figure 5.22.:** The amplitude (brightness) of the baseband signal of all the 256 pulse repetitions (left, in  $y$ -direction) corresponding to a single flow profile (right) 5 min after the start of the measurement. The spectral data is not normalized channel-wise to visualize the correspondences in the two plots.



**Figure 5.23.:** The baseband signal amplitude (brightness) of all the 256 pulse repetitions (in  $y$ -direction) and the corresponding profile at the end of the crystallization. The profile (power spectra) is not normalized but the resulting profile is indicated with crosses.

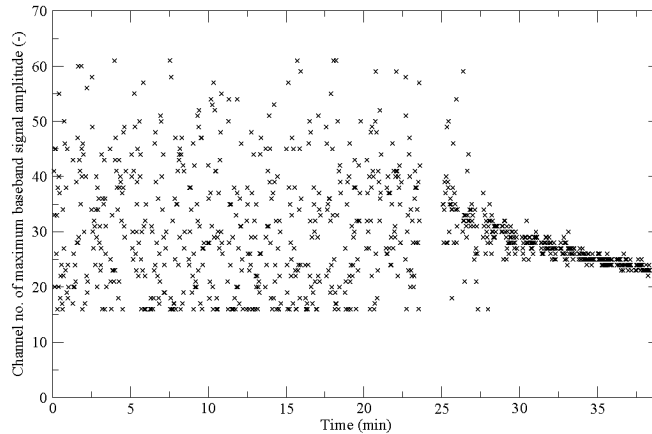


**Figure 5.24.:** Temporal behavior of the location (measurement channel) of the maximum value of the baseband signal during the crystallization. Maxima inside the cavity (before channel 15) are not considered.

same position. Then it reaches its maximum at channel 20 where the flow profile flattens and then decreases until channel 70 (distal pipe wall). This agrees with the increased attenuation in the crystal suspension also shown in figure 5.18. If the source of backscattering are only the fat crystals (which is not very evident as the density and compressibility differences between the disperse and the continuous phase are expected to be rather small) one would expect the amplitude to be closer towards the pipe wall. If it is the interface between the wall layer and the plug like flow in the center of the pipe which reflects the ultrasound waves then the structure in figure 5.23 in the baseband signal amplitude between channels 20 and 30 would be expected to look more homogeneous. So one could hypothesize that due to the increased velocity gradient near the pipe wall and the flattening of the flow profile in the central part, the reflectors (probably mostly air bubbles) concentrate in the zone of the end of the high shear rate and the begin of the flat region.

---

DC offset in the baseband signal occurs if the RF signal contains an important quantity of base frequency signals, e. g. from transducer ringing or echoes from pipe walls. If the spectral analysis is applied the DC offset is corrected individually for the measurement channels during the preconditioning of the signal.

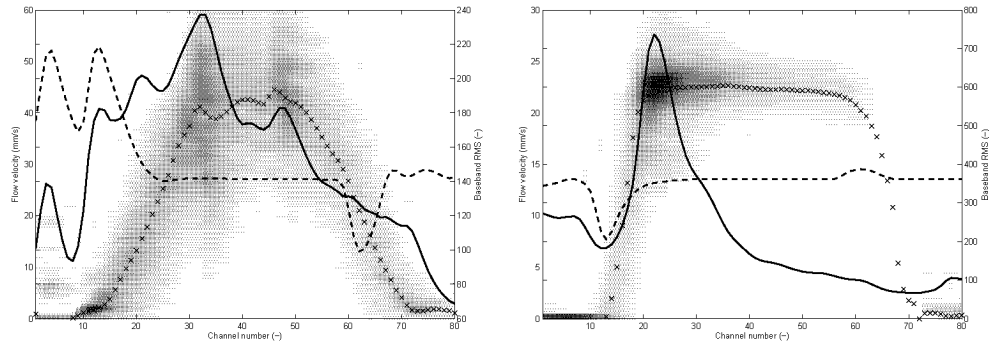


**Figure 5.25.:** Average over 30 flow profiles (crosses and spectral intensity as surface), RMS of the baseband signal (full line) and the average of the baseband signal (dashed line). On the left side a profile in the liquid cocoa butter, on the right side the crystal suspension. In contrast to other profile plots (e.g. figure 5.19) high spectral intensities are visualized by a darker shading which is not normalized channel wise. The average of the baseband signal results in the DC offset if it deviates from zero.

### 5.2.6. Rheological parameters

The experimental velocity profiles (a few are shown in figure 5.19) were fitted to the power law rheological model equation (3.11) to determine the values of  $n$  and  $K$  using the corresponding measured pressure drop in the pipe section after the shear crystallizer shown in figure 5.18.

The velocity profile in the central pipe region corresponding to the maximum cocoa butter crystal concentration at 36 min shown in figure 5.19 is flat. This could be considered as a plug corresponding to a yield stress during the flow of the suspension. Figure 5.26 shows the comparison between the experimental velocity profiles and those fitted to the power-law and Herschel Bulkley models equations (3.11) and (3.17) respectively. The values of the yield stress  $\tau_0$  and the plug radius  $R_*$  are listed in the figure caption. As mentioned by Wiklund et al. Wiklund *et al.* (2002), the accuracy of determination of the radius of the plug affects significantly the calculated yield stress as the Herschel Bulkley model has three parameters. However, the shear rate dependent viscosity predicted by the power law model is found to be the same as that determined using the Herschel-Bulkley model. Consequently, the present work utilizes the power law model.

The temporal evolution of the values of power law rheological model parameters  $n$  and  $K$  determined are shown in figure 5.27. As discussed in the previous section, cocoa butter was a Newtonian liquid in the cooling period (until about 18 min) which is confirmed by the fact that the value of  $n$  is equal to 1. The corresponding



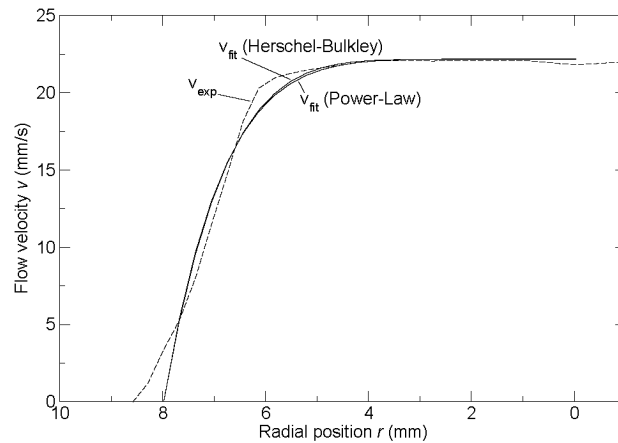


**Figure 5.26.:** The measured profile (dashed line) and the profiles resulting from the fits to the power law and Herschel-Bulkley models (full lines). The parameters of the power law fit are:  $n = 0.16$ ,  $K = 29.14 \text{ Pa}\cdot\text{s}^n$  and  $R^2 = 0.985$  (regression coefficient). For the Herschel-Bulkley model:  $n = 0.29$ ,  $K = 13 \text{ Pa}\cdot\text{s}^n$ ,  $\tau_0 = 16.6 \text{ Pa}$ ,  $R_* = 2.8 \text{ mm}$  and  $R^2 = 0.989$ .

value of  $K$  increased due to increase in pressure drop associated with the increase in viscosity as the temperature decreased from  $41^\circ\text{C}$  to  $30^\circ\text{C}$ . In the intermediate period, the concentration of cocoa butter crystals in the suspension increased with time due to crystallization in the shear crystallizer. Consequently, the value of  $n$  decreased to 0.34 at 25 min indicating that the crystal suspension is shear thinning, which is also reflected by the fact that the corresponding velocity profile in figure 5.19 is flat at the center of the pipe. For the isothermal shear crystallization period, the value of  $n$  further decreased to 0.175 at 36 min and the corresponding velocity profile in figure 5.19 is much flatter.

Figure 5.28 shows the temporal variation in viscosity during the three periods defined in previous section at two different shear rates using equations (3.14) and (3.15) with the values of  $n$  and  $K$  shown in figure 5.27. The variations in the position of the radius in the pipe corresponding to these two shear rates are also shown. In the cooling period up to about 18 min, the positions of the radii where the shear rates are 2.5 and 7.5 1/s respectively are virtually constant. However, the corresponding viscosities increased with time as expected due to the reduction in temperature. In contrast, as time increased during the intermediate and isothermal shear crystallization periods (after 18 min), the concentration of cocoa butter crystals in the suspension increased and consequently, the position of the radius corresponding to the higher shear rate ( $\dot{\gamma} = 7.5 \text{ 1/s}$ ) moved closer to the wall of the pipe than that for the lower shear rate ( $\dot{\gamma} = 2.5 \text{ 1/s}$ ). The viscosity at

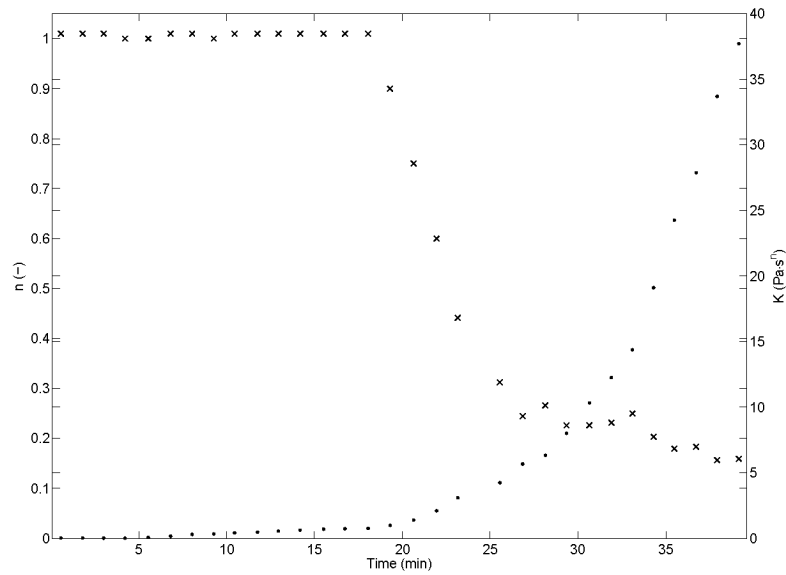


**Figure 5.27.:** Temporal variation in the values of  $K$  (•) and  $n$  (x) during the crystallization process.

36 min decreased from a value of 12.75 Pa·s to 5.5 Pa·s as the shear rate increased from 2.5 1/s to 7.5 1/s.

Figure 5.29 shows the distribution of the shear rate and viscosity along the radius of the pipe for the velocity profiles shown in figure 5.19. The shear rate can be seen to increase from a value of zero at the centre of the pipe to a maximum value at the pipe wall, the corresponding viscosity decreasing from a large value.

### 5.2.7. Limitations of the current ultrasound transducers and adapter

The pressure distribution along the ultrasound beam is irregular in the region, which is called the near field, close to the transducer. The region after the focal point is called the far field in which the pressure decays. Consequently, the measurements are carried out in the latter region by positioning the transducer in the PVC flow adaptor 17 mm away from the inner surface of the pipe as shown in figure 4.9. However, this causes three drawbacks: (i) the laminar fluid streamlines could be disturbed by the cavities, (ii) possibility of crystallization in the stagnant region of cavities, and (iii) averaging of sound velocity and amplitude of attenuated transmitted signal over the stagnant and flow regions of adaptor. These limitations should be solved by an improved design of a flow adaptor and an ultrasound transducer.

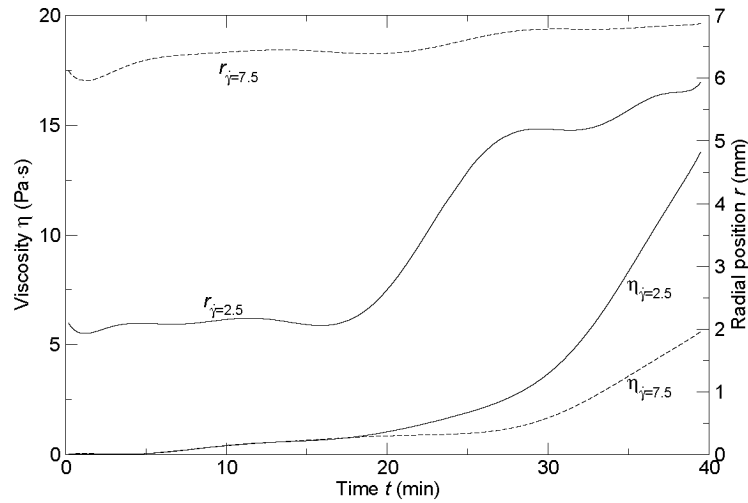


**Figure 5.28.:** Temporal variation in viscosities ( $\eta_{\dot{\gamma}=2.5}$  and  $\eta_{\dot{\gamma}=7.5}$ ) and radial positions ( $r_{\dot{\gamma}=2.5}$  and  $r_{\dot{\gamma}=7.5}$ ) in the pipe corresponding to shear rates  $\dot{\gamma}$  of 2.5 1/s (full lines) and 7.5 1/s (broken lines) respectively.

### 5.3. Seeded chocolate suspension

Chocolates are highly concentrated suspensions containing sugar crystals, whole milk powder, cocoa mass and other ingredients in addition to cocoa butter crystals (details are given in section 4.1.4). Consequently, the attenuation of the ultrasound is expected to be high and thereby reducing the quality of the velocity profiles. Therefore, velocity profiles were measured in chocolate processed in the compact shear crystallizer described in section 4.5.3 to investigate the profile quality and the penetration depth of ultrasound. In addition, the velocity of sound was also measured to examine its dependence on the seeding of cocoa butter.

#### 5.3.1. Attenuation of transmitted pulse signal

By using a flow adapter with two transducers facing each other (see section 4.3.3) it was possible to measure the signal transmitted through the chocolate. Figure 5.31 shows this throughput signal for pulse lengths between 1 and 4 cycles. For one cycle, the maximum amplitude is highest compared to the other pulse lengths. For 3 and 4 cycles, the central part of the pulse has a reduced amplitude. Both observations (which were also made in highly concentrated corn starch suspensions) can be explained with phase cancellation from scattered signals.

## 5. Results and Discussion

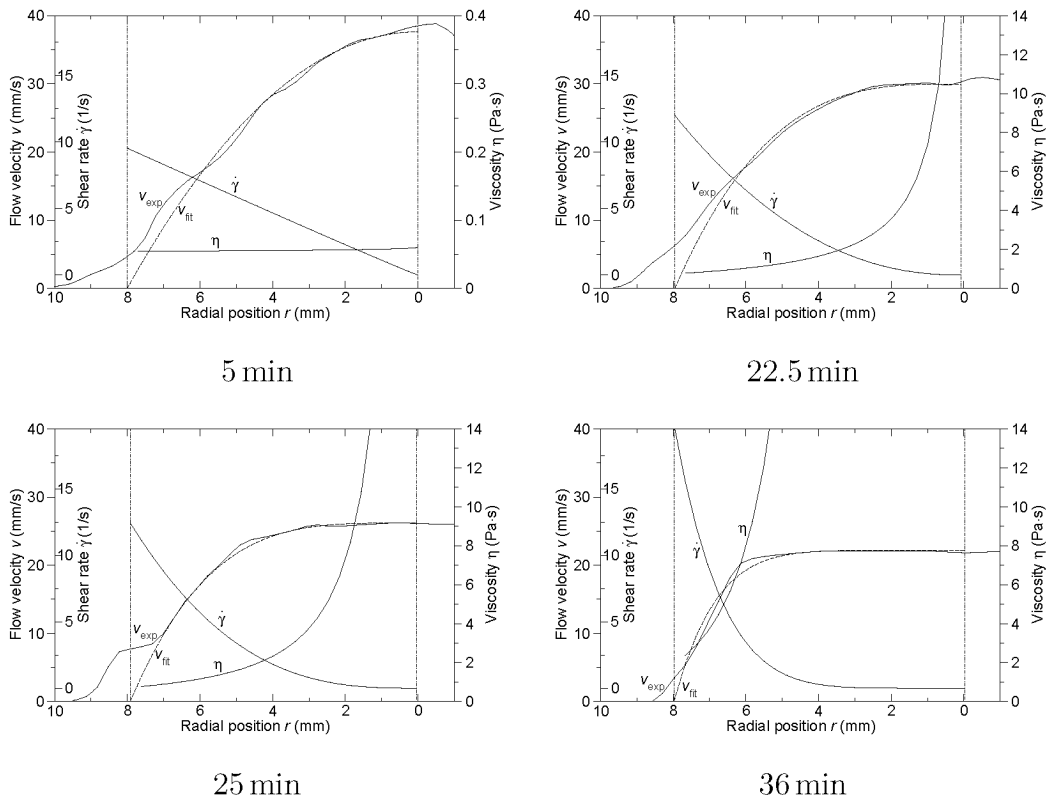


**Figure 5.29.:** Radial distribution of shear rate  $\dot{\gamma}$  and viscosity  $\eta$  for the velocity distributions (full line: experimental profile, dashed line: fitted profile) shown in figure 5.19.

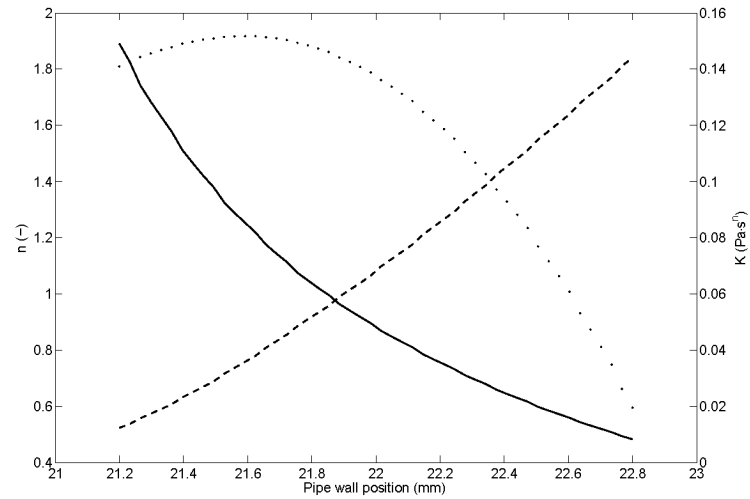


**Figure 5.30.:** Influence of the estimated pipe wall position on  $n$  (full line) and  $K$  (dashed line) and the corresponding error (dotted line) for the liquid cocoa butter.

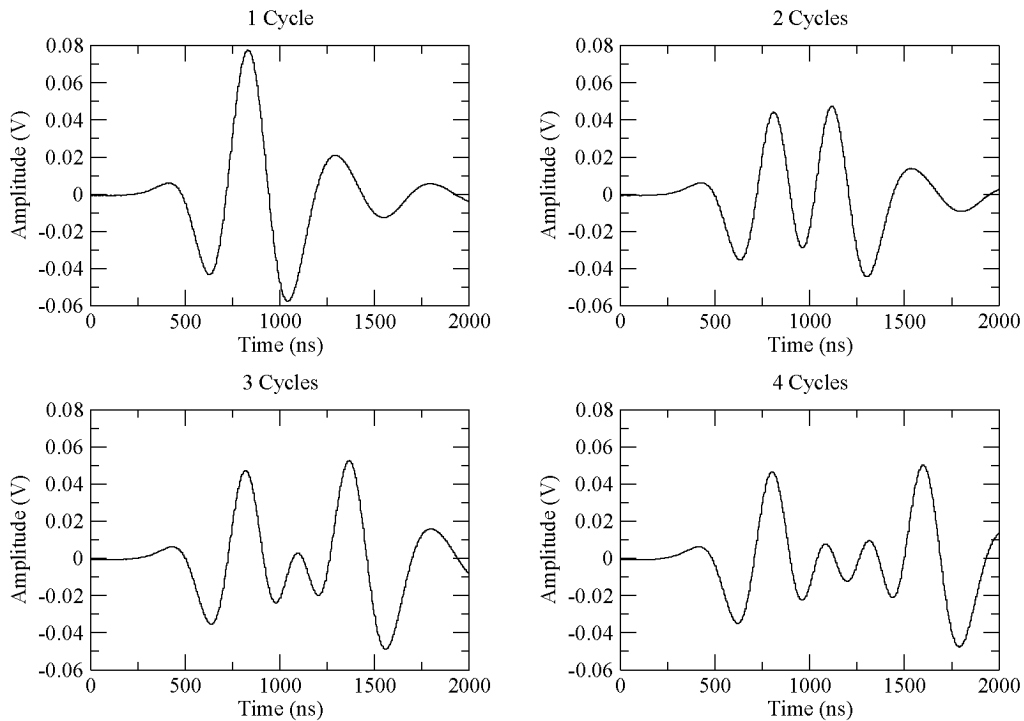


**Figure 5.31.:** Overview of the received signals when using 1 to 4 cycles. Sending from the TN, receiving with the TX transducer with a distance of 34 mm.

**Table 5.6.:** UVP parameters common for all profiles shown in section 5.3.2.

Parameter	Value
Transducer type	TN
Active diameter	5 mm
Number of profiles	25
Number of pulse repetitions	512
Pulse repetition frequency	2.40 kHz
Emission frequency	4 MHz
Voltage	150 V
Gain start	9
Gain end	9
Number of cycles	1, 2 and 4
Sound velocity	1669 m/s
Channel distance	0.417 mm
Window Start	1.46 mm

### 5.3.2. Number of cycles per pulse

The following measurements comparing the influence of varying the pulse length between 1 and 4 cycles were made using the parameters listed in table 5.6 with the transducer installed in flush with the pipe wall.

#### 5.3.2.1. Baseband signal amplitude

The received echo signal amplitude is approximately a linear function of the length of the pulse as shown in figure 5.32. The deviation from a linear relation can also be explained with the phase cancellation described in the previous section.

#### 5.3.2.2. Velocity profiles

The effect of ultrasound pulse length on the velocity profiles is shown in figure 5.33. Despite the big difference in the baseband signal amplitude, the profiles are similar although the penetration depth is increased for the 4 cycle pulse approximately 2mm compared to 1 cycle. As the first measurement volumes are very close to the transducer (window start at 1.42 mm), the near field, the transducer ringing and the receiving electronic elements in UVP overloaded from the pulse sent affect the velocity profile. This can be seen in figure 5.34, which shows the envelopes of the baseband signal of the received echoes. The first 5 to 10 channels have an

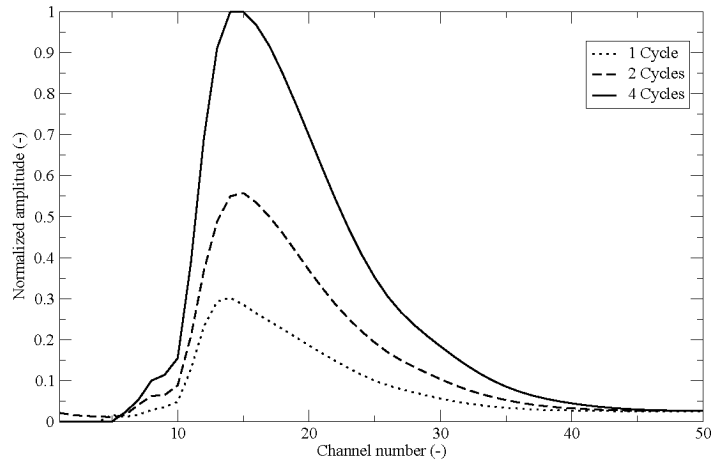


**Figure 5.32.:** Normalized amplitude of the baseband signal for 1, 2 and 4 cycles with maximum values 0.30, 0.55 and 1 respectively.

important DC offset (due to the sent pulse influencing the receiving hardware) which reduces the signal after the DC offset correction nearly to zero. For the 1 cycle signal (top row), the ADC limit is reached in the co-phase signal (top right) between channels 10 and 14. For the 4 cycle signal (bottom row), the ADC is saturated for the in-phase and co-phase signal between channels 10 and 20. As the DC offset influences the signal, the pulse length does not result in a significant difference in the profiles close to the wall as seen in figure 5.33 (bottom right).

From these measurements one can see, that for chocolate the pulse length has a significant influence on the amplitude of the received signal which increases proportional with the number of cycles. At the same time the profile quality and penetration depth show a relatively small variance with the pulse length. Using shorter pulses reduces the measurement volume which would reduce the size of the sample volume and should thus improve the accuracy. At the same time it would have to be investigated how the increased bandwidth with the decreased pulse length influences the measurements.

### 5.3.3. Frequency

The TN and TX series transducers with a central frequency of 4 MHz were also used at an emission frequency of 2 MHz as shown in Figure 5.35. The transducer position and most parameters were the same as used in the previous section,

## 5. Results and Discussion

---

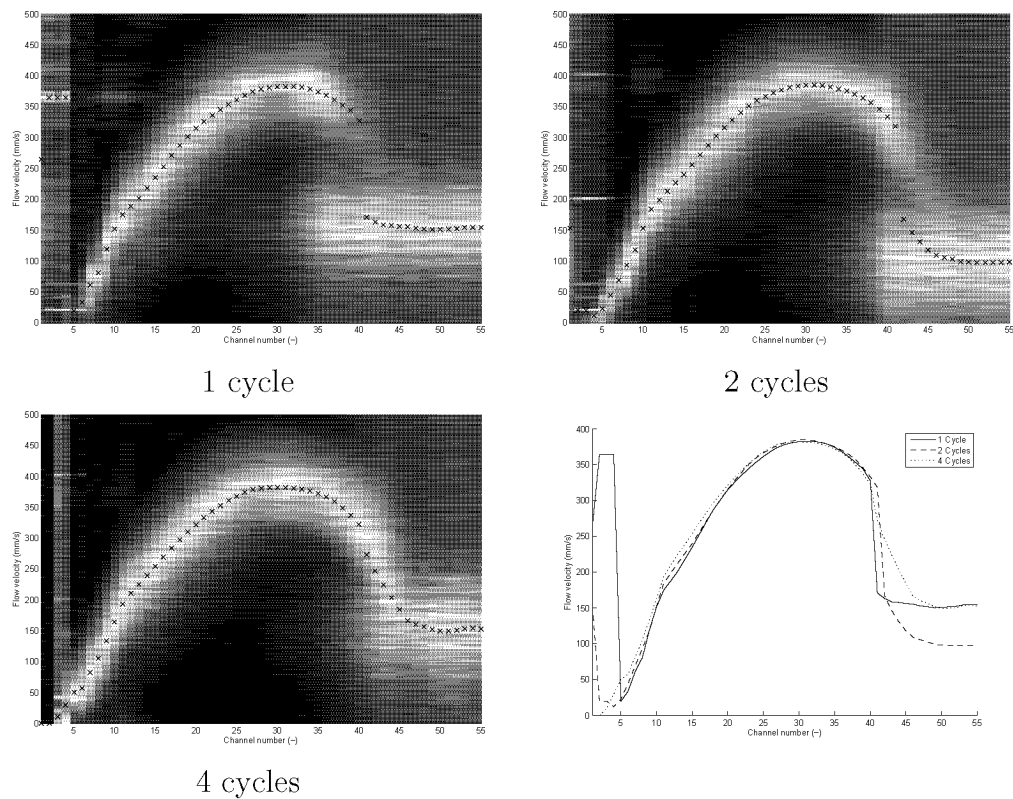


**Figure 5.33.:** Flow profiles with pulse lengths of 1, 2 and 4 cycles. With a summary of the estimated profiles in the plot on the bottom left.



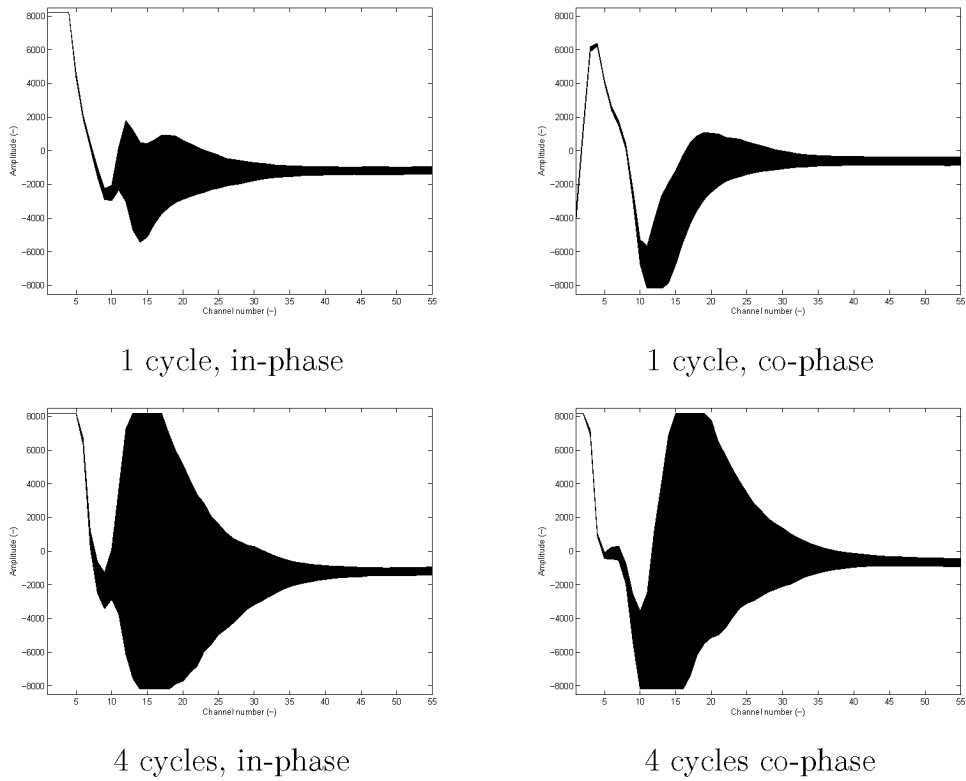


**Figure 5.34.:** Envelopes of the baseband signal amplitude (median of the 25 profiles) which is digitized at 14 bit for two different pulse lengths.

**Table 5.7.:** UVP parameters for profiles shown in figure 5.35 different from the ones given in table 5.6.

Parameter	Value
Number of profiles	20
Number of pulse repetitions	256
Pulse repetition frequency	1.08 kHz
Emission frequency	2 MHz
Number of cycles	2
Window Start	1.04 mm

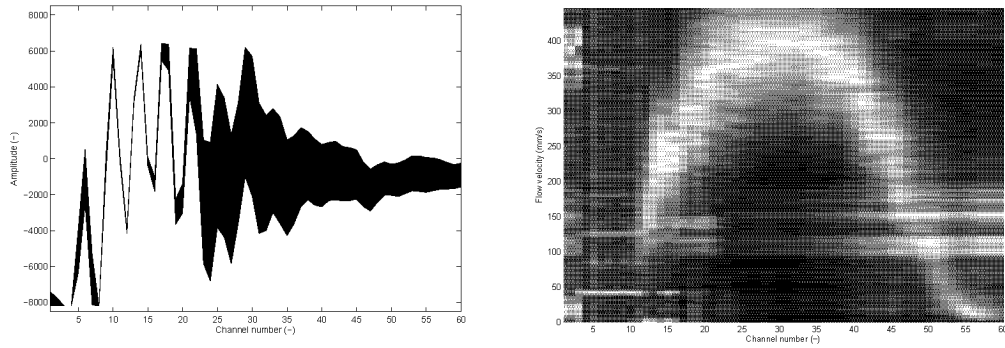


**Figure 5.35.:** Envelope of the in-phase part of the baseband signal (left side) and the flow profile (right side) measured with the parameters given in table 5.7.

the different ones being listed in table 5.7. The zone of DC-offset is elongated from channel 10 to channel 20 in contrast to that for the results (figure 5.34) with 4 MHz. This could be mainly due to the transducer characteristics (internal ringing) as the near field length is only half of that for 4 MHz. In spite of the small amplitude of Doppler signal after the DC off-set correction, it is possible to get a profile. However, the less quality in the corresponding region of the profile is reflected by the spectral broadening. Since the penetration depth for the 2 MHz is higher compared with that for 4 MHz, it is possible to measure the flow profile at the far end of the pipe wall. There seem to be some artifacts (horizontal bright stripes) visible in the second half of the profile.

It is interesting to know that the 4 MHz transducers can also measure at 2 MHz. The increased penetration depth is explained by the attenuation that increases with the square of the frequency. This option could be used to measure the first part of the profile with a lower frequency than the second. As our transducers are designed for a single base frequency it would be necessary to check the pressure field and other parameters before applying this method systematically.

**Table 5.8.:** UVP parameters for the measurements with the TX transducer presented in section 5.3.4.

Parameter	Value
Transducer type	TX
Active diameter	5 mm
Number of profiles	500
Number of pulse repetitions	256
Pulse repetition frequency	3.59 kHz
Emission frequency	4 MHz
Voltage	150 V
Gain start	6
Gain end	9
Number of cycles	2
Sound velocity	1670 m/s
Channel distance	0.417 mm
Window Start	0.417 mm

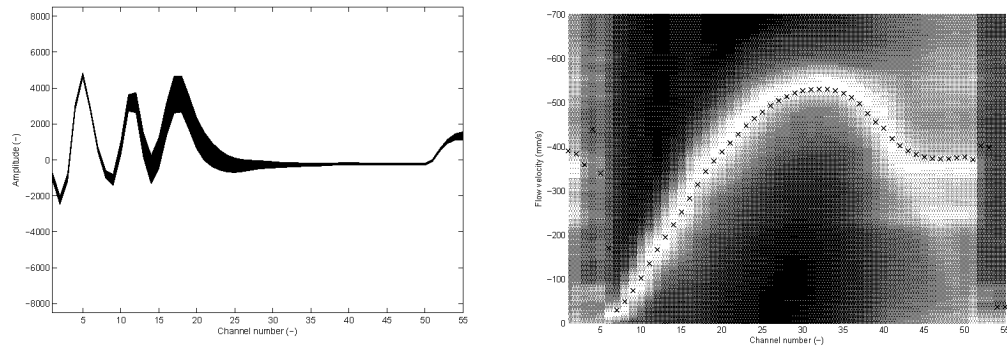
#### 5.3.4. Comparison of TN and TX transducers

Figure 5.36 shows the envelope of the in-phase baseband signal and the velocity profile measured with the 4 MHz TX transducer positioned in flush with the pipe wall using the parameters given in table 5.8. As the sensitivity of the newer TX transducer series is increased, it was possible to reduce the gain start value from 9 to 6 and still obtain a penetration depth reaching nearly the distal pipe wall. The quality of the measurement of the profile close to the pipe wall is also enhanced as the ADC was not saturated due to the lower signal amplification.

With the window start depth of 0.417 mm and the position of the transducer with one edge in flush with the pipe wall one would expect the profile to start just at the second channel in figure 5.36 as the distance from the center of the transducer front plate to the pipe is 0.8 mm. There are three obvious reasons why this is not the case. First there is an inherent delay in the analog electronics from the amplifiers and filters which causes a delay of approximately  $1.5 \mu\text{s}$  which corresponds to 3 channels. Second there is the transfer function of the transducer (see 5.31) which delays the signal approximately one cycle, corresponding to another half channel. Third there is the front plate of the transducer with a thickness of one quarter of a wavelength which is passed by the sent and the received signal.

## 5. Results and Discussion

---



**Figure 5.36.:** Envelope of the baseband signal and a velocity profile (average of 500 single profiles) measured with the TX transducer.

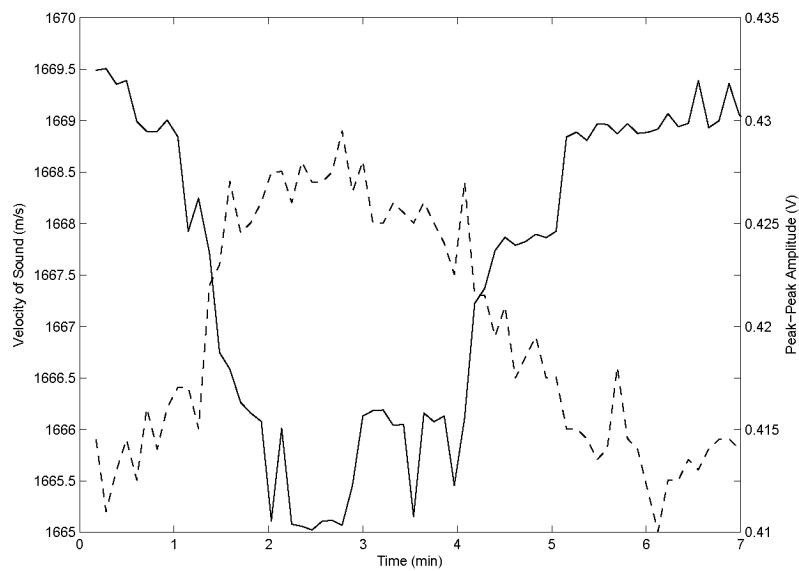


**Figure 5.37.:** Dynamic development of the sound velocity (full line) and transmitted signal amplitude (dashed line) due to step changes (increase and decrease) in the seeding of chocolate with 0.4% (by volume) cocoa butter crystal suspension.

### 5.3.5. Influence of cocoa butter seeding on sound velocity

Figure 5.37 shows the measured temporal variations in the sound velocity and transmitted signal amplitude during step changes in seeding of the chocolate with 0.4% cocoa butter crystal suspension at a constant temperature of 27.6°C. The mean flow velocity was about 500 mm/s and the sound velocity was measured at 1.5 m upstream of the location of seeding after a static mixer. This involved 10 sound velocity measurements per minute (limited by the 9600 baud serial connection to the oscilloscope). The sound velocity dropped with a short delay, due to the mentioned distance of 1.5 m, after the start of the seeding. It continued to decrease because of the dilution by the added cocoa butter suspension and attains a constant value at about 2 min, which depends on homogenization by the static mixer. The sound velocity drops by 4 m/s as its value in the cocoa butter crystal suspension is about 1430 m/s. The amplitude of the transmitted signal increases as the attenuation in the cocoa butter is lower than that in the chocolate. The seeding was stopped at 3 : 45 min, which resulted in an increase in the velocity of sound while the transmitted signal amplitude decreased.

## 5.4. Open channel flow with hydrogen bubbles

The effect of the concentration of hydrogen bubble reflectors on the quality of the velocity profiles during turbulent flow of water in a 0.5 m wide and 40 m long open channel set-up installed by T. Meile at EPFL (École Polytechnique Fédérale, Lausanne) relevant to hydraulic engineering applications was investigated. The details of the experimental set-up including the electrolysis method to generate hydrogen bubbles by varying applied current between two electrodes were described by Meile *et al.* (2006). The Reynolds number  $Re$  was about  $1.5 \times 10^4$  in the used configuration. The wires for the hydrolysis were installed 2.5 m upstream from the flow measurement. The experiments were carried out at constant volume flow rate of water with the UVP parameters listed in table 5.9. The profiles were measured with the following voltage/current combinations: 0/0, 2.5/50, 6/100, 10/150, 13/200, 18.5/300, 28.5/400 and 30 V/500 mA.

### 5.4.1. Flow profiles and baseband signal

Figure 5.38 shows that the measured velocity profiles are similar when applied current is larger than 100 mA. In contrast, they change drastically for the lowest voltage and when no bubble generation (0 V) was used. The amplitude of the

**Table 5.9.:** UVP parameters common for all profiles shown in section 5.4.

Parameter	Value
Transducer type	TN
Active diameter	10 mm
Number of profiles	25
Number of pulse repetitions	512
Pulse repetition frequency	1.62 kHz
Emission frequency	2 MHz
Voltage	90 V
Gain start	3
Gain end	4
Number of cycles	2
Sound velocity	1480 m/s
Channel distance	0.74 mm
Window Start	6.1 mm

baseband signal can be seen in figures 5.39 and 5.40 to increase more or less linearly with the applied current.

The spectra of the channel 30 are shown in figure 5.41 for different applied currents. The order of the intensities at the actual flow velocity (about 400 mm/s) correspond to the order of the currents. It is interesting to note that the peak around zero velocity seems to be independent of the applied current. This could be an artifact from either the electronics or the transducer or internal echoes of the cavity, where the transducer is fixed. The width of the peak is more or less independent of the signal amplitude. If no current is applied (lowest curve in fig. 5.41) the intensity at the flow velocity of 400 mm/s is the lower than that at 0 mm/s. Consequently, the estimated velocity (fig. 5.38) even under flow conditions is zero.

Further details on two examples of baseband signal data sets (each corresponding to the data used to calculate one FFT based profile) for the measurement where no current was applied, are shown in figure 5.42. These were picked out of 25 profiles by choosing the data sets with the minimum and maximum values of the maximum of the sum of the squares of in-phase ( $I$ ) and co-phase ( $Q$ ) signal. The top row (lowest maximum baseband amplitude) shows a typical speckle pattern in the baseband signal and the frequencies are distributed around zero. In contrast, the bottom row shows a bright (high echo intensity) region (channels 20 to 34) in the surface plot of the baseband signal amplitude. This corresponds to the region with a meaningful velocity in the power spectra plot on the right side, which implies that the structure is a reflector flowing with the water. The Doppler angle

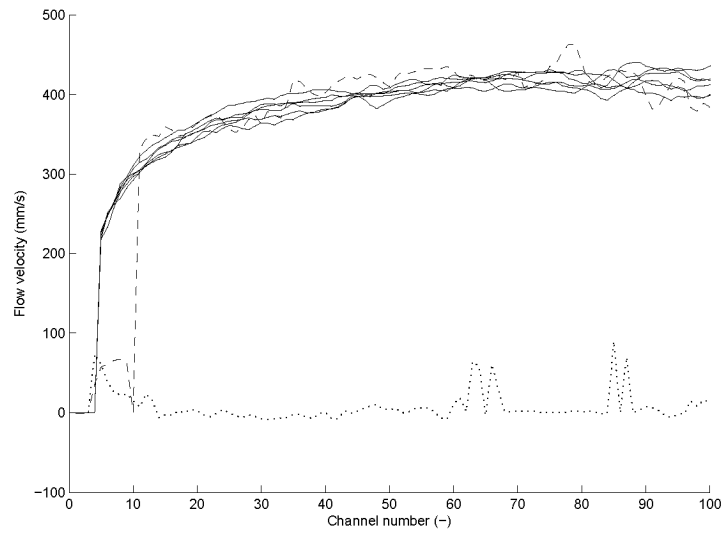


**Figure 5.38.:** Velocity profiles for the eight different applied currents. Dotted line: no current applied; dashed line: 2.5 V/50 mA; full lines: 6 V/100 A to 30 V/500 mA.

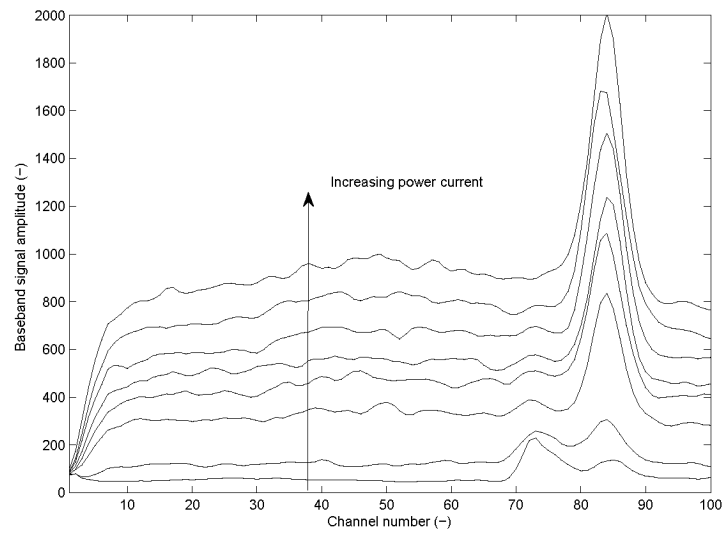


**Figure 5.39.:** The root mean square of the normal part of the demodulated echo amplitude (baseband signal) for the eight applied power currents. The amplitude increases with the current. The peak indicates the location of the water surface.

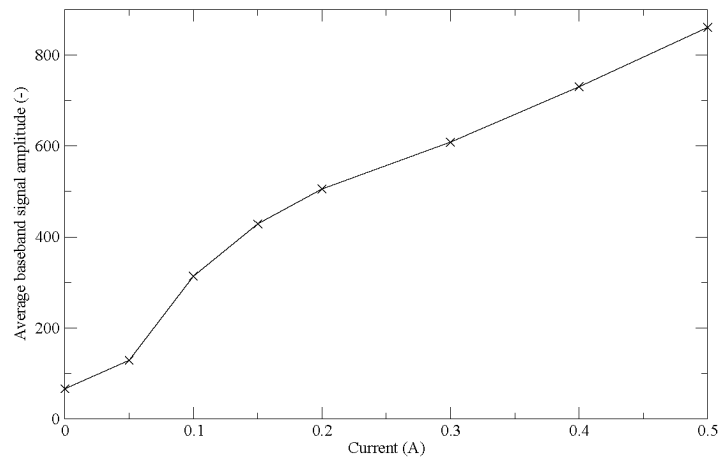


**Figure 5.40.:** The average amplitude of the baseband signal shown in figure 5.39 between channels 1 and 80 in function of the applied current.

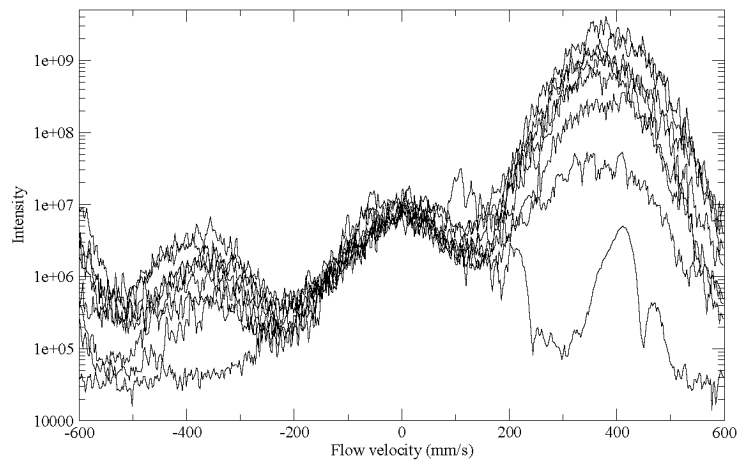


**Figure 5.41.:** Spectra averaged over 20 profile data sets at channel 30 for the different currents.



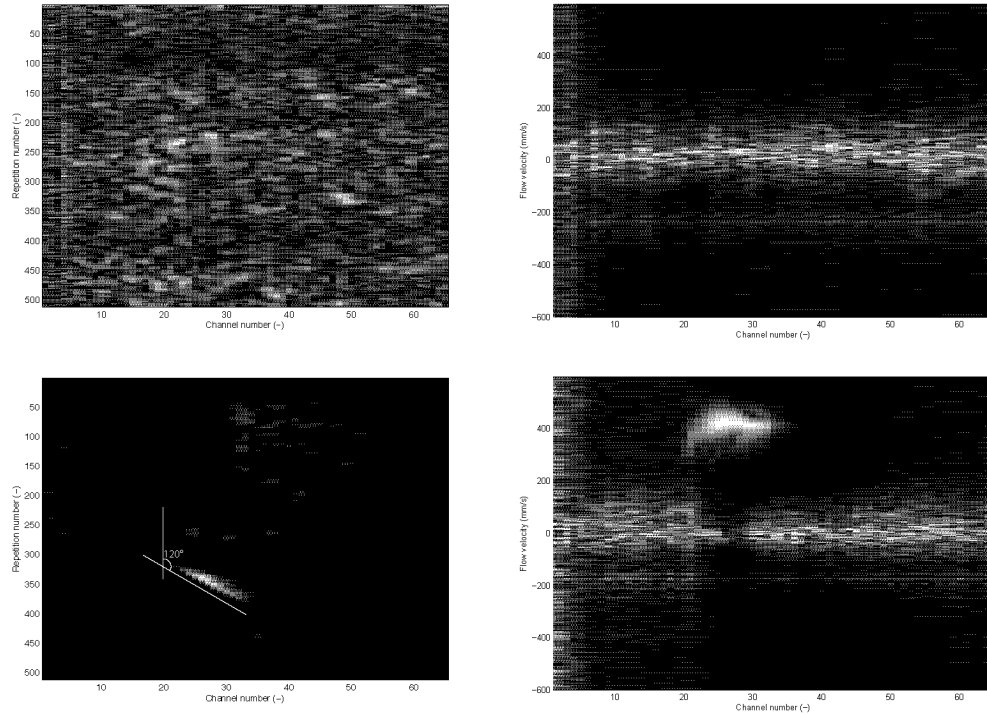


**Figure 5.42.:** Two examples of the baseband signal amplitudes and corresponding power spectra from the measurement with no current (no bubble generation) applied. Top left shows the sum of the squares of  $I$  and  $Q$  for the 512 repetitions and the first 65 channels. The maximum value (white) is 82 000 (which is the minimum of the maxima of the 25 data sets acquired). Top right are the corresponding channel wise power spectra. Bottom left are the demodulated echo amplitudes for the data set with the highest maximum value (3 720 000). The corresponding power spectra are shown bottom right.

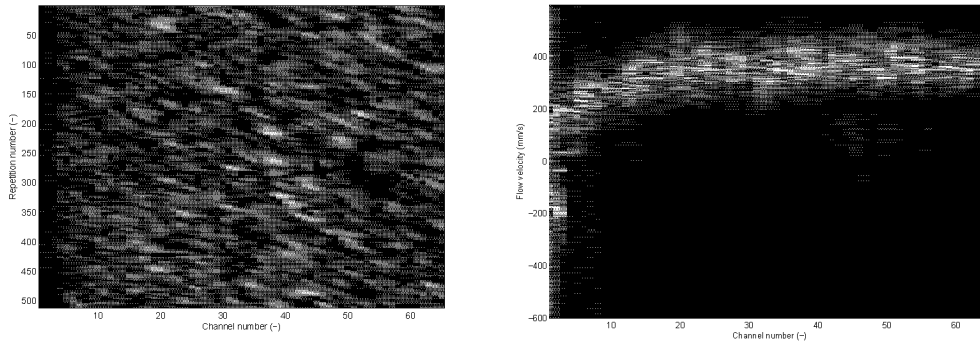


**Figure 5.43.:** Baseband signal amplitudes and corresponding power spectra for a data set with the highest current applied. White corresponds to amplitude of  $28 \times 10^6$ .

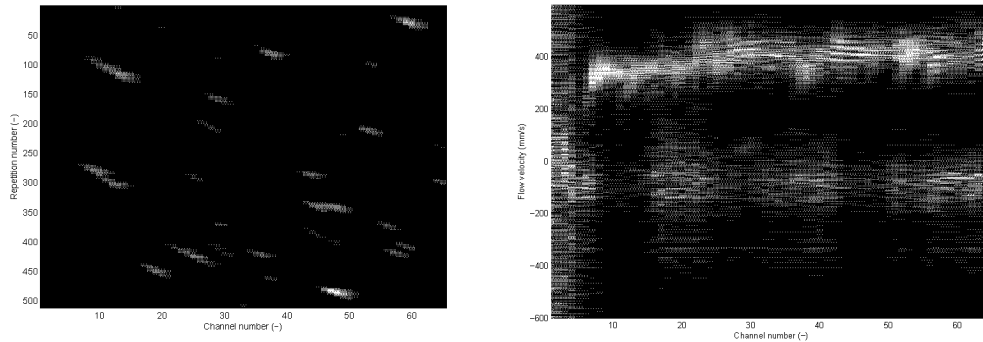
used for the measurements was  $120^\circ$ , this corresponds to the angle with which the structure seems to drift away from the transducer with increasing number of repetitions. The structure is visible for about 50 pulse repetitions corresponding to 31 ms. In that time the flow at 400 mm/s covers 12 mm. The near field length is 34 mm (corresponding to channel 38) for the 2 MHz transducer with an active diameter of 10 mm. The values seem to be realistic considering the fact that the assumed diameter of the bubbles lies between 50 and 100  $\mu\text{m}$ . Unfortunately, the spatial resolution of this measurement is not high enough to measure the creaming velocity of the bubbles.

Figure 5.43 shows a single data set for the measurement where the highest current was applied. Instead of only a single there are many corresponding structures.

### 5.4.2. Concentration of gas bubbles

Assuming that the average bubble diameter is equal to that of the wire (100  $\mu\text{m}$ ) and that a direct correlation of the current to the number of hydrogen bubbles generated exists, it is possible to calculate the number of generated hydrogen bubbles using ideal gas law:  $PV = Nk_B T$ , where  $P$  is the pressure,  $V$  is the volume,  $N$  is the number of molecules and  $T$  is the absolute temperature of the gas bubbles,  $k$  being the Boltzmann's constant. This results in 1500 to 15 000 bubbles per second (for minimum and maximum currents) or 12 000 to 120 000 bubbles per second if the bubble diameter is reduced to 50  $\mu\text{m}$ .

The volume flow rate of water is about 10  $\ell/\text{s}$  so that the concentration of bubbles lies between 0.1 and 1 bubbles per  $\text{m}\ell$  water for the lowest value of the applied current. As the total sample volume in the beam is 50  $\text{m}\ell$  and the total sampling



**Figure 5.44.:** Baseband signal and power spectrum for the case with the minimum current applied.

time for one data set is 0.3 s, one would expect to see between 6.5 and 65 visible bubbles per measurement (in 50 ml + 15 ml). Picking one of the data sets with the minimum current (figure 5.44), these numbers seem to be realistic as approximately 20 bubbles are visible. In view of the assumptions made, one cannot expect a precision higher than an order of magnitude.

As the quality of velocity profile was good for 0.15 A current, one can conclude that even a very low concentration of bubbles of 2 per ml is sufficient, which corresponds to a volume concentration of about 6 ppm for 100  $\mu$ m diameter bubbles.

## 5.5. Rotating cylinder evaluation

In order to test the accuracy of the flow velocity measured by UVP, a rotating cylinder (section 4.2.4) was used in which the flow velocity of a suspension of 0.1 % polyamide particles in water is known. Further details on the setup and the results can be found in Shafiei (2005). In contrast to the previously shown measurements in the current chapter the flow profiles in the rotating cylinder were estimated using the time domain algorithm implemented on the UVP-Duo instrument. Only section 5.5.4.4 shows measurements which were calculated via FFT from the baseband signal.

### 5.5.1. Polyamide reflector particles

Figure 5.45 shows a picture of the polyamide particles obtained from the microscope (Leica DM IRB). The particles look similar to the 11 respectively 90  $\mu$ m polyamide particles from a different supplier shown in figure 5.1. The particle size

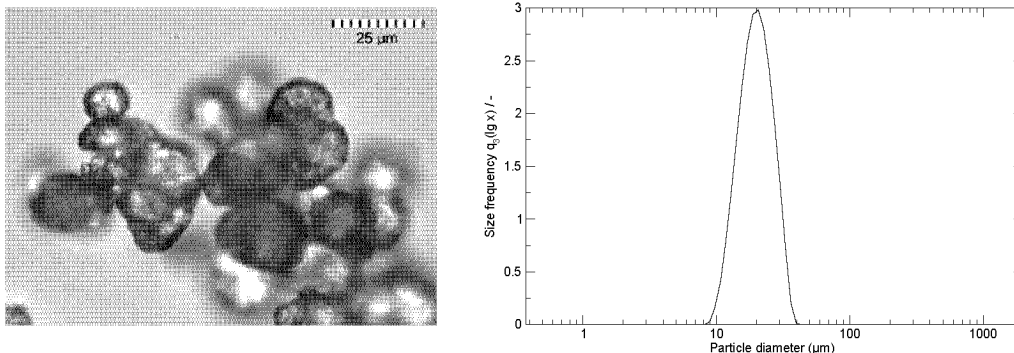


**Figure 5.45.:** On the left side a microscopy image of polyamide suspension in water and on the right side the size distribution of polyamide particles. The average size of particles is about 20 μm.

distribution shown on the right side of figure 5.45 (also measured with the Coulter particle size analyzer) is quite sharp around 20 μm as specified by the supplier Dantec Dynamics.

### 5.5.2. Velocity development

In order to estimate the required waiting time between mixing the content of cylinder (for a homogenous distribution of the polyamide particles which sedimented slowly) and starting the measurement, the development of the velocity over the time after switching on the rotation was measured. It could be seen that after about 120s, the measured velocity reached a steady value. This was then used as minimum waiting time between mixing or changing the rotation speed and conducting a measurement.

### 5.5.3. Reference measurement

Figure 5.46 shows the results of velocity measurements in the big and small cylinders. For both cylinders there is a good agreement between the velocity measured by the UVP and the theoretical velocity calculated from transducer position and rotation speed. The experiments were carried out at two different motor speeds of nominally 30 and 50. The transducer was placed respectively for each motor speed at different positions from 10 mm to 60 mm distance  $\Delta y$  from the center of cylinder (see figure 4.4 on page 48). The relative error averages between 0.7%

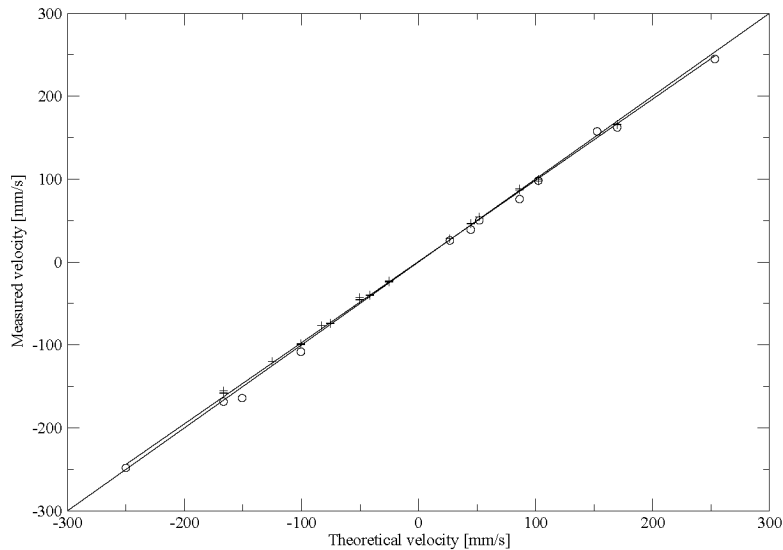


**Figure 5.46.:** The measured velocity versus the theoretical velocity in small (+) and big (O) cylinders. The good agreement between the measured (dashed line) and theoretical velocities (full line) can be observed.

to 12% for the big cylinder and between 0.5% to 15% for the small cylinder. The geometry of cylinder does not seem to make a significant difference in the results.

## 5.5.4. UVP parameters

### 5.5.4.1. Number of repetitions

The number of repetitions is the number of pulses sent and received for a single valid profile measurement. This can be adjusted from 32 to 240 (4095 in the most recent software version) in the UVP. The influence of this parameter on the velocity profile is investigated by varying the number of repetitions between 60 and 240 and comparing the resulting standard deviations in the flow velocity. As a result 120 repetitions were chosen for the further measurements. It is a compromise between the profile quality (mean standard deviation) and the measurement time for a single complete profile. The mean measured velocity from the profile is not significantly influenced by the number of repetitions.

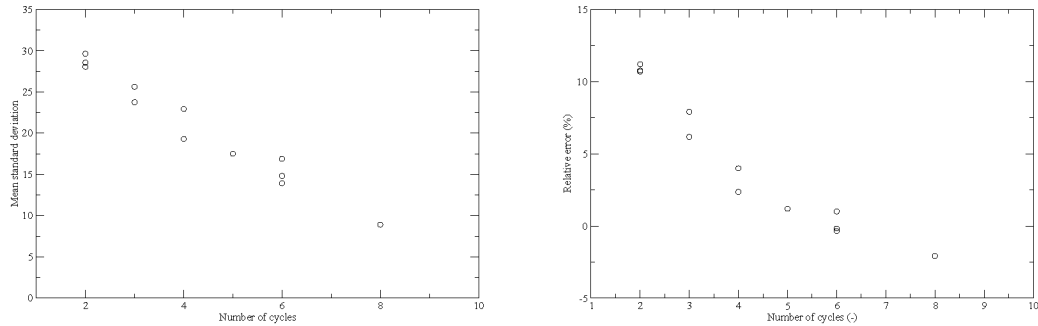


**Figure 5.47.:** The plot on the left side shows mean standard deviation versus number of cycles. The plot on the right side illustrates the % relative error versus number of cycles. Both errors become smaller with an increasing pulse length. Theoretical flow velocity:  $-150.66$  mm/s, transducer position:  $-39.93$  mm.

### 5.5.4.2. Number of cycles

The number of cycles  $n$  multiplied by the wavelength gives the pulse length. The results in figure 5.47 show that the mean standard deviation decreases with the number of cycles. On the other hand, there is a correlation between the pulse length and the spatial resolution which is not important in the case of the rotating cylinder as the projected flow velocity is constant while for the flow profile with the velocity gradient there is strong impact from the length of the pulse (Jorgensen *et al.*, 1973). Adjusting the number of cycles to 4 produces an acceptable relative error (fig. 5.47).

### 5.5.4.3. Rotation speed of cylinder

At a fixed position of the transducer, increasing the speed of rotation of cylinder from 1 to 50 decreased the relative error as indicated in figure 5.48. A low standard deviation at high rotation speed indicates also the quality of measurements, which means that the distribution width is closely around the mean value of velocity.

### 5.5.4.4. FFT based measurement

While the rotating cylinder measurements presented in the previous sections were made using the flow profiles calculated with the time domain algorithm on the UVP instrument this section presents the first data processed in the frequency domain using FFT. The baseband signal was acquired with a custom software

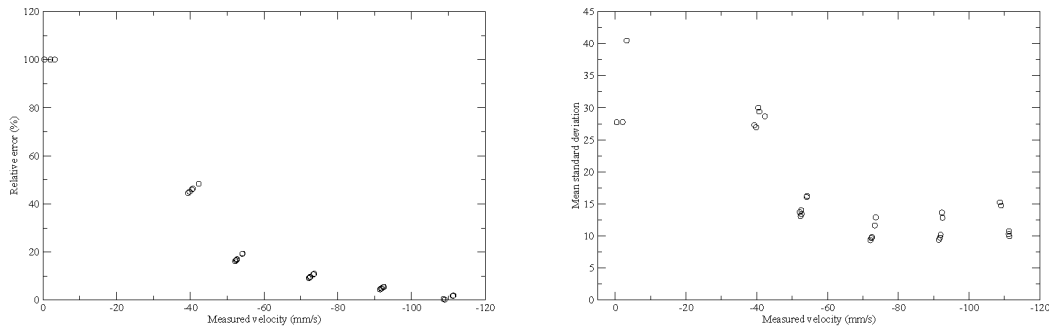


**Figure 5.48.:** The left graph shows the % relative error versus measured velocity and the other graph shows the standard deviation of the measured velocity at different motor speeds. The position of transducer was constant ( $-29.93$  mm) during the measurement.

running directly on the PC inside the UVP instrument that had certain limitations, e. g. the number of repetitions was fixed to 128.

Figure 5.49 illustrates the corresponding results from the experiments with a suspension of polyamide particles in water in the small rotating cylinder. The rather bright area (which is due to the channel wise normalization of the data) on the left side of the plots are in the water around the cylinder which is not seeded with reflectors and which only should only move in a small layer around the cylinder. Then there is a region with the total reflection from the surface of the solid wall of rotating cylinder which has therefore a velocity of zero. The first four plots of figure 5.49 show a zero velocity inside the cylinder volume. This can be explained with the total reflection of the pulse at the cylinder wall and the transducer and its holder (made of metal). The returned echo (having no Doppler shift in the frequency) is superimposed on the echo from along the actual beam path inside the cylinder which is weaker. The effect decreases with increasing  $\Delta y$  as the angle between beam and cylinder wall deviates from normal due to the cylinder curvature and thus the direction of the reflection at the cylinder wall is less directed towards the transducer. The measured velocity and the velocity calculated from the rotation speed are in a good agreement for all the positions, only in the last case with  $\Delta y = 3$  cm the velocity decreases slightly with increasing distance. This can be explained with the curvature of the cylinder (see figure 4.3 on page 47).

## 5. Results and Discussion

---

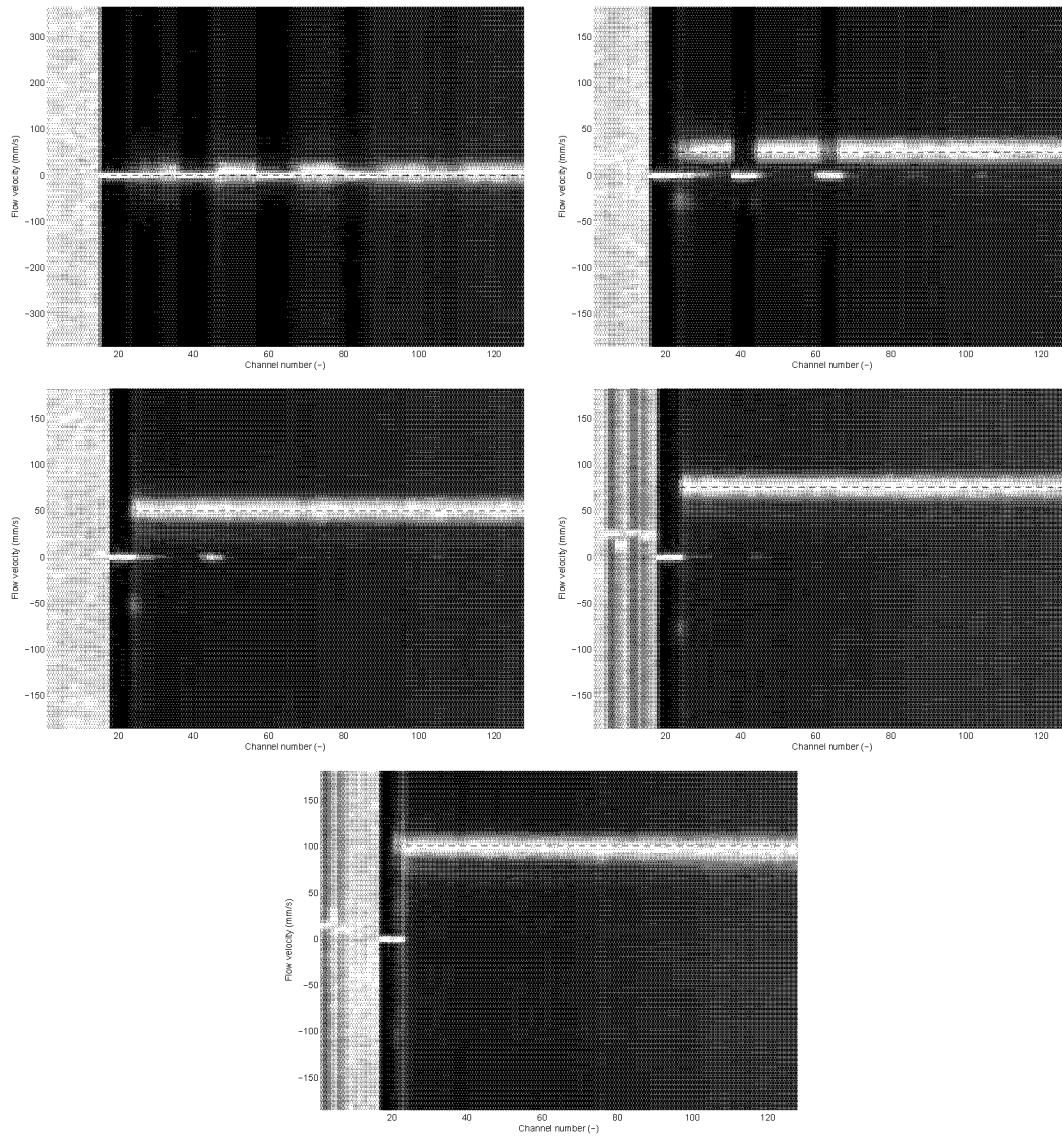


**Figure 5.49.:** Average spectra over 100 measurements of the Doppler shift frequencies for the single channels for the measurements in the small rotating cylinder at different transducer positions ( $\Delta y$  0, 1, 2 and 3 cm) with a constant rotation speed of nominally 30. The velocities calculated from rotation speed (0, 25.5, 50.3, 75.5 and 100.6 mm/s) are shown as dashed lines.



## 6. Conclusions

1. The ultrasound Doppler based velocity profile (UVP) and pressure drop (PD) measurement technique was used effectively for in-line rheological characterization of model particulate suspensions by determining the shear rate using the gradient of the velocity profile along the radius of the pipe. The radial variation in shear stress is obtained by measuring the pressure drop in a pipe section of known length. The corresponding shear rate dependent viscosity determined agreed reasonably well with that measured using the off-line stress controlled rheometer. The viscosity of suspensions of a given concentration of 11  $\mu\text{m}$  diameter unimodal polyamide particles in rapeseed oil decreased with the shear rate indicating shear thinning behaviour. This implies that the migration and sedimentation of particles in the pipe flow appear to be negligible. The viscosity increased with increase in concentration of particles (up to 25 %) but decreased for larger particles (90  $\mu\text{m}$ ). The simultaneously measured sound velocity increased with particle concentration and decreased with particle size.
2. The UVP-PD technique combined with the simultaneous measurement of sound velocity and attenuation was shown to be valuable for the in-line monitoring of rheological properties due to dynamic changes in cocoa butter fat crystallization process parameters relevant to industrial applications. The velocity of sound increased almost linearly with the solid fat content in the cocoa butter crystal suspension, which was found to be shear thinning.
3. The addition of a spectral analysis of the baseband signal to the time domain approach for the determination of the flow velocity profiles proved to be valuable as it not only provided additional quality information (signal amplitude, signal to noise ratio) but also simplified identification of the source of causes of the velocity measurement errors.
4. The application of the power law flow model for the rheological characterization was unrealistic as the fitted parameters were sensitive to the position of the pipe wall and vary significantly even over the minimum distance (370  $\mu\text{m}$ ) of the velocity sampling points. Consequently, the above alternative direct gradient method was found to be more robust and accurate.

## 6. Conclusions

---

5. The accuracy of measurement of flow velocities in suspensions using UVP was evaluated by comparing with the results obtained from experimental investigations of reference rotating cylinder containing dilute aqueous suspensions of reflector particles. The agreement was found to be good.
6. The method of electrolysis to generate gas bubbles to measure ultrasound based velocity profiles in open channel flow enabled the determination of minimum concentration of gas bubbles needed to obtain the actual velocity distribution. The required concentration was found to be in the range of several ppm in water.
7. Ultrasound Doppler based technique demonstrated that it was possible to measure the velocity profiles during the pipe flow of milk chocolate suspension when the pulse length was as low as 1 cycle, the measurement was close to the transducer (about 1 mm) and higher penetration depth was obtained using a lower frequency.
8. The accuracy of the profile measurement could be further improved by investigating the acoustic pressure field, and the size and pressure distribution inside the sample volume. Latter would enable the deconvolution of the profile, which would be relevant for the rheological calculations especially in the vicinity of the pipe wall.

# Appendix



## A. Near field pressure field

The pressure field can be described by the Rayleigh integral (equation (A.1)) which is a reduction of the Kirchhoff-Helmholtz integral:

$$p(\vec{x}, t) = \frac{\rho}{2\pi} \iint \frac{\dot{v}_n(x_S, y_S, t - R/c)}{R} dx_S dy_S \quad (\text{A.1})$$

( $R^2 = z^2 + (x - x_S)^2 + (y - y_S)^2$ ;  $x_S, y_S$ : position on surface S;  $v_n$ : normal velocity of the transducer surface (figure A.1))

The field of an oscillating circular piston is not necessarily easy to describe at intermediate radial distances. However, a simple expression results for the field along the symmetry axis ( $x=0, y=0$ ).

The coordinate system of equation (A.1) is replaced by cylindrical coordinates  $w_S, \phi_S$  and  $z$  ( $x_S = w_S \cos \phi_S, y_S = w_S \sin \phi_S$ ).

$$p(0, 0, z, t) = \frac{\rho}{2\pi} \int_0^{2\pi} \int_0^a \frac{\dot{v}_n(t - R/c)}{R} w_S dw_S d\phi_S \quad (\text{A.2})$$

( $R^2 = z^2 + w_S^2, a$ : active transducer radius)

Integrated one gets

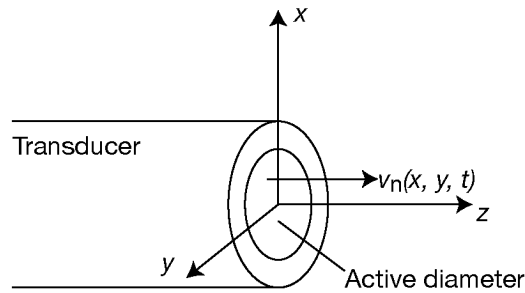


**Figure A.1.:** Scheme of the coordinate system and the normal velocity of the transducer surface.

### A. Near field pressure field

---

$$p = \rho c \left( v_n \left( t - \frac{z}{c} \right) - v_n \left( t - \frac{\sqrt{z^2 + a^2}}{c} \right) \right) \quad (\text{A.3})$$

This can be regarded as the superposition of two waves, one propagating from the center of the piston and the other (with a minus sign prefixed) propagating from the edge of the piston ( $w_S = a$ ).

When the piston is oscillating with constant angular frequency  $\omega$ , the two terms in equation (A.3) may cancel for certain values of  $z$ . With the complex amplitude  $\hat{v}_n \exp(i\omega\tau) = v_n(t - \tau)$  one gets the complex pressure  $\hat{p}$ :<sup>1</sup>

$$\hat{p} = -2i\rho c \hat{v}_n \exp \left\{ \frac{ik \left[ z + \sqrt{z^2 + a^2} \right]}{2} \right\} \sin \left[ \frac{k\sqrt{z^2 + a^2} - kz}{2} \right] \quad (\text{A.5})$$

( $k$ : wave number ( $k = \omega/c$ ))

---

<sup>1</sup>Complex notation: An acoustic disturbance is of constant frequency if the field variables oscillate sinusoidally with time, such that (for the acoustic pressure  $p$ )

$$p = p_{\text{pk}} \cos(\omega t - \phi) = p_{\text{pk}} \sin(\omega t - \phi') = \Re \hat{p} \exp(-i\omega t) \quad (\text{A.4})$$

( $p_{\text{pk}}$ : amplitude or peak pressure;  $\omega$ : angular frequency;  $\hat{p}$ : complex pressure amplitude;  $\phi$ : phase constant.)

The complex-number representation in equation (A.4) is convenient in theoretical studies; in particular, it replaces the amplitude and phase by a single complex number and condenses the writing of mathematical relations. (Pierce, 1981)

# Bibliography

- Adjadj, Laurent P., Alexander K. Hipp, Giuseppe Storti, and Massimo Morbidelli: *Characterization of dispersions by ultrasound spectroscopy*. In Birkhofer *et al.* (2006b), pp. 9–13.
- Akulichev, V. A. and V. N. Bulanov: *Sound propagation in a crystallizing liquid*. Soviet Physics - Acoustics, 27(5):377–381, 1981.
- Alam, S. Kaisar and Kevin J. Parker: *Implementation issues in ultrasonic flow imaging*. Ultrasound in Medicine & Biology, 29(4):895–905, 2003.
- Álava, J. M., S. S. Sahi, J. García-Álvarez, A. Turó, J. A. Chávez, M. J. García, and J. Salazar: *Use of ultrasound for the determination of flour quality*. Ultrasonics, 46:270–276, 2007.
- Allam, M. E. and J. F. Greenleaf: *Isomorphism between pulsed-wave Doppler ultrasound and direction-of-arrival estimation. I. Basic principles*. IEEE Transactions on Ultrasonics, Ferroelectrics, and Frequency Control, 43(5):911–922, 1996.
- Allam, M. E., R. R. Kinnick, and J. F. Greenleaf: *Isomorphism between pulsed-wave Doppler ultrasound and direction-of-arrival estimation. II. Experimental results*. IEEE Transactions on Ultrasonics, Ferroelectrics, and Frequency Control, 43(5):923–935, 1996.
- Allegra, J. R. and S. A. Hawley: *Attenuation of sound in suspensions and emulsions: Theory and experiments*. The Journal of the Acoustical Society of America, 51(5 (Part 2)):1545–1564, 1972.
- Angelsen, Bjørn A. J.: *A theoretical study of the scattering of ultrasound from blood*. IEEE Transactions on Biomedical Engineering, 27(2):61–67, 1980.
- Archer, G. P., C. J. Kennedy, and M. J. W. Povey: *Investigations of ice nucleation in water-in-oil emulsions using ultrasound velocity measurements*. Cryo-Letters, 17:391–396, 1996.
- Arnolds, B. J., D. Kunz, and G. M. von Reutern: *Spatial resolution of transcranial pulsed Doppler technique in vitro evaluation of the sensitivity distribution of the sample volume*. Ultrasound in Medicine & Biology, 15(8):729–735, 1989.
- Arola, Darren F., Geoffrey A. Barrall, Robert L. Powell, Kathryn L. McCarthy, and Michael J. McCarthy: *Use of nuclear magnetic resonance imaging as a viscometer for process monitoring*. Chemical Engineering Science, 52(13):2049–2057, 1997.

- Atkinson, C. M. and H. K. Kytömaa: *Acoustic wave speed and attenuation in suspensions*. International Journal of Multiphase Flow, 18(4):577–592, 1992.
- Atkinson, C. M. and H. K. Kytömaa: *Acoustic properties of solid-liquid mixtures and the limits of ultrasound diagnostics I: Experiments*. Journal of Food Engineering, 115:665–675, 1993.
- Awad, Tareck S.: *Ultrasonic studies of the crystallization behavior of two palm fats o/w emulsions and its modification*. Food Research International, 37:579–586, 2004.
- Bachelet, C., Ph. Dantan, and P. Flaud: *Indirect on-line determination of Newtonian fluid viscosity based on numerical flow simulations*. European Physical Journal - Applied Physics, pp. 67–73, 2003. doi: 10.1051/epjap:2002104.
- Bachelet, C., Ph. Dantan, and P. Flaud: *Indirect on-line determination of the rheological behavior of a power law fluid based on numerical flow simulations*. European Physical Journal - Applied Physics, 25:209–217, 2004.
- Baker, Donald W.: *Pulsed ultrasonic Doppler blood-flow sensing*. IEEE Transactions on Sonics and Ultrasonics, 17(3):170–185, July 1970.
- Baker, Donald W. and William G. Yates: *Technique for studying the sample volume of ultrasonic Doppler devices*. Medical and Biological Engineering, 11(6):766–770, 1973.
- Bamberger, J. A. and M. S. Greenwood: *Non-invasive characterization of fluid foodstuffs based on ultrasonic measurements*. Food Research International, 37(6):621–625, 2004.
- Bambi, G., T. Morganti, S. Ricci, E. Boni, F. Guidi, C. Palombo, and P. Tortoli: *A novel ultrasound instrument for investigation of arterial mechanics*. Ultrasonics, 42:731–737, 2003.
- Barabell, A.: *Improving the resolution performance of eigenstructure-based direction-finding algorithms*. In *IEEE International Conference on Acoustics, Speech, and Signal Processing (ICASSP '83)*, pp. 336–339, 1983.
- Barber, William D., Jefferey W. Eberhard, and Steven G. Karr: *A new time domain technique for velocity measurements using Doppler ultrasound*. IEEE Transactions on Biomedical Engineering, 32(3):213–229, 1985.
- Bascom, P. A. J., R. S. C. Cobbold, and B. H. M. Roelofs: *Influence of spectral broadening on continuous wave Doppler ultrasound spectra: A geometric approach*. Ultrasound in Medicine & Biology, 12(5):387–395, 1986.
- Bascom, Peter A. J. and Richard S. C. Cobbold: *On a fractal packing approach for understanding ultrasonic backscattering from blood*. The Journal of the Acoustical Society of America, 98(6):3040–3049, 1995.
- Bastos, Carlos A. C., Peter J. Fish, Robin Steel, and Francisco Vaz: *Doppler power spectrum from a Gaussian sample volume*. Ultrasonics, 37(9):623–632, 2000.
- Batchelor, G. K.: *The effect of Brownian motion on the bulk stress in a suspension of spherical particles*. Journal of Fluid Mechanics, 83:97–117, 1977.
- Berger, N. E., R. J. Lucas, and V. Twersky: *Polydisperse scattering theory and*



- comparisons with data for red blood cells*. The Journal of the Acoustical Society of America, 89(3):1394–1401, 1991.
- Birkhofer, B., S. A. K. Jeelani, B. Ouriev, and E. J. Windhab: *In-line characterization and rheometry of concentrated suspensions using ultrasound*. In Takeda *et al.* (2004), pp. 65–68.
- Birkhofer, Beat, Jean-Claude Eischen, David Megias-Alguacil, Peter Fischer, and Erich J. Windhab: *Computer-controlled flow cell for the study of particle and drop dynamics in shear flow fields*. Industrial & Engineering Chemistry Research, 44(17):6999–7009, 2005.
- Birkhofer, Beat H., Shaik A. K. Jeelani, Klaus-Jochen Lisner Erich J. Windhab and Boris Ouriev, Peter Braun, and Yuantong Zeng: *Monitoring of fat crystallization process using UVP-PD technique*. In Birkhofer *et al.* (2006b).
- Birkhofer, Beat H., Shaik A. K. Jeelani, and Erich J. Windhab (editors): *Proceedings of the 5th International Symposium on Ultrasonic Doppler Methods for Fluid Mechanics and Fluid Engineering*, 2006b.
- Black, R.A. and T.V. How: *Pulsed Doppler ultrasound system for the measurement of velocity distributions and flow disturbances in arterial prostheses*. Journal of Biomedical Engineering, 11(1):35–42, 1989.
- Bohs, Laurence N., Barry H. Friemel, and Gregg E. Trahey: *Experimental velocity profiles and volumetric flow via two-dimensional speckle tracking*. Ultrasound in Medicine & Biology, 21(7):885–898, 1995.
- Brady, John F.: *Model hard-sphere dispersions: statistical mechanical theory, simulations, and experiments*. Current opinion in Colloid & Interface Science, 1: 472–480, 1996.
- Brandestini, M.: *Topoflow – a digital full range Doppler velocity meter*. IEEE Transactions on Sonics and Ultrasonics, 25(5):287–292, 1978.
- Brands, Peter J., Arnold P. G. Hoeks, Leo Hofstra, and Robert S. Reneman: *A noninvasive method to estimate wall shear rate using ultrasound*. Ultrasound in Medicine & Biology, 21(2):171–185, 1995.
- Brunn, Peter O., Thomas Wunderlich, and Markus Müller: *Ultrasonic rheological studies of a body lotion*. Flow Measurement and Instrumentation, 15(3):139–144, 2004.
- Brunn, P.O., J. Vorwerk, and R. Steger: *Optical and acoustic rheometers: three examples*. Applied Rheology, 3:1(3):20–27, March 1993.
- Butler, Jason E. and Roger T. Bonnecaze: *Imaging of particle shear migration with electrical impedance tomography*. Physics of Fluids, 11(8):1982–1994, 1999.
- Butler, Jason E., Paul D. Majors, and Roger T. Bonnecaze: *Observations of shear-induced particle migration for oscillatory flow of a suspension within a tube*. Physics of Fluids, 11(10):2865–2877, 1999.
- Buyevich, Yu. A. and S. K. Kaprsov: *Segregation of a fine suspension in channel flow*. Journal of Non-Newtonian Fluid Mechanics, 86(1-2):157–184, 1999.
- Cantz, S.: *Anwendung der Ultraschalldoppleranemometrie zur Ermittlung von*

- Rohrströmungsgeschwindigkeitsprofilen in Abhängigkeit von rheologischen Stoffgrößen.* Semesterarbeit, ETH Zürich, 1994.
- Carlson, J. and R. K. Ing: *Ultrasonic particle velocimetry in multiphase flows.* In *IEEE Int. Ultrason. Symp. 2002 (Munich, Germany)*, pp. 740–743. IEEE, 2002.
- Challis, R. E., M. J. W. Povey, M. L. Mather, and A. K. Holmes: *Ultrasound techniques for characterizing colloidal dispersions.* Reports on Progress in Physics, 68(1541-1637):1541–1637, 2005.
- Chang, Chingyi and Robert L. Powell: *Dynamic simulation of bimodal suspensions of hydrodynamically interacting spherical particles.* Journal of Fluid Mechanics, 253:1–25, 1993.
- Chang, Chingyi and Robert L. Powell: *Effect of particle size distributions on the rheology of concentrated bimodal suspensions.* Journal of Rheology, 38(1):85–98, 1994.
- Chaplin, Martin: *Water structure and science*, 2007. <http://www.lsbu.ac.uk/water/explan2.html>.
- Chen, J.-F., J. A. Zagzebski, and E. L. Madsen: *Tests of backscatter coefficient measurement using broadband pulses.* IEEE Transactions on Ultrasonics, Ferroelectrics, and Frequency Control, 40(5):603–607, 1993.
- Chen, Jian-Feng and J. A. Zagzebski: *Frequency dependence of backscatter coefficient versus scatterer volume fraction.* IEEE Transactions on Ultrasonics, Ferroelectrics, and Frequency Control, 43(3):345–353, 1996.
- Choi, Y.J., K.L. McCarthy, and M.J. McCarthy: *Tomographic techniques for measuring fluid flow properties.* Journal of Food Science, 67(7):2718–2724, 2002.
- Choi, Young Jin, Kathryn L. McCarthy, and Michael J. McCarthy: *A MATLAB graphical user interface program for tomographic viscometer data processing.* Computers and Electronics in Agriculture, 47(1):59–67, 2005.
- Choi, Young Jin, Rebecca R. Milczarek, Charles E. Fleck, T. Casey Garvey, Kathryn L. McCarthy, and Michael J. McCarthy: *In-line monitoring of tomato concentrate physical properties during evaporation.* Journal of Food Process Engineering, 29:615–632, 2006.
- Chong, J. S., E. B. Christiansen, and A. D. Baer: *Rheology of concentrated suspensions.* Journal of Applied Polymer Science, 15(8):2007–2021, August 1971.
- Cloostermans, M. J. T. M. and J. M. Thijssen: *A beam corrected estimation of the frequency dependent attenuation of biological tissues from backscattered ultrasound.* Ultrasonic Imaging, 5(2):136–147, 1983.
- Cloutier, G. and Z. Qin: *Ultrasound backscattering from non-aggregating and aggregating erythrocytes – A review.* Bioirheology, 34(6):443–470, 1997.
- Cloutier, G. and K. Kirk Shung: *Cyclic variation of the power of ultrasonic Doppler signals backscattered by polystyrene microspheres and porcine erythrocyte suspensions.* IEEE Transactions on Biomedical Engineering, 40(9):953–962, 1993.
- Cloutier, G., L. Allard, Z. Guo, and L.-G. Durand: *The effect of averaging cardiac Doppler spectrograms on the reduction of their amplitude variability.* Medical &

- Biological Engineering & Computing, 30:177–186, 1992.
- Coupland, John N.: *Low intensity ultrasound*. Food Research International, 37: 537–543, 2004.
- Coupland, John N. and Raffaella Saggin: *Ultrasonic sensors for the food industry*. Advances in food and nutrition research, 45:101–166, 2003.
- Silva, M. Salgueiro da, R.S. Eccleston, J. Bessa Sousa, and S.B. Palmer: *Automated measurement of ultrasound velocity and attenuation*. Ultrasonics, 30(6):347–350, 1992.
- deMan, J. M.: *X-ray diffraction spectroscopy in the study of fat polymorphism*. Food Research International, 25:471–476, 1992.
- Aarssen, M. Van den, W. A. Verhoef, and J. M. Thijssen: *Influence of absorbing and scattering media on the propagation of ultrasound*. The Journal of the Acoustical Society of America, 85(2):567–575, 1989.
- Dickinson, Eric, Michael I. Goller, David J. McClements, Sarah Peasgood, and Malcolm J. W. Povey: *Ultrasonic monitoring of crystallization in an oil-in-water emulsion*. Journal of the Chemical Society, Faraday Transactions, 86: 1147–1148, 1990.
- Dickinson, Eric, David J. McClements, and Malcolm J. W. Povey: *Ultrasonic investigation of the particle size dependence of crystallization in n-hexadecane-in-water emulsions*. Journal of Colloid and Interface Science, 142(1):103–110, 1991.
- Dickinson, Eric, Fokko-Jan Kruizenga, Malcolm J. W. Povey, and Mirjam van der Molen: *Crystallization in oil-in-water emulsions containing liquid and solid droplets*. Colloids and Surfaces A: Physicochemical and Engineering Aspects, 81(13):273–279, 1993.
- Dobromyslov, N. A. and N. I. Koshkin: *Velocity of sound in molecular crystals near the melting point*. Soviet Physics - Acoustics, 15(3):386–387, 1970.
- Dogan, N., M.J. McCarthy, and R.L. Powell: *In-line measurement of rheological parameters and modeling of apparent wall slip in diced tomato suspensions using ultrasonics*. Food Engineering and Physical Properties, 67(6):2235–2240, 2002.
- Dogan, Nihan, Michael J. McCarthy, and Robert L. Powell: *In-line flow and rheology measurements of complex, opaque fluids with velocimeter based rheometry using ultrasonics*. In Peter Fischer, Irene Marti, Erich J. Windhab (editor), *Proceedings of the 3rd International Symposium on Food Rheology and Structure (ISFRS 2003)*, pp. 453–454, 2003a.
- Dogan, Nihan, Michael J. McCarthy, and Robert L. Powell: *Comparison of in-line consistency measurement of tomato concentrates using ultrasonics and capillary methods*. Journal of Food Process Engineering, 25:571–587, 2003b.
- Dogan, Nihan, Michael J. McCarthy, and Robert L. Powell: *Application of an in-line rheological characterization method to chemically modified and native corn starch*. Journal of Texture Studies, 36:237–254, 2005a.
- Dogan, Nihan, Michael J. McCarthy, and Robert L. Powell: *Measurement of poly-*

- mer melt rheology using ultrasonics-based in-line rheometry*. Measurement Science and Technology, 16:1684–1690, 2005b.
- Drost, Martyn: *Anwendung der Ultraschall-dopplernemometrie zur Charakterisierung von Fliesseigenschaften*. Master's thesis, ETH Zürich, Food Process Engineering, 1995.
- Dukhin, A. S. and P. J. Goetz: *Ultrasound for Characterizing Colloids, Particle Sizing, Zeta Potential, Rheology*. Studies in Interface Science. Elsevier, 2002.
- Durst, F., S. Ray, B. Ünsal, and O. A. Bayoumi: *The development lengths of laminar pipe and channel flows*. Journal of Fluids Engineering, 127(6):1154–1160, 2005.
- Durst, Franz, Yasushi Takeda, and Jürgen Vorwerk: *Messungen momentaner Geschwindigkeitsprofile in einer pulsierenden Rohrströmung*. Verfahrenstechnik, 268(6):50–54, 1992.
- Einstein, A.: *Eine neue Bestimmung der Moleküldimensionen*. Annalen der Physik, 324(2):289–306, 1906.
- Einstein, A.: *Berichtigung zu meiner Arbeit: "Eine neue Bestimmung der Moleküldimensionen"*. Annalen der Physik, 339(3):591–592, 1911.
- Elmehdi, H. M., J. H. Page, and M. G. Scanlon: *Monitoring dough fermentation using acoustic waves*. Transactions of the Institution of Chemical Engineers. Part C, Food and bioproducts processing, 81(C3):217–223, 2003.
- Epstein, Paul S. and Richard R. Carhart: *The absorption of sound in suspensions and emulsions. I. Water fog in air*. The Journal of the Acoustical Society of America, 25(3):553–565, 1953.
- Evans, David H. and W. Norman McDicken: *Doppler ultrasound: Physics, instrumentation and signal processing*. Chichester: Wiley, 2nd edition, 2000.
- Evans, J. M. and K. Attenborough: *Coupled phase theory for sound propagation in emulsions*. The Journal of the Acoustical Society of America, 102(1):278–282, 1997.
- Farris, R. J.: *Prediction of the viscosity of multimodal suspensions from unimodal viscosity data*. Transactions of the Society of Rheology/Journal of Rheology, 12(2):281–301, July 1968.
- Fidanzati, Paolo, Tiziano Morganti, and Piero Tortoli: *Real-time software processing and audio reproduction of directional Doppler signals*. Ultrasound in Medicine & Biology, 31(12):1735–1741, 2005.
- Fink, M., F. Hottier, and J. F. Cardoso: *Ultrasonic signal processing for in vivo attenuation measurement: Short time fourier analysis*. Ultrasonic Imaging, 5(2):117–135, 1983.
- Fink, Mathias A. and Jean-François Cardoso: *Diffraction effects in pulse-echo measurement*. IEEE Transactions on Sonics and Ultrasonics, 31(4):313–329, 1984.
- Fischer, Stéphane: *Développement d'une instrumentation pour la mesure des vitesses des liquides dans les conduites à l'aide d'ondes ultrasonores pulsées*. PhD

- thesis, Université Louis Pasteur de Strasbourg, 2004.
- Fischer, Stéphane, Philippe Schmitt, and Benoît Schwaller: *Spectral reconstruction method for liquid velocity measurement beyond the Nyquist limit*. In Takeda *et al.* (2004), pp. 115–120.
- Fischer, Stéphane, Philippe Schmitt, Denis Ensminger, Fares Abda, and Anne Pallares: *A new velocity estimation method using spectral identification of noise*. In Birkhofer *et al.* (2006b).
- Fish, P. J. and J. A. Cope: *Effect of frequency dependent processes on pulsed Doppler sample volume*. *Ultrasonics*, 29(4):275–282, 1991.
- Fish, P. J., P. R. Hoskins, C. Moran, and W. N. McDicken: *Developments in cardiovascular ultrasound: Part 1: Signal processing and instrumentation*. *Medical and Biological Engineering and Computing*, 35(6):561–569, 1997.
- Fish, Peter J.: *The Doppler effect and blood flow: An instrument optimisation programme*. In Povey, M. J. W. and D. J. McClements (editors), *Developments in Acoustics & Ultrasonics*, pp. 91–127. IOP Physical Acoustics Group, Leeds, UK, Institute of Physics Publishing, Bristol and Philadelphia, 1992.
- Flaud, P. and A. Bensalah: *Blood viscosity measurement: an integral method using Doppler ultrasonic profiles*. *European Physical Journal - Applied Physics*, 32: 213–221, 2005.
- Flaud, Patrice, Aziz Bensalah, and Pierre Peronneau: *Deconvolution process in measurement of arterial velocity profiles via an ultrasonic pulsed Doppler velocimeter for evaluation of the wall shear rate*. *Ultrasound in Medicine & Biology*, 23(3):425–436, 1997.
- Fowles, William W.: *Liquid metal flow measurements using an ultrasonic Doppler velocimeter*. *Nature Physical Science*, 242:12–13, March 1973.
- Franca, M. J. and U. Lemmin: *Eliminating velocity aliasing in acoustic Doppler velocity profiler data*. *Measurement Science and Technology*, 17:313–322, 2006.
- Frankel, N. A. and Andreas Acrivos: *On the viscosity of a concentrated suspension of solid spheres*. *Chemical Engineering Science*, 22(6):847–853, June 1967.
- Fryer, Peter and Kerstin Pinschower: *The materials science of chocolate*. *MRS Bulletin*, 25(12):25–29, December 2000.
- Garbini, Joseph L., Fred K. Forster, and Jens E. Jorgensen: *Measurement of fluid turbulence based on pulsed ultrasound techniques. Part 1. Analysis*. *Journal of Fluid Mechanics*, 118:445–470, 1982a.
- Garbini, Joseph L., Fred K. Forster, and Jens E. Jorgensen: *Measurement of fluid turbulence based on pulsed ultrasound techniques. Part 2. Experimental investigation*. *Journal of Fluid Mechanics*, 118:471–505, 1982b.
- Garbolino, Chiara, Gregory R. Ziegler, and John N. Coupland: *Ultrasonic determination of the effect of shear on lipid crystallization*. *The journal of the American Oil Chemists' Society (AOCS)*, 77(2):157–162, 2000.
- Garside, John and Maan R. Al-Dibouni: *Velocity-voidage relationships for fluidization and sedimentation in solid-liquid systems*. *Industrial & engineering*

- chemistry process design and development, 16(2):206–214, 1977.
- Gibson, Richard L. and M. Nafi Toksöz: *Viscous attenuation of acoustic waves in suspensions*. The Journal of the Acoustical Society of America, 85(5):1925–1934, 1989.
- Gill, Robert W.: *Measurement of blood flow by ultrasound: Accuracy and sources of error*. Ultrasound in Medicine & Biology, 11(4):625–641, 1985.
- Gladwell, N., C. Javanaud, K. E. Peers, and R. R. Rahalkar: *Ultrasonic behavior of edible oils: Correlation with rheology*. The journal of the American Oil Chemists' Society (JAOCS), 62(8):1231–1236, 1985.
- Gondret, Philippe and Luc Petit: *Dynamic viscosity of macroscopic suspensions of bimodal sized solid spheres*. Journal of Rheology, 41(6):1261–1274, 1997.
- Guidi, G., V. L. Newhouse, and P. Tortoli: *Doppler spectrum shape analysis based on the summation of flow-line spectra*. IEEE Transactions on Ultrasonics, Ferroelectrics, and Frequency Control, 42(5):907–915, 1995.
- Guidi, Gabriele, Leonardo Corti, and Piero Tortoli: *Application of autoregressive methods to multigate spectral analysis*. Ultrasound in Medicine & Biology, 26(4):585–592, 2000.
- Haïder, Leïla, Jacques Tatibouët, Arnaud Lafaurie, and Laurent Ferry: *In-line ultrasonic characterization of shear dispersion processes of polydisperse fillers in polymer melts*. Journal of Physics: Condensed Matter, 14:4943–4961, 2002.
- Hampton, R. E., A. A. Mammoli, A. L. Graham, N. Tetlow, and S. A. Altobelli: *Migration of particles undergoing pressure-driven flow in a circular conduit*. Journal of Rheology, 41(3):621–640, 1997.
- Harker, A. H. and J. A. G. Temple: *Velocity and attenuation of ultrasound in suspensions of particles in fluids*. Journal of Physics D: Applied Physics, 21:1576–1588, 1988.
- Hein, I. A. and William D. O'Brien: *Current time-domain methods for assessing tissue motion by analysis from reflected ultrasound echoes – A review*. IEEE Transactions on Ultrasonics, Ferroelectrics, and Frequency Control, 40(2):84–102, 1993.
- Hernqvist, L.: *Polymorphism of triglycerides a crystallographic review*. Food Structure, 9:39–44, 1990.
- Hiemenz, P. C. and R. Rajagopalan: *Principles of colloid and surface chemistry*. Marcel Dekker, 3rd edition, 1997.
- Hill, C. R. (editor): *Physical principles of medical ultrasound*. Wiley, 2nd edition, 2004.
- Hindle, Scott, Malcolm J. W. Povey, and Kevin Smith: *Kinetics of crystallization in n-hexadecane and cocoa butter oil-in-water emulsions accounting for droplet collision-mediated nucleation*. Journal of Colloid and Interface Science, 232:370–380, 2000.
- Ho, B. P. and L. G. Leal: *Inertial migration of rigid spheres in two-dimensional unidirectional flows*. Journal of Fluid Mechanics, 65:365–400, 1974.

- Hodate, Y., S. Ueno, J. Yano, T. Katsuragi, Y. Tezuka, T. Tagawa, N. Yoshimoto, and K. Sato: *Ultrasonic velocity measurement of crystallization rates of palm oil in oil-water emulsions*. Colloids and Surfaces A: Physicochemical and Engineering Aspects, 128(1):217–224, 1997.
- Hoeks, A. P. G., C. J. Ruissen, P. Hick, and R. S. Reneman: *Methods to evaluate the sample volume of pulsed Doppler systems*. Ultrasound in Medicine & Biology, 10(4):427–434, 1984.
- Hoeks, Arnold P. G., Michael Hennerici, and Robert S. Reneman: *Spectral composition of Doppler signals*. Ultrasound in Medicine & Biology, 17(8):751–760, 1991.
- Hoffman, Richard L.: *Factors affecting the viscosity of unimodal and multimodal colloidal dispersions*. Journal of Rheology, 36(5):947–965, July 1992.
- Holmes, Andrew K., Richard E. Challis, and David J. Wedlock: *A wide bandwidth study of ultrasound velocity and attenuation in suspensions: Comparison of theory with experimental measurements*. Journal of Colloid and Interface Science, 156:261–268, 1993.
- Holmes, Andrew K., Richard E. Challis, and David J. Wedlock: *A wide bandwidth study of ultrasound velocity and attenuation in suspensions: The variation of velocity and attenuation with particle size*. Journal of Colloid and Interface Science, 168:339–348, 1994.
- Hoskins, P. R.: *Choice of moving target for a string phantom: I. Measurement of filament backscatter characteristics*. Ultrasound in Medicine & Biology, 20(8):773–780, 1994a.
- Hoskins, P. R.: *Choice of moving target for a string phantom: II. On the performance testing of Doppler ultrasound systems*. Ultrasound in Medicine & Biology, 20(8):781–789, 1994b.
- Hoskins, P. R., T. Loupas, and W. N. McDicken: *A comparison of three different filters for speckle reduction of Doppler spectra*. Ultrasound in Medicine & Biology, 16(4):375–389, 1990.
- Hughes, P. E. and T. V. How: *Quantitative measurement of wall shear rate by pulsed Doppler ultrasound*. Journal of Medical Engineering & Technology, 17(2):58–64, 1993.
- Hughes, P. E. and T. V. How: *Pulsatile velocity distribution and wall shear rate measurement using pulsed Doppler ultrasound*. Journal of Biomechanics, 27(1):103–110, 1994.
- Hung, B. N. and A. Goldstein: *Acoustic parameters of commercial plastics*. IEEE Transactions on Sonics and Ultrasonics, 30(4):249–254, 1983.
- Hunt, John W., Marcel Arditi, and F. Stuart Foster: *Ultrasound transducers for pulse-echo medical imaging*. IEEE Transactions on Biomedical Engineering, 30(8):453–481, 1983.
- Hussin, A. B. B. H. and M. J. W. Povey: *A study of dilatation and acoustic propagation in solidifying fats and oils: II. Experimental*. The journal of the

- American Oil Chemists' Society (JAOCS), 61(3):560–564, March 1984.
- Insana, Michael F., Ernest L. Madsen, Timothy J. Hall, and James A. Zagzebski: *Tests of the accuracy of a data reduction method for determination of acoustic backscatter coefficients*. The Journal of the Acoustical Society of America, 79(5):1230–1236, 1986.
- Javanaud, C.: *Applications of ultrasound to food systems*. Ultrasonics, 26:117–123, May 1988.
- Jeelani, S.A.K., G. Benoist, K. S. Joshi, R. Gunde, D. Kellenberger, and E.J. Windhab: *Creaming and aggregation of particles in suspensions*. Colloids and Surfaces A: Physicochem. Eng. Aspects, 263:379–389, 2005.
- Jensen, J. A., J. Mathorne and T. Gravesen, and B. Stage: *Deconvolution of in vivo ultrasound B-Mode images*. Ultrasonic Imaging, 15(2):122–133, 1993.
- Jensen, Jørgen Arendt: *A model for the propagation and scattering of ultrasound in tissue*. The Journal of the Acoustical Society of America, 89(1):182–190, 1991.
- Jensen, Jørgen Arendt: *Estimation of blood velocities using ultrasound: A signal processing approach*. Cambridge University Press, 1996.
- Jensen, Jørgen Arendt: *Algorithms for estimating blood velocities using ultrasound*. Ultrasonics, 38:358–362, 2000.
- Johansson, Matthias and Johan Wiklund: *In-line rheological measurements of complex model fluids using an ultrasound UVP-PD based method*. Master's thesis, Swiss Federal Institute of Technology (Zurich), Swedish Institute for Food and Biotechnology (Gothenburg), Chalmers University of Technology, 2001.
- Jones, Steven A.: *Fundamental sources of error and spectral broadening in Doppler ultrasound signals*. Critical Reviews in Biomedical Engineering, 21(5):399–483, 1993.
- Jorgensen, J. E. and J. L. Garbini: *An analytical procedure of calibration for the pulsed ultrasonic Doppler flow meter*. Transactions of the ASME/Journal of Fluids Engineering, 96:158–167, June 1974.
- Jorgensen, J. E., D. N. Campau, and D. W. Baker: *Physical characteristics and mathematical modeling of pulsed ultrasonic flowmeter*. Medical and Biological Engineering, 11(4):404–421, 1973.
- Karnis, A., H. L. Goldsmith, and S. G. Mason: *The kinetics of flowing dispersions: I. Concentrated suspensions of rigid particles*. Journal of Colloid and Interface Science, 22(6):531, 1966.
- Kell, George S.: *Density, thermal expansivity, and compressibility of liquid water from 0° to 150°C: Correlations and tables for atmospheric pressure and saturation reviewed and expressed on 1968 temperature scale*. Journal of Chemical and Engineering Data, 20(1):97–105, 1975.
- Kikura, H., G. Yamanaka, and M. Aritomi: *Effect of measurement volume size on turbulent flow measurement using ultrasonic Doppler method*. Experiments in Fluids, 36(1):187–196, 2004.



- Kim, Hyungsuk and Tomy Varghese: *Attenuation estimation using spectral cross-correlation*. IEEE Transactions on Ultrasonics, Ferroelectrics, and Frequency Control, 54(3):510–519, 2007.
- Kishiro, Masami, Noritomo Hirayama, Hironobu Yao, Toshihiro Yamamoto, and Yasushi Takeda: *Analysis of frequency characteristics on non-invasive ultrasonic-Doppler flow measurement for metal pipes*. In Takeda et al. (2004), pp. 95–100.
- Kloek, William, Pieter Walstra, and Ton van Vliet: *Nucleation kinetics of emulsified triglyceride mixtures*. The journal of the American Oil Chemists' Society (JAOCS), 77(6):643–652, 2000.
- Koh, Christopher J., Philip Hookham, and L. G. Leal: *An experimental investigation of concentrated suspension flows in a rectangular channel*. Journal of Fluid Mechanics, 266:1–32, 1994.
- Kowalewski, T. A.: *Velocity profiles of suspension flowing through a tube*. Archives of Mechanics, 32(6):857–865, 1980.
- Krieger, Irvin M. and Thomas J. Dougherty: *Mechanism for non-Newtonian flow in suspensions of rigid spheres*. Transactions of the Society of Rheology/Journal of Rheology, 3(1):137–152, 1959.
- Kulmyrzaev, Asylbek and David Julian McClements: *High frequency dynamic shear rheology of honey*. Journal of Food Engineering, 45(4):219–224, 2000.
- Kytömaa, H. K. and C. M. Atkinson: *Sound propagation in suspensions and acoustic imaging of their microstructure*. Mechanics of Materials, 16(1-2):189–197, 1993.
- Kytömaa, Harri K.: *Theory of sound propagation in suspensions: A guide to particle size and concentration characterization*. Powder Technology, 82(1):115–121, 1995.
- Lareo, C., C.A. Branch, and P.J. Fryer: *Particle velocity profiles for solid-liquid food flows in vertical pipes. Part I. Single particles*. Powder Technology, 93: 23–34, 1997a.
- Lareo, C., P. J. Fryer, and M. Barigou: *The fluid mechanics of two-phase solid-liquid food flows: A review*. Transactions of the Institution of Chemical Engineers. Part C, Food and bioproducts processing, 75(C2):73–105, June 1997b.
- Lareo, C., R. M. Nedderman, and P. J. Fryer: *Particle velocity profiles for solid-liquid food flows in vertical pipes. Part II. Multiple particles*. Powder Technology, 93(1):35–45, 1997c.
- Larson, Ronald G.: *The structure and Rheology of Complex Fluids*. Topics in Chemical Engineering. Oxford University Press, 1999.
- Larsson, K.: *Classification of glyceride crystal forms*. Acta Chemica Scandinavica, 20(8):2255, 1966.
- Law, Y. F., K. W. Johnston, H. F. Routh, and R. S. C. Cobbold: *On the design and evaluation of a steady flow model for Doppler ultrasound studies*. Ultrasound in Medicine & Biology, 15(5):505–516, 1989.

- Law, Y. F., P. A. J. Bascom, K. W. Johnston, P. Vaitkus, and R. S. C. Cobbold: *Experimental study of the effects of pulsed Doppler sample volume size and position on the Doppler spectrum*. Ultrasonics, 29(5):404–410, 1991.
- Lee, Paul P. K. and Robert C. Waag: *Spectral analysis of pulsed ultrasound for blood flow measurement in the presence of noise*. In *Ultrasonics Symposium*, 1978.
- Leighton, David and Andreas Acrivos: *The shear-induced migration of particles in concentrated suspensions*. Journal of Fluid Mechanics, 181:415–439, 1987.
- Lemmin, Ulrich and Thierry Rolland: *Acoustic velocity profiler for laboratory and field studies*. Journal of Hydraulic Engineering, 123(12):1089–1098, 1997.
- Lhermitte, R. and U. Lemmin: *Open-channel flow and turbulence measurement by high-resolution Doppler sonar*. Journal of Atmospheric and Ocean Technology, 11:1295–1308, October 1994.
- Lhermitte, Roger and Robert Serafin: *Pulse-to-pulse coherent Doppler sonar signal processing techniques*. Journal of Atmospheric and Oceanic Technology, 1(4): 293–308, 1984.
- Lin, Yu-Hong and K. Kirk Shung: *Ultrasonic backscattering from porcine whole blood of varying hematocrit and shear rate under pulsatile flow*. Ultrasound in Medicine & Biology, 25(7):1151–1158, 1999.
- Liu, D. C., J. Kim, and M. Schardt: *Modified autocorrelation method compared with maximum entropy method and RF cross correlation method as mean frequency estimator for Doppler ultrasound*. In *1991 Ultrasonics Symposium*, volume 2, pp. 1285–1290. IEEE, 1991.
- Lloyd, P. and M. V. Berry: *Wave propagation through an assembly of spheres: IV. Relations between different multiple scattering theories*. Proceedings of the Physical Society, 91:678–688, 1967.
- Lockwood, G. R., L. K. Ryan, J. W. Hunt, and F. S. Foster: *Measurement of the ultrasonic properties of vascular tissues and blood from 35–65 MHz*. Ultrasound in Medicine & Biology, 17(7):653–666, 1991.
- Lombardi, R., G. Danese, and F. Leporati: *Flow rate profiler: An instrument to measure blood velocity profiles*. Ultrasonics, 39:143–150, 2001.
- Loupas, T., R. B. Peterson, and R. W. Gill: *Experimental evaluation of velocity and power estimation for ultrasound blood flow imaging, by means of a two-dimensional autocorrelation approach*. IEEE Transactions on Ultrasonics, Ferroelectrics, and Frequency Control, 42(4):689–699, 1995a.
- Loupas, T., J. T. Powers, and R. W. Gill: *An axial velocity estimator for ultrasound blood flow imaging, based on a full evaluation of the Doppler equation by means of a two-dimensional autocorrelation approach*. IEEE Transactions on Ultrasonics, Ferroelectrics, and Frequency Control, 42(4):672–688, 1995b.
- Lyon, M. K. and L. G. Leal: *An experimental study of the motion of concentrated suspensions in two-dimensional channel flow. Part 1. Monodisperse systems*. Journal of Fluid Mechanics, 363:25–56, 1998a.

- Lyon, M. K. and L. G. Leal: *An experimental study of the motion of concentrated suspensions in two-dimensional channel flow. Part 2. Bidisperse systems.* Journal of Fluid Mechanics, 363:57–77, 1998b.
- Macosko, Christopher W.: *Rheology: Principles, measurements, and applications.* VCH Publishers, Inc., 1994.
- Madsen, Ernest L., Michael F. Insana, and James A. Zagzebski: *Method of data reduction for accurate determination of acoustic backscatter coefficients.* The Journal of the Acoustical Society of America, 76(3):913–923, 1984.
- Maier, S. E., D. Meier, P. Boesiger, U. T. Moser, and A. Vieli: *Human abdominal aorta: Comparative measurements of blood flow with MR imaging and multi-gated Doppler US.* Radiology, 171:487–492, 1989.
- Manneville, Sébastien, Lydiane Bécu, and Annie Colin: *High-frequency ultrasonic speckle velocimetry in sheared complex fluids.* The European Physical Journal - Applied Physics, 2003.
- Marangoni, Alejandro G. and Sara E. McGauley: *Relationship between crystallization behavior and structure in cocoa butter.* Crystal Growth & Design, 3(1): 95–108, 2003.
- Marasek, Krzysztof and Andrzej Nowicki: *Comparison of the performance of three maximum Doppler frequency estimators coupled with different spectral estimation methods.* Ultrasound in Medicine & Biology, 20(7):629–638, 1994.
- Markou, Christos P. and David N. Ku: *Accuracy of velocity and shear rate measurements using pulsed Doppler ultrasound: A comparison of signal analysis techniques.* Ultrasound in Medicine & Biology, 17(8):803–814, 1991.
- Martini, Silvana, Constatin Bertoli, Maria Lidia Herrera, Ian Neeson, and Alejandro Marangoni: *Attenuation of ultrasonic waves: Influence of microstructure and solid fat content.* The journal of the American Oil Chemists' Society (JAOCS), 82(5):319–328, May 2005.
- Matas, Jean-Philippe, Virginie Glezer, Élisabeth Guazzelli, and Jeffrey F. Morris: *Trains of particles in finite-Reynolds-number pipe flow.* Physics of Fluids, 16 (11):4192–4195, 2004.
- McArdle, Andrew and Vernon L. Newhouse: *Doppler bandwidth dependence on beam to flow angle.* The Journal of the Acoustical Society of America, 99(3): 1767–1778, 1996.
- McClements, D. J. and P. Fairley: *Ultrasonic pulse echo reflectometer.* Ultrasonics, 29:58–62, January 1991.
- McClements, D. J. and M. J. W. Povey: *Solid fat content determination using ultrasonic velocity measurements.* International Journal of Food Science and Technology, 22:491–499, 1987a.
- McClements, D. J. and M. J. W. Povey: *Comparison of pulsed NMR and ultrasonic velocity techniques for determining solid fat content.* International Journal of Food Science and Technology, 23:159–170, 1988a.
- McClements, D. J. and M. J. W. Povey: *Ultrasonic velocity measurements in some*

- liquid triglycerides and vegetable oils*. The journal of the American Oil Chemists' Society (JAOCS), 65(11):1787–1790, November 1988b.
- McClements, D. J. and M. J. W. Povey: *Investigation of phase transitions in glyceride/paraffin oil mixtures using ultrasonic velocity measurements*. The journal of the American Oil Chemists' Society (JAOCS), 65(11):1791–1795, November 1988c.
- McClements, D. J. and M. J. W. Povey: *Scattering of ultrasound by emulsions*. Journal of Physics D: Applied Physics, 22:38–47, 1989.
- McClements, D. J. and Malcolm J.W. Povey: *Ultrasonic analysis of edible fats and oils*. Ultrasonics, 30(6):383–388, 1992.
- McClements, D. J., M. J. W. Povey, M. Jury, and E. Betsanis: *Ultrasonic characterization of a food emulsion*. Ultrasonics, 28:266–272, July 1990.
- McClements, D. Julian: *Ultrasonic characterization of foods and drinks: Principles, methods, and applications*. Critical Reviews in Food Science and Nutrition, 37(1):1–46, 1997.
- McClements, D. Julian, Eric Dickinson, Stephanie R. Dungan, John E. Kinsella, Jian G. Ma, and Malcolm J. W. Povey: *Effect of emulsifier type on the crystallization kinetics of oil-in-water emulsions containing a mixture of solid and liquid droplets*. Journal of Colloid and Interface Science, 160(2):293–297, 1993a.
- McClements, D. Julian, Malcolm J.W. Povey, and Eric Dickinson: *Absorption and velocity dispersion due to crystallization and melting of emulsion droplets*. Ultrasonics, 31(6):433–437, 1993b.
- McClements, David Julian: *Handbook on Ultrasonic and Dielectric characterization Techniques for Suspended Particulates*, chapter Ultrasonic Characterization of Food Emulsions, pp. 305–316. The American Ceramic Society, 1998.
- McClements, David Julian and Malcolm James William Povey: *Ultrasonic velocity as a probe of emulsions and suspensions*. Advances in Colloid and Interface Science, 27:285–316, 1987b.
- McDicken, W. N.: *A versatile test-object for the calibration of ultrasonic Doppler flow instruments*. Ultrasound in Medicine & Biology, 12(3):245–249, 1986.
- Meagher, S., T.L. Poepping, K.V. Ramnarine, R.A. Black, and P.R. Hoskins: *Anatomical flow phantoms of the nonplanar carotid bifurcation, Part II: Experimental validation with Doppler ultrasound*. Ultrasound in Medicine & Biology, 33(2):303–310, 2006.
- Meile, Tobias, Giovanni de Cesare, Koen Blanckaert, and Anton J. Schleiss: *Improving acoustic Doppler velocimetry in steady and unsteady flow by means of seeding with hydrogen bubbles*. In Birkhofer *et al.* (2006b), pp. 97–100.
- Miles, C. A. and G. A. J. Fursey: *Measurement of the fat content of meat using ultrasonic waves*. Food Chemistry, 2(2):107–118, 1977.
- Miles, Christopher A., Graham A. J. Fursey, and Richard C. D. Jones: *Ultrasonic estimation of solid/liquid ratios in fats, oils and adipose tissue*. Journal of the science of food and agriculture, 36:215–228, 1985.

- Miller, Ryan M. and Jeffrey F. Morris: *Normal stress-driven migration and axial development in pressure-driven flow of concentrated suspensions*. Journal of Non-Newtonian Fluid Mechanics, 135(2-3):149–165, 2006.
- Mo, L. Y. L., Y.-I. Kuo, K. Kirk Shung, L. Ceresne, and R. S. C. Cobbold: *Ultrasound scattering from blood with hematocrits up to 100%*. IEEE Transactions on Biomedical Engineering, 41(1):91–95, 1994.
- Müller, M., P.O. Brunn, and C. Harder: *New rheometric technique: The gradient-ultrasound pulse Doppler method*. Applied Rheology, 7(5):204–210, 1997.
- Müller-Fischer, Nadina and Erich J. Windhab: *Influence of process parameters on microstructure of food foam whipped in a rotor-stator device within a wide static pressure range*. Colloids and Surfaces A: Physicochemical and Engineering Aspects, 263:353–362, 2005.
- Murakawa, Hideki, Hiroshige Kikura, and Masonori Aritomi: *Application of ultrasonic Doppler method for bubbly flow measurement using two ultrasonic frequencies*. Experimental Thermal and Fluid Science, 29:843–850, 2005.
- Newhouse, V. L. and Israel Amir: *Time dilation and inversion properties and the output spectrum of pulsed Doppler flowmeters*. IEEE Transactions on Sonics and Ultrasonics, 30(3):175–179, 1983.
- Norman, Jay T. and Roger T. Bonnecaze: *Measurement of solids distribution in suspension flows using electrical resistance tomography*. The Canadian Journal of Chemical Engineering, 83(1):24–36, 2005.
- Norman, Jay T., Hebri V. Nayak, and Roger T. Bonnecaze: *Migration of buoyant particles in low-Reynolds-number pressure-driven flows*. Journal of Fluid Mechanics, 523:1–35, 2005.
- Nott, Prabhu R. and John F. Brady: *Pressure-driven flow of suspensions: Simulation and theory*. Journal of Fluid Mechanics, 275:157–199, 1994.
- Nowak, M.: *Wall shear stress measurement in a turbulent pipe flow using ultrasound Doppler velocimetry*. Experiments in Fluids, 33:249–255, 2002.
- Ouriev, B.: *Investigation of the wall slip effect in highly concentrated disperse systems by means of non-invasive UVP-PD method in the pressure driven shear flow*. Colloid Journal, 64(6):740–745, November 2002.
- Ouriev, B. and E. J. Windhab: *Rheological study of concentrated suspensions in pressure-driven shear flow using a novel in-line ultrasound Doppler method*. Experiments in Fluids, pp. 204–211, 2002.
- Ouriev, Boris: *Ultrasound Doppler Based In-Line Rheometry of Highly Concentrated Suspensions*. PhD thesis, ETH Zürich, 2000.
- Ouriev, Boris and Erich Windhab: *Transient flow of highly concentrated suspensions investigated using the ultrasound velocity profiler-pressure difference method*. Measurement Science and Technology, 14(11):1963–1972, 2004.
- Ouriev, Boris and Erich Windhab: *Novel ultrasound based time averaged flow mapping method for die entry visualization in flow of highly concentrated shear-thinning and shear-thickening suspensions*. Measurement Science and Technol-

- ogy, 14(1):140–147, January 2003.
- Ouriev, Boris, Erich Windhab, Peter Braun, Yuantong Zeng, and Beat Birkhofer: *Industrial application of ultrasound based in-line rheometry: Visualization of steady shear pipe flow of chocolate suspension in pre-crystallization process*. Review of Scientific Instruments, 74(12):5255–5259, 2003.
- Ouriev, Boris, Erich Windhab, Peter Braun, and Beat Birkhofer: *Industrial application of ultrasound based in-line rheometry: From stationary to pulsating pipe flow of chocolate suspension in precrystallization process*. Review of Scientific Instruments, 75(10):3164–3168, 2004.
- Padar, Stefan: *The colloidal properties of cocoa butter crystal suspensions*. Master’s thesis, ETH Zürich, 2003.
- Pedersen, Morten H., Thanassis X. Misaridis, and Jørgen A. Jensen: *Clinical evaluation of chirp-coded excitation in medical ultrasound*. Ultrasound in Medicine & Biology, 29(6):895–905, 2003.
- Peronneau, Pierre: *Ultrasound pulsed Doppler velocimetry*. In *Engineering in Medicine and Biology Society, Vol.14. Proceedings of the Annual International Conference of the IEEE*, volume 7, pp. 2863–2866, 1992.
- Pfund, David M., Margaret S. Greenwood, Judith Ann Bamberger, and Richard A. Pappas: *In-line ultrasonic rheometry by pulsed Doppler*. Ultrasonics, 44:e477–e482, 2006.
- Phillips, Ronald J., Robert C. Armstrong, Robert A. Brown, Alan L. Graham, and James R. Abbott: *A constitutive equation for concentrated suspensions that accounts for shear-induced particle migration*. Physics of Fluids, 4(1):30–40, 1992.
- Phung, Thanh N., John F. Brady, and Georges Bossis: *Stokesian dynamics simulation of brownian suspensions*. Journal of Fluid Mechanics, 313:181–207, 1996.
- Pierce, Allan D.: *Acoustics; An Introduction to Its Physical Principles and Applications*. McGraw-Hill Series in Mechanical Engineering. McGraw-Hill Book Company, 1981.
- Pinfield, Valerie J. and Malcolm J. W. Povey: *Thermal scattering must be accounted for in the determination of adiabatic compressibility*. Journal of physical chemistry. B, Condensed matter, materials, surfaces, interfaces and biophysical, 101(7):1110–1112, 1997.
- Pinfield, Valerie J., Malcolm J. W. Povey, and Eric Dickinson: *The application of modified forms of the Urick equation to the interpretation of ultrasound velocity in scattering systems*. Ultrasonics, 33(3):243–251, 1995.
- Pinkel, Robert: *Observations of strongly nonlinear internal motion in the open sea using a range-gated Doppler sonar*. Journal of Physical Oceanography, 9(4):675–686, 1979.
- Poslinski, A. J., M. E. Ryan, R. K. Gupta, S. G. Seshadri, and F. J. Frechette: *Rheological behavior of filled polymeric systems II: The effect of a bimodal size distribution of particulates*. Journal of Rheology, 32(8):751–771, November 1988.

- Povey, M. J. W.: *Ultrasonics in food engineering. Part II: Applications*. Journal of Food Engineering, 9(1):1–20, 1989.
- Povey, M. J. W. and D. J. McClements: *Ultrasonics in food engineering. Part I: Introduction and experimental methods*. Journal of Food Engineering, 8(4): 217–245, 1988.
- Povey, Malcolm J. W.: *A study of dilatation and acoustic propagation in solidifying fats and oils: I. Theoretical*. The journal of the American Oil Chemists' Society (JAOCs), 61(3):558–559, 1984.
- Povey, Malcolm J. W.: *Ultrasonics of food*. Contemporary Physics, 39(6):467–478, 1998.
- Povey, Malcolm J.W.: *Ultrasonic Techniques for Fluids Characterization*. Academic Press, 1997.
- Povey, Malcolm J.W. and Timothy J. Mason: *Ultrasound in Food Processing*. Blackie Academic & Professional, 1998.
- Powell, Robert and David Pfund: *Non-invasive diagnostics for measuring physical properties and processes in high level wastes*. Technical report, University of California Davis (US), 2005. [http://www.osti.gov/bridge/product.biblio.jsp?osti\\_id=841672](http://www.osti.gov/bridge/product.biblio.jsp?osti_id=841672).
- Probstein, R. F., M. Z. Sengun, and T-C. Tseng: *Bimodal model of concentrated suspension viscosity for distributed particle sizes*. Journal of Rheology, 38(4): 811–829, July 1994.
- Regner, Mårten, Marcus Henningsson, Johan Wiklund, Karin Östergren, and Christian Trägårdh: *Predicting the displacement of yoghurt by water in a pipe using CFD*. Chemical Engineering Technology, 30(7):1–11, 2007.
- Ricci, S., E. Boni, T. Morganti, G. Bambi, F. Guidi, and P. Tortoli: *An integrated system for full digital processing of echographic signals*. In *The European DSP Education and Research Symposium (EDERS)*, Birmingham UK, 2004. <http://eprints.unifi.it/archive/00000883/>.
- Ricci, S., E. Boni, F. Guidi, T. Morganti, and P. Tortoli: *A programmable real-time system for development and test of new ultrasound investigation methods*. IEEE Transactions on Ultrasonics, Ferroelectrics, and Frequency Control, 53 (10):1813–1819, 2006.
- Rickey, D. W., P. A. Picot, D. A. Christopher, and A. Fenster: *A wall-less vessel phantom for Doppler ultrasound studies*. Ultrasound in Medicine & Biology, 21 (9):1163–1176, 1995.
- Riebel, Ulrich and Friedrich Löffler: *The fundamentals of particle size analysis by means of ultrasonic spectrometry*. Particle and Particle Systems Characterization, 6:135–143, March 1989.
- Rivara, Guido: *Indagine sul comportamento reologico e fluidodinamico di sospensioni opache mediante l'utilizzo di moderne tecniche ultrasoniche*. Master's thesis, Politecnico di Torino, Facoltà di Ingegneria, Corso di Laurea Specialistica in Ingegneria Meccanica, Sede di Mondovì, 2004.

- Rouffiac, Valérie, Jean-Paul Guglielmi, Alain Barbet, Nathalie Lassau, and Pierre Peronneau: *Application of validated ultrasound indices to investigate erythrocyte aggregation in pigs. Preliminary in vivo results.* Ultrasound in Medicine & Biology, 30(1):35–44, 2004.
- Round, W. H. and R. H. T. Bates: *Modification of spectra of pulses from ultrasonic transducers by scatterers in non-attenuating and in attenuating media.* Ultrasonic Imaging, 9(1):18–28, 1987.
- Saggin, R. and J.N. Coupland: *Concentration measurement by acoustic reflectance.* Journal of Food Science, 66(5):681–685, 2001a.
- Saggin, Raffaella and John N. Coupland: *Oil viscosity measurement by ultrasonic reflectance.* The journal of the American Oil Chemists' Society (JAOCS), 78(5):509–511, 2001b.
- Saggin, Raffaella and John N. Coupland: *Measurement of solid fat content by ultrasonic reflectance in model systems and chocolate.* Food Research International, 35:999–1005, 2002.
- Saggin, Raffaella and John N. Coupland: *Rheology of xanthan/sucrose mixtures at ultrasonic frequencies.* Journal of Food Engineering, 65:49–53, 2004a.
- Saggin, Raffaella and John N. Coupland: *Shear and longitudinal ultrasonic measurements of solid fat dispersions.* The journal of the American Oil Chemists' Society (JAOCS), 81(1):27–32, 2004b.
- Sandrin, Laurent, Sébastien Manneville, and Mathias Fink: *Ultrafast two-dimensional ultrasonic speckle velocimetry: A tool in flow imaging.* Applied Physics Letters, 78(8):1155–1157, 2001.
- Satomura, Shigeo: *Ultrasonic Doppler method for the inspection of cardiac functions.* The Journal of the Acoustical Society of America, 29(11):1181–1185, 1957.
- Schaafsma, Arjen S. and Alex E. Hay: *Attenuation in suspensions of irregularly shaped sediment particles: A two-parameter equivalent spherical scatterer model.* The Journal of the Acoustical Society of America, 102(3):1485–1502, 1997.
- Segré, G. and A. Silberberg: *Non-Newtonian behavior of dilute suspensions of macroscopic spheres in a capillary viscometer.* Journal of Colloid Science, 18(4):312–317, 1963.
- Sengun, M. Z. and R. F. Probstein: *Bimodal model of slurry viscosity with application to coal-slurries. Part 1. Theory and experiment.* Rheologica Acta, 28(5):382–393, September 1989a.
- Sengun, M. Z. and R. F. Probstein: *Bimodal model of slurry viscosity with application to coal-slurries. Part 2. High shear limit behavior.* Rheologica Acta, 28(5):394–401, September 1989b.
- Sengun, M. Z. and R. F. Probstein: *Bimodal model of suspension viscoelasticity.* Journal of Rheology, 41(4):811–819, 1997.
- Sengun, Mehmet Z. and Roland F. Probstein: *High-shear-limit viscosity and the maximum packing fraction in concentrated monomodal suspensions.* PCH



- PhysicoChemical Hydrodynamics, 11(2):229–241, 1989c.
- Shaaban, Akram M. and André J. Duerinckx: *Wall shear stress and early atherosclerosis*. American Journal of Roentgenology, 174:1657–1665, 2000.
- Shafiei, Tina: *Acoustic properties of oil and water based suspensions for in-line velocity profile measurements*. Master’s thesis, ETH Zurich, 2005.
- Shapiro, Andrew P. and Ronald F. Probst: *Random packings of spheres and fluidity limits of monodisperse and bidisperse suspensions*. Physical Review Letters, 68(9):1422 – 1425, March 1992.
- Shapley, Nina C., Robert A. Brown, and Robert C. Armstrong: *Evaluation of particle migration models based on laser Doppler velocimetry measurements in concentrated suspensions*. Journal of Rheology, 48(2):255–279, 2004.
- Shekarriz, A. and D. M. Sheen: *Slurry pipe flow measurements using tomographic ultrasonic velocimetry and densitometry*. In *Proceedings of FEDMS '98, 1998 ASME Fluids Engineering Division Summer Meeting, June 21-25, 1998 Washington, D.C., USA*, pp. 1–8. ASME, June 1998a.
- Shekarriz, Alireza and David M. Sheen: *Method and apparatus for ultrasonic Doppler velocimetry using speed of sound and reflection mode pulsed wideband Doppler*. Patent, June 1998b.
- Shen, C. and U. Lemmin: *Ultrasonic measurements of suspended sediments: A concentration profiling system with attenuation compensation*. Measurement Science and Technology, 7:1191–1194, 1996.
- Shung, K. K., Y. W. Yuan, and D. Y. Fei: *Effect of flow disturbance on ultrasonic backscatter from blood*. The Journal of the Acoustical Society of America, 75 (4):1265–1272, 1984.
- Shung, K. Kirk and Dong-Guk Paeng: *Ultrasound: An unexplored tool for blood flow visualization and hemodynamic measurements*. Japanese Journal of Applied Physics Part 1, 42(5B):2901–2908, 2003.
- Shung, KoPing K., Rubens A. Sigelmann, and John M. Reid: *Scattering of ultrasound by blood*. IEEE Transactions on Biomedical Engineering, 23(6):460–467, November 1976.
- Sigelmann, Rubens A. and John M. Reid: *Analysis and measurement of ultrasound backscattering from an ensemble of scatterers excited by sine-wave bursts*. The Journal of the Acoustical Society of America, 53(5):1351–1355, 1973.
- Singh, Anad Pal, D. J. McClements, and A. G. Marangoni: *Solid fat content determination by ultrasonic velocimetry*. Food Research International, 37:545–555, 2004.
- Sleefe, Gerard E. and Padmakar P. Lele: *On estimating the number density of random scatterers from backscattered acoustic signals*. Ultrasound in Medicine & Biology, 14(8):709–727, 1988.
- Stickel, Jonathan J. and Robert L. Powell: *Fluid mechanics and rheology of dense suspensions*. Annual Review of Fluid Mechanics, 37:129–149, January 2005.
- Storti, G., A. K. Hipp, and M. Morbidelli: *Monitoring latex reactors by ultrasonics*.

- Polymer Reaction Engineering, 8(1):77–94, 2000.
- Szabo, Thomas L., Basak Ülker Karbeyaz, Robin O. Cleveland, and Eric L. Miller: *Determining the pulse-echo electromechanical characteristic of a transducer using flat plates and point targets*. The Journal of the Acoustical Society of America, 115(1):90–96, 2004.
- Takeda, Y.: *Velocity profile measurement by ultrasonic Doppler shift method*. International journal of numerical methods for heat and fluid flow, 7:313, 1986.
- Takeda, Y. and M. Haefeli: *Velocity profile measurements by ultrasonic Doppler shift method – evaluation of shape reproducibility*. In Keffer, J. F., R. K. Shan, and E. N. Ganić (editors), *Proceedings of the Second World Conference on Experimental Heat Transfer, Fluid mechanics, and Thermodynamics held June 23-28, 1991 in Dubrovnik, Yugoslavia*, pp. 369–374. Elsevier, 1991.
- Takeda, Y., Y. Murai, H. Kikura, and N. Furuichi (editors): *Fourth International Symposium on Ultrasonic Doppler Methods for Fluid Mechanics and Fluid Engineering (4th ISUD)*, Hokkaido University, Sapporo, Japan, September 2004.
- Takeda, Yashushi: *Measurement of velocity profile of mercury flow by ultrasound Doppler-shift method*. Nuclear Technology, 79(1):120–124, 1987.
- Teirlinck, Carolus J. P. M., Robert A. Bezemer, Christian Kollmann, Jaap Lubbers, Peter R. Hoskins, Peter Fish, Knud-Erik Fredfeldt, and Ulrich G. Schaarschmidt: *Development of an example flow test object and comparison of five of these test objects, constructed in various laboratories*. Ultrasonics, 36(1-5):653–660, 1998.
- Tezuka, Kenichi, Michitsugu Mori, Takeshi Suzuki, and Toshimasa Kanamine: *Application of ultrasonic pulse-Doppler flow meter for hydraulic power plant*. In Birkhofer *et al.* (2006b), pp. 105–108.
- Thijssen, J. M., M. C. van Wijk, and M. H. M. Cuypers: *Performance testing of medical echo/Doppler equipment*. European Journal of Ultrasound, 15(3):151–164, 2002.
- Thijssen, Johan M.: *Ultrasonic speckle formation, analysis and processing applied to tissue characterization*. Pattern Recognition Letters, 24(4-5):659–675, 2003.
- Thijssen, Johan M., Gert Weijers, and Chris L. de Korte: *Objective performance testing and quality assurance of medical ultrasound equipment*. Ultrasound in Medicine & Biology, 33(3):460–471, 2007.
- Thompson, R. S. and G. K. Aldis: *Effect of a cylindrical refracting interface on ultrasound intensity and the CW Doppler spectrum*. IEEE Transactions on Biomedical Engineering, 43(5):451–459, 1996.
- Thompson, Rosemary S., Piero Tortoli, and Geoffrey K. Aldis: *Selective transmission of a focused Doppler ultrasound beam through a plastic layer*. Ultrasound in Medicine & Biology, 26(8):1333–1346, 2000.
- Thorne, Peter D. and Michael J. Buckingham: *Measurements of scattering by suspensions of irregularly shaped sand particles and comparison with a single parameter modified sphere model*. The Journal of the Acoustical Society of

- America, 116(5):2876–2889, 2004.
- Thorne, Peter D., Peter J. Hardcastle, and Richard L. Soulsby: *Analysis of acoustic measurements of suspended sediments*. Journal of Geophysical Research, 98(C1): 899–910, 1993.
- Tortoli, P. and F. Andreuccetti: *A high-speed FFT unit based on a low cost digital signal processor*. IEEE Transactions on Ultrasonics, Ferroelectrics, and Frequency Control, 35(11):1434–1438, 1988.
- Tortoli, P., R. S. Thompson, P. Berti, and F. Guidi: *Flow imaging with pulsed Doppler ultrasound and flow phantoms*. IEEE Transactions on Ultrasonics, Ferroelectrics, and Frequency Control, 46(6):1591–1596, 1999.
- Tortoli, Piero: *A tracking FFT processor for pulsed Doppler analysis beyond the Nyquist limit*. IEEE Transactions on Biomedical Engineering, 36(2):232–237, 1989.
- Tortoli, Piero, Francesco Guidi, Gabriele Guidi, and Carlo Atzeni: *Spectral velocity profiles for detailed ultrasound flow analysis*. IEEE Transactions on Ultrasonics, Ferroelectrics, and Frequency Control, 43(4):654–659, July 1996.
- Tortoli, Piero, Gabriele Guidi, Paolo Berti, Francesco Guidi, and Daniele Righi: *An FFT-based flow profiler for high-resolution in vivo investigations*. Ultrasound in Medicine & Biology, 23(6):899–910, 1997.
- Tortoli, Piero, Tiziano Morganti, Giacomo Bambi, Carlo Palombo, and Kumar V. Ramnarine: *Noninvasive simultaneous assessment of wall shear rate and wall distension in carotid arteries*. Ultrasound in Medicine & Biology, 32(11):1661–1670, 2006.
- Tsou, Jean K., Jie Liu, and Michael F. Insana: *Modeling and phantom studies of ultrasonic wall shear rate measurements using coded pulse excitation*. IEEE Transactions on Ultrasonics, Ferroelectrics, and Frequency Control, 53(4):724–734, 2006.
- Twersky, Victor: *Low-frequency scattering by mixtures of correlated nonspherical particles*. The Journal of the Acoustical Society of America, 84(1):409–415, 1988.
- Ueda, Mitsuhiro and Yasuhiko Ozawa: *Spectral analysis of echoes for backscattering coefficient measurement*. The Journal of the Acoustical Society of America, 77(1):38–47, 1985.
- Urick, R. J.: *A sound velocity method for determining the compressibility of finely divided substances*. Journal of Applied Physics, 18:983–987, 1947.
- Vaitkus, P. J. and R. S. C. Cobbold: *A comparative study and assessment of Doppler ultrasound spectral estimation techniques part i: Estimation methods*. Ultrasound in Medicine & Biology, 14(8):661–672, 1988.
- Vaitkus, P. J. and R. S. C. Cobbold: *A new time-domain narrowband velocity estimation technique for Doppler ultrasound flow imaging. I. Theory*. IEEE Transactions on Ultrasonics, Ferroelectrics, and Frequency Control, 45(4):939–954, 1998.

- Vaitkus, P. J., R. S. C. Cobbold, and K. W. Johnston: *A comparative study and assessment of Doppler ultrasound spectral estimation techniques part ii: Methods and results*. *Ultrasound in Medicine & Biology*, 14(8):673–688, 1988.
- Vaitkus, P. J., R. S. C. Cobbold, and K. W. Johnston: *A new time-domain narrowband velocity estimation technique for Doppler ultrasound flow imaging. II. Comparative performance assessment*. *IEEE Transactions on Ultrasonics, Ferroelectrics, and Frequency Control*, 45(4):955–971, 1998.
- Heiden, Maurits S. van der, Machteld G. M. de Kroon, Nicolaas Bom, and Cornelius Borst: *Ultrasound backscatter at 30 MHz from human blood: Influence of rouleau size affected by blood modification and shear rate*. *Ultrasound in Medicine & Biology*, 21(5):817–826, 1995.
- Malssen, Kees van, René Peschar, Claudia Brito, and Henk Schenk: *Real-time X-ray powder diffraction investigations on cocoa butter. III. Direct  $\beta$ -crystallization on cocoa butter: Occurrence of a memory effect*. *The journal of the American Oil Chemists' Society (JAOCs)*, 73(10):1225–1230, 1996a.
- Malssen, Kees van, René Peschar, and Henk Schenk: *Real-time X-ray powder diffraction investigations on cocoa butter. I. Temperature-dependent crystallization behavior*. *The journal of the American Oil Chemists' Society (JAOCs)*, 73(10):1209–1215, 1996b.
- Malssen, Kees van, René Peschar, and Henk Schenk: *Real-time X-ray powder diffraction investigations on cocoa butter. II. The relationship between melting behavior and composition of  $\beta$ -cocoa butter*. *The journal of the American Oil Chemists' Society (JAOCs)*, 73(10):1217–1223, 1996c.
- Malssen, Kees van, Arjen van Langevelde, René Peschar, and Henk Schenk: *Phase behavior and extended phase scheme of static cocoa butter investigated with real-time X-ray powder diffraction*. *The journal of the American Oil Chemists' Society (JAOCs)*, 76(6):669–676, 1999.
- Vieli, A., U. Moser, S. Maier, D. Meier, and P. Boesiger: *Velocity profiles in the normal human abdominal aorta: A comparison between ultrasound and magnetic resonance data*. *Ultrasound in Medicine & Biology*, 15(2):113–119, 1989.
- Wada, Sanehiro, Hiroshige Kikura, Masanori Aritomi, Michitsugu Mori, and Yashushi Takeda: *Development of pulse ultrasonic Doppler method for flow rate measurement in power plant. Multilines flow rate measurement on metal pipe*. *Journal of Nuclear Science and Technology*, 41(3):339–346, 2004.
- Walker, Andrew R., David J. Philips, and Jeffry E. Powers: *Evaluating Doppler devices using a moving string test target*. *Journal of Clinical Ultrasound*, 10(1): 25–30, 1982.
- Wang, Shyh-Hau and K. K. Shung: *In vivo measurements of ultrasonic backscattering in blood*. *IEEE Transactions on Ultrasonics, Ferroelectrics, and Frequency Control*, 48(2):425–431, 2001.
- Wang, Shyh-Hau and K. Kirk Shung: *An approach for measuring ultrasonic backscattering from biological tissues with focused transducers*. *IEEE Trans-*

- actions on Biomedical Engineering, 44(7):549–554, 1997.
- Waterman, P. C. and Rohn Truell: *Multiple scattering of waves*. Journal of Mathematical Physics, 2(4):512–537, 1961.
- Wells, P. N. T.: *A range-gated ultrasonic Doppler system*. Medical and Biological Engineering, 7:641–652, 1969.
- Wiklund, J., M. Johansson, J. Shaik, P. Fischer, E. Windhab, M. Stading, and A.M. Hermansson: *In-line rheological measurements of complex model fluids using an ultrasound UVP-PD based method*. In *Annual Transactions - The Nordic Rheology Society, 10th Anniversary conference, Trondheim, Norway*, pp. 128–130, 2001.
- Wiklund, Johan: *Rheological in-line techniques based on ultrasound Doppler methods for the food industry. A literature survey*. Technical Report SR-710, SIK, Göteborg, Sweden, 2003, ISBN 91-7290-225-X.
- Wiklund, Johan: *Ultrasound Doppler Based In-Line Rheometry – Development, Validation and Application*. PhD thesis, Lund University, 2007, ISBN 978-91-628-7025-6.
- Wiklund, Johan and Mats Stading: *Application of in-line ultrasound Doppler based UVP-PD method to concentrated model and industrial suspensions*. In Birkhofer *et al.* (2006b), pp. 145–148.
- Wiklund, Johan, Matthias Johansson, Jeelani Shaik, Peter Fischer, Erich Windhab, Mats Stading, and Anne-Marie Hermansson: *In-line ultrasound based rheometry of industrial and model suspensions flowing through pipes*. In *Papers of the Third International Symposium on Ultrasonic Doppler Methods for Fluid Mechanics and Fluid Engineering*, pp. 69–76. EPFL Lausanne, Paul Scherrer Institut, 2002.
- Wiklund, Johan, J. Pettersson, A. Rasmuson, and M. Stading: *A comparative study between UVP and LDA techniques for highly concentrated pulp suspensions in pipe flow*. In Takeda *et al.* (2004), pp. 69–75.
- Wiklund, Johan, Mats Stading, A. J. Pettersson, and A. Rasmuson: *A comparative study of UVP and LDA techniques for pulp suspensions in pipe flow*. AIChE Journal, 52(2):484–495, 2006.
- Wiklund, Johan, Iman Shahram, and Mats Stading: *Methodology for in-line rheology by ultrasound Doppler velocity profiling and pressure difference techniques*. Chemical Engineering Science, 62:4277–4293, 2007.
- Wille, R. L. and E. S. Lutton: *Polymorphism of cocoa butter*. The journal of the American Oil Chemists’ Society (JAOCs), 43(8):491–496, 1966.
- Windhab, E. J.: *Fluid immobilization – a structure-related key mechanism for the viscous flow behavior of concentrated suspension systems*. Applied Rheology, 10(3):134–139, 2000.
- Windhab, E. J., M. Dressler, K. Feigl, P. Fischer, and D. Megias-Alguacil: *Emulsion processing – from single-drop deformation to design of complex processes and products*. Chemical Engineering Science, 60:2101–2113, 2005.

- Windhab, Erich J.: *Sensoren zur On-Line Messung am Beispiel von Struktur- und Fließparametern in der Schokoladentechnologie*. In *Schoko-Technik, Internationale ZDS-Fachtagung SIC-14*, Gürzenich in Köln, Martinstrasse 27-31, D-50667 Köln, December 1994. Zentralfachschule der Deutschen Süßwarenwirtschaft/Solingen.
- Wood, A. B.: *A textbook of Sound*. Bell and Sons, London, 3rd edition, 1964.
- Wunderlich, Th. and P. O. Brunn: *Ultrasound pulse Doppler method as a viscometer for process monitoring*. *Flow Measurement and Instrumentation*, 10 (4):201–205, 1999.
- Yamanaka, G., H. Kikura, Y. Takeda, and M. Aritomi: *Flow measurement on an oscillating pipe flow near the entrance using the UVP method*. *Experiments in Fluids*, 32(2):212–220, 2002.
- York, George and Yongmin Kim: *Ultrasound processing and computing: Review and future directions*. *Annual Review of Biomedical Engineering*, 1:559–588, 1999.
- Zeng, Yuanqun: *Impf- und Scherkristallisation von Schokoladen*. PhD thesis, ETH Zürich, 2000.

# List of Figures

2.1. Electrical and acoustic bursts and shape of the sample volume. . .	7
2.2. Deconvolution of a fully-developed laminar flow. . . . .	8
3.1. Flow profiles of Newtonian and non-Newtonian fluid pipe flow. . .	23
3.2. Backscattering coefficient in function of the hematocrit. . . . .	34
4.1. The different cocoa butter crystal conformations, their stability and packing. . . . .	44
4.2. Microscopy picture of a diluted sample of the suspension produced in the shear crystallization process. There are single, spherical to rod like particles below 10 $\mu$ m in diameter and a few larger aggregates with a diameter larger than 10 $\mu$ m. . . . .	45
4.3. Rotating cylinder and the calculated beam paths. . . . .	47
4.4. Scheme of rotating cylinder. . . . .	48
4.5. Pressure field and near field zone generated by the transducer. . .	50
4.6. Flow adapter with two ultrasound transducers. . . . .	52
4.7. Data flow chart with the data inputs on the left side and the processing resulting in the rheological parameters. . . . .	55
4.8. Flow loop for the model suspension. . . . .	56
4.9. Scheme of the shear crystallizer flow loop, its instrumentation and data acquisition devices. . . . .	57
5.1. Microscopic image of 11 $\mu$ m and 90 $\mu$ m polyamide particles in rapeseed oil. . . . .	60
5.2. Distributions of volume mean diameters for two mean diameter (11 and 90 $\mu$ m) polyamide particles. . . . .	60
5.3. Velocity of sound and attenuation in rapeseed oil in function of the temperature. . . . .	61
5.4. The measured velocity of sound in function of the particle concentration and result from the fit to the Urick equation. . . . .	62
5.5. Temporal development velocity of sound during the measurement of the 25 % suspension of 90 $\mu$ m polyamide particles. . . . .	63
5.6. Flow curves measured in-line and off-line for 11 $\mu$ m polyamide particles in rapeseed oil. . . . .	64

5.7. Flow curves measured in-line and off-line for 90 $\mu\text{m}$ polyamide particles in rapeseed oil. . . . .	65
5.8. Flow curves measured in-line and off-line for bimodal suspensions of polyamide particles in rapeseed oil. . . . .	66
5.9. Radial velocity profile in the pipe during the flow of a suspension of 5 % by volume of 11 $\mu\text{m}$ diameter polyamide particles in rapeseed oil. . . . .	67
5.10. Radial velocity profile in the pipe during the flow of a suspension of 25 % by volume of 11 $\mu\text{m}$ diameter polyamide particles in rapeseed oil. . . . .	68
5.11. Radial velocity profile in the pipe during the flow of a suspension of 25 % by volume of 90 $\mu\text{m}$ diameter polyamide particles in rapeseed oil. . . . .	68
5.12. Radial velocity profile in the pipe during the flow of a suspension of a constant total concentration of 25 % by volume of a bimodal mixture of 20 % 11 $\mu\text{m}$ and 5 % 90 $\mu\text{m}$ polyamide particles in rapeseed oil. . . . .	69
5.13. Radial velocity profile in the pipe during the flow of a suspension of a constant total concentration of 25 % by volume of a bimodal mixture of 20 % 11 $\mu\text{m}$ and 5 % 90 $\mu\text{m}$ polyamide particles in rapeseed oil. . . . .	69
5.14. Comparison of shear rate dependent viscosities determined using off-line rheometry and in-line power law and gradient methods. . . . .	74
5.15. The measured velocity profile in 5%/11 $\mu\text{m}$ polyamide suspension and the fitted power law velocity profiles for three different pipe wall positions 300 $\mu\text{m}$ apart from each other. . . . .	75
5.16. Sound velocity, SFC and temperature during crystallization in the one stage shear crystallizer. . . . .	76
5.17. Velocity of sound as a function of the solid fat content (both quantities originally measured as function of the time). . . . .	76
5.18. Temporal variation in the measured values of the process and acoustic parameters in a pipe section after the shear crystallizer. . . . .	78
5.19. Velocity profiles (average of 30 single profiles) given as channel-wise normalized baseband signal power spectra and estimated velocity profiles along the pipe diameter at different times after the start-up of shear crystallizer. . . . .	79
5.20. Development of the baseband signal envelope in the liquid cocoa butter after switching on the shear crystallizer. . . . .	82
5.21. Temporal and spatial distribution of the amplitude of the baseband signal. . . . .	83
5.22. The amplitude of the baseband signal of all the 256 pulse repetitions corresponding to a single profile 5 min after the start of the measurement . . . . .	84



5.23. The baseband signal amplitude of all the 256 pulse repetitions and the corresponding profile at the end of the crystallization. . . . .	84
5.24. Temporal behavior of the location (measurement channel) of the maximum value of the baseband signal during the crystallization. . . . .	85
5.25. Average over 30 flow profiles, RMS of the baseband signal and the average of the baseband signal for liquid cocoa butter and crystal suspension. . . . .	86
5.26. The measured profile and the profiles resulting from the fits to the power law and Herschel-Bulkley models. . . . .	87
5.27. Temporal variation in the values of $K$ and $n$ during the crystallization process. . . . .	88
5.28. Temporal variation in viscosities ( $\eta_{\dot{\gamma}=2.5}$ and $\eta_{\dot{\gamma}=7.5}$ ) and radial positions ( $r_{\dot{\gamma}=2.5}$ and $r_{\dot{\gamma}=7.5}$ ) in the pipe corresponding to shear rates $\dot{\gamma}$ of 2.5 1/s and 7.5 1/s respectively. . . . .	89
5.29. Radial distribution of shear rate $\dot{\gamma}$ and viscosity $\eta$ for the velocity distributions shown in figure 5.19. . . . .	90
5.30. Influence of the estimated pipe wall position on $n$ and $K$ and the corresponding error for the liquid cocoa butter. . . . .	91
5.31. Overview of the received signals when using 1 to 4 cycles. Sending from the TN, receiving with the TX transducer with a distance of 34 mm. . . . .	91
5.32. Normalized amplitude of the baseband signal for 1, 2 and 4 cycles with maximum values 0.30, 0.55 and 1 respectively. . . . .	93
5.33. Flow profiles with pulse lengths of 1, 2 and 4 cycles. With a summary of the estimated profiles in the plot on the bottom left. . . . .	94
5.34. Envelopes of the baseband signal amplitude (median of the 25 profiles) which is digitized at 14 bit for two different pulse lengths. . . . .	95
5.35. Envelope of the in-phase part of the baseband signal and the flow profile measured at 2 MHz. . . . .	96
5.36. Envelope of the baseband signal and a velocity profile (average of 500 single profiles) measured with the TX transducer. . . . .	98
5.37. Dynamic development of the sound velocity and transmitted signal amplitude due to step changes (increase and decrease) in the seeding of chocolate with 0.4% (by volume) cocoa butter crystal suspension. . . . .	98
5.38. Velocity profiles for the eight different applied currents. . . . .	101
5.39. The root mean square of the normal part of the demodulated echo amplitude (baseband signal) for the eight applied power currents. . . . .	101
5.40. The average amplitude of the baseband signal shown in figure 5.39 between channels 1 and 80 in function of the applied current. . . . .	102
5.41. Spectra averaged over 20 profile data sets at channel 30 for the different currents. . . . .	102

5.42. Baseband signal amplitudes and corresponding power spectra for the measurement with no current applied. . . . .	103
5.43. Baseband signal amplitudes and corresponding power spectra for a data set with the highest current applied. . . . .	104
5.44. Baseband signal and power spectrum for the case with the minimum current applied. . . . .	105
5.45. On the left side a microscopy image of polyamide suspension in water and on the right side the size distribution of polyamide particles. The average size of particles is about 20 $\mu\text{m}$ . . . . .	106
5.46. The measured velocity versus the theoretical velocity in small and big cylinders . . . . .	107
5.47. Graph shows Mean stdev versus number of cycles . . . . .	108
5.48. Graph shows the % relative error versus measured velocity . . . . .	109
5.49. Frequency spectra of measurements in rotating cylinder. . . . .	110
A.1. Scheme of the coordinate system and the normal velocity of the transducer surface. . . . .	115

# List of Tables

3.1. Fluids and suspensions used for UVP-PD measurements in literature.	24
3.2. Parameters of UVP-PD measurements in literature. . . . .	25
3.3. Articles on fat crystallization. . . . .	41
5.1. Values of measured flow, acoustic and UVP parameters for sus- pensions of different concentrations of 11 $\mu\text{m}$ diameter polyamide particles in rapeseed oil. . . . .	70
5.2. Values of measured flow, acoustic and UVP parameters for sus- pensions of different concentrations of 90 $\mu\text{m}$ diameter polyamide particles in rapeseed oil. . . . .	71
5.3. Values of measured flow, acoustic and UVP parameters for sus- pensions of different concentrations of bimodal polyamide sized polyamide particles in rapeseed oil. . . . .	71
5.4. Effect of the wall position on the values of the power law parameters $n$ and $K$ . . . . .	73
5.5. UVP parameters for the measurement during the crystallization process. . . . .	82
5.6. UVP parameters common for all profiles shown in section 5.3.2. . .	92
5.7. UVP parameters for profiles shown in figure 5.35 different from the ones given in table 5.6. . . . .	96
5.8. UVP parameters for the measurements with the TX transducer presented in section 5.3.4. . . . .	97
5.9. UVP parameters common for all profiles shown in section 5.4. . .	100

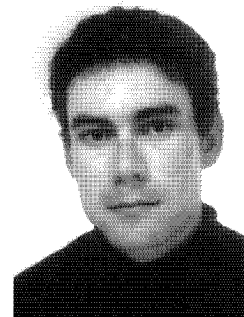


# Curriculum Vitae

Beat H. Birkhofer

## Personal Data

date of birth January 14, 1977  
place of birth Basel  
citizen of Liestal (BL) and  
Neuhausen am Rheinfall (SH)



## Education and Stages

- 2003 – 2007 Doctoral student and research assistant at the Swiss Federal Institute of Technology (ETH) Zurich, Switzerland, Institute of Food Science and Nutrition, Laboratory of Food Process Engineering.
- 1996 – 2002 Diploma Studies in Food Engineering and Technology at ETH Zurich
- Diploma thesis: «Design and setup of an optical computer-controlled flow cell and real time measurement of the droplet deformation in simple shear flow.»
- Mobility semester at the ENSIA (École Nationale Supérieure des Industries Agricoles et Alimentaires) in Massy (Paris).
- 9 months of practical experience at
- Swiss Federal Institute of Environmental Science and Technology
  - Waterworks Zurich
  - Toni AG (diary factory), Basel
- 1996 Matura, typus C (natural science) in Liestal (BL)